Reference

DOT-HS-806-962
DOT-TSC-NHTSA-86-1

Crash Padding Research

Volume III: Impact Analysis and Model Validation

Oscar Orringer
David Y. Jeong
Pin Tong
Kevin T. Knadle
John F. Mandell

Transportation Systems Center
Cambridge MA 02142

July 1986
Final Report

U.S. Department of Transportation
National Highway Traffic Safety Administration

Office of Research and Development
Office of Crashworthiness Research
Washington DC 20590

Technical Report Documentation Page

1. Report No.	2. Government Accession No.	3. Recipient's Catalog No.
DOT-HS-806-962		

4. Title and Subtitle	5. Report Date
CRASH PADDING RESEARCH Volume III: Impact Analysis and Model Validation	July 1986
	6. Performing Organization Code DTS-44
7. Author(s) O. Orringer, D.Y. Jeong, P. Tong, K.T. Knadle, F. Mandell*	8. Performing Organization Report No. DOT-TSC-NHTSA-86-1
9. Performing Organization Name and Address U.S. Department of Transportation Research and Special Programs Administration Transportation Systems Center Cambridge, MA 02142	10. Work Unit No. (TRAIS) HS-476/R4431
	11. Contract or Grant No.
12. Sponsoring Agency Name and Address U.S. Department of Transportation National Highway Traffic Safety Administration Office of Research and Development Washington, DC 20590	13. Type of Report and Period Covered Final Report April 1982 - June 1984
	14. Sponsoring Agency Code NRD-10

15. Supplementary Notes

*Department of Materials Science and Engineering
Massachusetts Institute of Technology
Cambridge, MA 02139

16. Abstract

This final volume of Crash Padding Research report summarizes the application of the laboratory material model developed in Volumes I and II to the prediction of impact behavior. This involved embedding the material model in a simplified dynamic simulation of the occupant-vehicle impact. The simulation is a computer program predicting force, acceleration, etc., versus time, based on fundamental inputs of the occupant's initial speed, mass, and geometry, the vehicle's structural stiffness, and the laboratory model for padding.

By comparing simulation predictions with impact test results, the computer simulation has been validated for impact scenarios involving metal structures similar to an automobile dashboard.

17. Key Words	18. Distribution Statement
Crash Padding, Mechanical Properties, Viscoelastic Materials, Constitutive Equation, State Equation	DOCUMENT IS AVAILABLE TO THE PUBLIC THROUGH THE NATIONAL TECHNICAL INFORMATION SERVICE, SPRINGFIELD VIRGINIA 22161

19. Security Classif. (of this report)	20. Security Classif. (of this page)	21. No. of Pages	22. Price
UNCLASSIFIED	UNCLASSIFIED	98	

Form DOT F 1700.7 (8-72) Reproduction of completed page authorized

PREFACE

The analytical work described herein was conducted at the DOT Transportation Systems Center, Cambridge, Massachusetts. The experimental work was conducted at the Massachusetts Institute of Technology, Cambridge, Massachusetts. The work was sponsored by the National Highway Traffic Safety Administration under Project Plan Agreement HS-476. This series of reports is specifically concerned with evaluating the impact response characteristics of foam-type crash padding materials. This report is the last of three volumes in the series. Volume I covered the results of laboratory tests to determine the basic dynamic mechanical properties of a typical foam rubber. Volume II covered the derivation of foam-rubber constitutive equation models and the procedures used to fit the model parameters to the laboratory test results. This report covers application and validation of the best model for impact response prediction.

METRIC CONVERSION FACTORS

Approximate Conversions to Metric Measures

Symbol	When You Know	Multiply by	To Find	Symbol
		LENGTH		
in	inches	*2.5	centimeters	cm
ft	feet	30	centimeters	cm
yd	yards	0.9	meters	m
mi	miles	1.6	kilometers	km
		AREA		
in^2	square inches	6.5	square centimeters	cm^2
ft^2	square feet	0.09	square meters	m^2
yd^2	square yards	0.8	square meters	m^2
mi^2	square miles	2.6	square kilometers	km^2
	acres	0.4	hectares	ha
		MASS (weight)		
oz	ounces	28	grams	g
lb	pounds	0.45	kilograms	kg
	short tons (2000 lb)	0.9	tonnes	t
		VOLUME		
tsp	teaspoons	5	milliliters	ml
Tbsp	tablespoons	15	milliliters	ml
fl oz	fluid ounces	30	milliliters	ml
c	cups	0.24	liters	l
pt	pints	0.47	liters	l
qt	quarts	0.96	liters	l
gal	gallons	3.8	liters	l
ft^3	cubic feet	0.03	cubic meters	m^3
yd^3	cubic yards	0.76	cubic meters	m^3
		TEMPERATURE (exact)		
°F	Fahrenheit temperature	5/9 (after subtracting 32)	Celsius temperature	°C

*1 in. = 2.64 cm (exactly). For other exact conversions and more detail tables see NBS Misc. Publ. 286, Units of Weight and Measures. Price $2.25 SD Catalog No. C13 10 286.

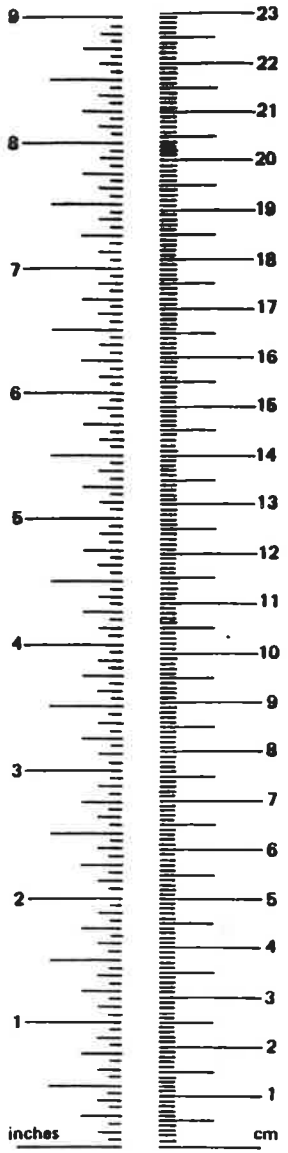

Approximate Conversions from Metric Measures

Symbol	When You Know	Multiply by	To Find	Symbol
		LENGTH		
mm	millimeters	0.04	inches	in
cm	centimeters	0.4	inches	in
m	meters	3.3	feet	ft
m	meters	1.1	yards	yd
km	kilometers	0.6	miles	mi
		AREA		
cm^2	square centimeters	0.16	square inches	in^2
m^2	square meters	1.2	square yards	yd^2
km^2	square kilometers	0.4	square miles	mi^2
ha	hectares (10,000 m^2)	2.5	acres	
		MASS (weight)		
g	grams	0.035	ounces	oz
kg	kilograms	2.2	pounds	lb
t	tonnes (1000 kg)	1.1	short tons	
		VOLUME		
ml	milliliters	0.03	fluid ounces	fl oz
l	liters	2.1	pints	pt
l	liters	1.06	quarts	qt
l	liters	0.26	gallons	gal
m^3	cubic meters	36	cubic feet	ft^3
m^3	cubic meters	1.3	cubic yards	yd^3
		TEMPERATURE (exact)		
°C	Celsius temperature	9/5 (then add 32)	Fahrenheit temperature	°F

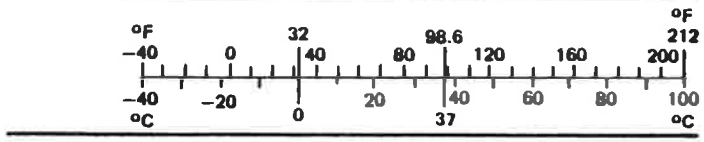

TABLE OF CONTENTS

LIST OF ILLUSTRATIONS

LIST OF ILLUSTRATIONS

LIST OF TABLES

SUMMARY

Selection of materials for energy-absorbent performance is an important consideration for automobile interior padding, which must provide the greatest occupant protection for the least padding thickness possible. Padding material dynamic properties, including energy absorption, can be determined by laboratory tests on small specimens. Such tests were performed on Uniroyal Ensolite AAC foam rubber padding, and constitutive equations embodying the energy-absorption characteristics of this material were developed. The results of these phases of the work were reported in Volume I and Volume II, respectively.

The present volume summarizes the application of the laboratory material model to the predicton of impact behavior. For this purpose, the material model has been embedded in a simplified dynamic simulation of the occupant-vehicle impact. The simulation is a computer program which predicts force, acceleration, etc., versus time, based on fundamental inputs of the occupant's initial speed, mass, and geometry, the automobile's metal structure stiffness, and the laboratory model of the padding.

The computer simulation has been validated for impact scenarios involving metal structure similar to the automobile dashboard. The validation was accomplished by comparing the simulation predictions with impact test results.

1. INTRODUCTION

The first two volumes of this report summarized the characterization of Uniroyal Ensolite AAC foam rubber, a recoverable closed-cell crash padding material. The first volume dealt with the results of laboratory tests to determine the one-dimensional (uniform compression) material dynamic properties. The second volume dealt with the development of constitutive equations to model the observed uniform compression properties. Two empirical models were developed, one with 9 parameters and one with 21 parameters. These models were applied to the Ensolite test data, with the result that the 21-parameter model fit the data well over the entire range of interest, while the 9-parameter model provided a reasonable fit only over a limited range.

This volume summarizes the application of the empirical models to the problem of predicting impact responses. The type of impact problem to be considered involves the collision of an unrestrained vehicle occupant with padded components of an automobile's interior structure during a crash.

The occupant-to-vehicle impact problem can be defined as follows: Let M_1 and M_2 be the effective masses of the occupant and vehicle, respectively; let V_1' and V_2' be their post-impact velocities. The impact can be assumed to have a short duration, i.e. short enough so that external forces do not substantially change the vehicle velocity during the event.

The impact involves exchange of momentum and kinetic energy between the two bodies and absorption of some kinetic energy by their deformable parts. If the energy absorption is characterized by a coefficient of restitution, C, then the momentum and energy conservation laws can be used to derive the following expressions for the post-impact velocities:

$$V_1' = \left[(M_1 - M_2\sqrt{C})V_1 + (1 + \sqrt{C})M_2V_2 \right] / (M_1 + M_2) \quad (1)$$

$$V_2' = \left[(1 + \sqrt{C})M_1V_1 + (M_2 - M_1\sqrt{C})V_2 \right] / (M_1 + M_2) \quad (2)$$

If the occupant's effective mass is small compared to the vehicle mass, and if the impact is described in coordinates at rest with respect to the vehicle, then Eqs. 1 and 2 reduce to $V'_1 \simeq -\sqrt{C}\, V_1$ and $V'_2 \simeq V_2 = 0$. The quantity 1-C is, by definition, the fraction of available kinetic energy that is absorbed by deformations:

$$1\text{-}C = E_{ABSORBED}/E_{AVAILABLE} \tag{3}$$

where

$$E_{AVAILABLE} = \frac{M_1 M_2 (V_1 - V_2)^2}{2 (M_1 + M_2)} \simeq M_1 V_1^2/2 \tag{4}$$

Impact analysis of crash pads has two objectives. The first is to estimate the coefficient of restitution or the equivalent post-impact velocities. These results can be used as inputs to computer programs such as the NHTSA Crash Victim Simulator[1], which predicts the path of an unrestrained occupant engaging in multiple impacts with different parts of the automobile's passenger compartment. The second objective is to estimate the force-time history of the pad's reaction on the occupant. Such force-time histories can be used as inputs to biomechanical models [2] from which injury severity indices are calculated.

Either objective requires analysis of both the loading and unloading phases, although the requirements for model accuracy are more stringent for the second objective than for the first. The loading phase encompasses the instant of contact to the point at which the pad reaches maximum compression. The unloading phase begins at the maximum-compression point and ends when the rebounding occupant loses contact with the pad.

The analysis is performed by coupling the occupant's equations of motion with the constitutive equation of the padding material. The equations of motion supply the strain and strain-rate fields imposed on the pad, while the constitutive equation supplies the reaction stress field and the net force on the occupant. In general, the part of the occupant's body involved in the impact is a flexible curved surface, and the resulting interaction is more complex than the one-dimensional uniform compression tests used to determine padding material properties. Section 2 summarizes the development of impact analysis procedures. The development emphasizes a simplified case in which the occupant is replaced by a rigid sphere, although other cases have been discussed elsewhere [3].

The rigid-sphere approximation is a useful device in two important ways. First, it is reasonable to treat the occupant as a rigid body in some cases, for example, impacts that involve the occupant's head. In such cases, the skull and its thin covering of skin are much less flexible than, say, the padding which covers the dashboard. Second, solid metal projectiles with spherical surfaces can be used in validation experiments to check the analysis method. Section 3 summarizes the procedures and results of a series of such validation experiments. Section 4 compares the test results with predictions made by the impact analysis method.

2. PREDICTION OF IMPACT RESPONSE

A basic impact analysis model has been developed, in which the occupant is replaced by a rigid spherical mass and the padding is assumed to be supported by an elastic structure. The properties of the sphere can be estimated to obtain rough equivalence to the effective mass and local surface curvature of body components. The force-deflection characteristics of the support structure can be linear or nonlinear, but do not include energy loss through hysteresis. Thus, the model is limited to cases in which the supporting structure should be expected to survive without significant permanent deformation.

Section 2.1 summarizes the system equations for the model. These include the equation of motion of the mass and the constitutive equation of the padding. The effects of nonuniform contact are introduced via the strain and strain-rate fields associated with the contact geometry. An integral of the nonuniform stress field provides the pad reaction force and, thereby, couples the constitutive equation to the equation of motion.

The system equations are too complicated to be solved by analytical methods, especially when either of the two empirical constitutive equations for Ensolite foam rubber is used. Section 2.2 deals with reduction of the system equations to numerical solution procedures. These procedures are based on finite-difference approximation of time derivatives and trapezoid approximation of the stress integral. Also, as is usual in numerical solution of nonlinear differential equations, it is found that an "equilibrium-check" term must be introduced to deal with the stress-strain nonlinearity and special provision must be made to avoid "hard-boundary" instabilities. Section 2.3 summarizes the results of an example analysis.

2.1 MODEL CONFIGURATION AND SYSTEM EQUATIONS

Figure 2-1 illustrates the configuration of the model at the instant of initial contact (t=o). A rigid sphere of mass M and radius R, travelling to the right at velocity V, just touches the flat surface of the pad at the joint P on the line of approach. Only the local effects of the sphere-to-pad contact are to be analyzed, i.e. lateral boundary effects on the pad are neglected. The padding is assumed to be a macroscopically homogeneous material of thickness L and with a given constitutive equation $\dot{\sigma} = f(\varepsilon, \dot{\varepsilon}, \sigma)$ for uniform compression, where σ and ε are engineering stress and strain, respectively, and where a dot over a quantity represents its time derivative. The pad is supported by an elastic structure with stiffness K_S, which may, in general, be nonlinear.

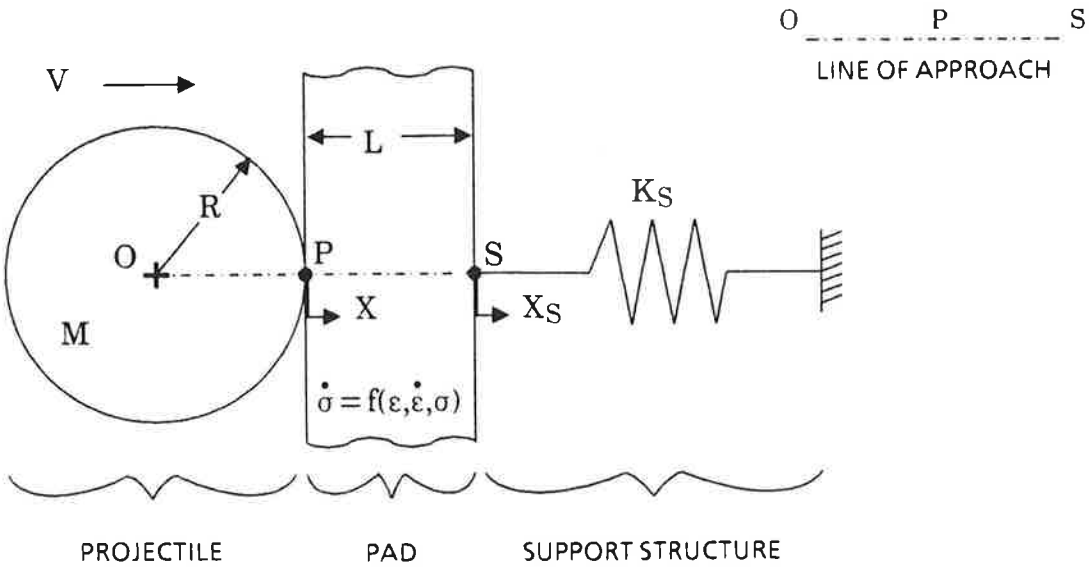

FIGURE 2-1. MODEL CONFIGURATION

The motion X of the point P corresponds to the motion of the sphere's center of mass. This motion is divided into the support structure deformation X_S and the pad compression on the line of approach, $X_P = X - X_S$. The convention $X = 0$ at $t = 0$ is adopted.

As the impact proceeds the deformations establish reaction forces F in the system, as shown in the free-body diagrams in Figure 2-2. The customary sign convention is used, i.e., the force F is negative when the pad and structure are under compression. Corresponding to this convention, compressive strain in the pad is also negative, and the constitutive equation must be expressed in terms of stress and strain magnitudes.

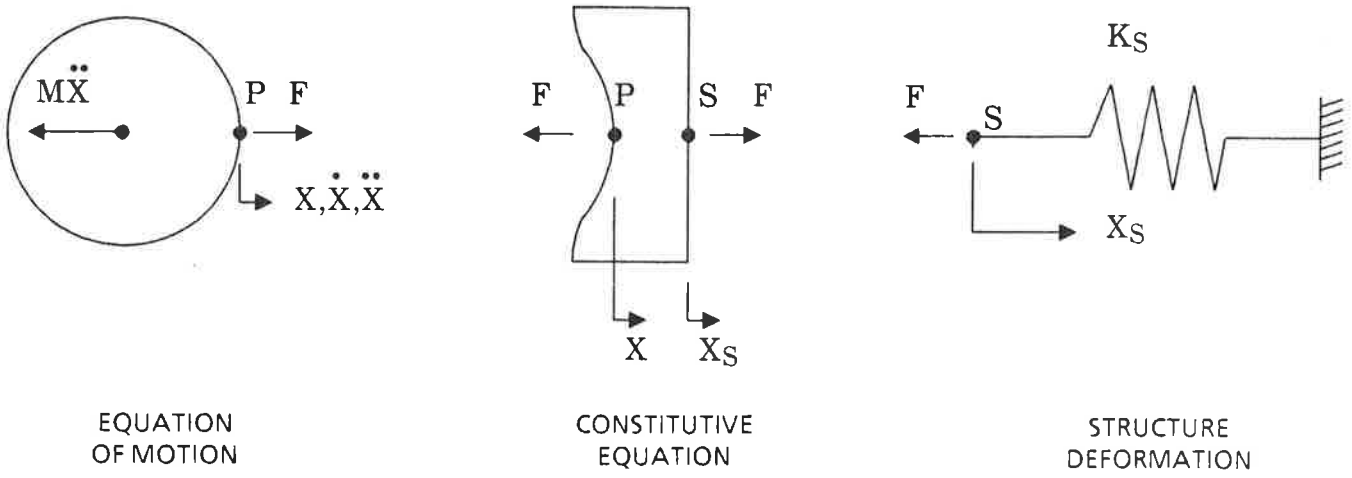

FIGURE 2-2. SUBSYSTEM FREE-BODY DIAGRAMS

The equation of motion and the structure's stiffness characteristics are used to update the motion variables, while the force F is calculated from the pad's constitutive equation. Before F can be calculated, however, some assumptions must be made about the characteristics of the local deformation in the pad.

The assumption adopted here is similar to the one used by Lockett et al. [4] in an earlier experimental investigation of crash padding materials. The sphere is assumed to impose its shape on the pad surface, as shown in Figure 2-3. The local deformation of the pad surface is given by the axially symmetric function:

$$W(r) = X_p - R\left[1 - \sqrt{1-(r/R)^2}\right]; \quad 0 \leq r \leq r_{max} \tag{5}$$

where the radial coordinate, r, is measured from the line of approach, and where r_{max} is the contact radius.

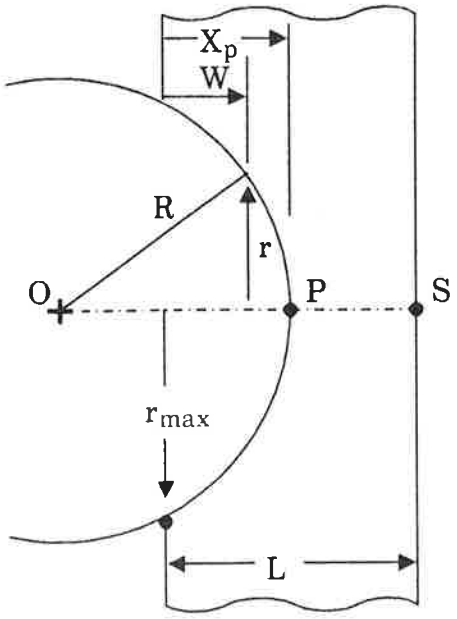

FIGURE 2-3. ASSUMED CONTACT GEOMETRY

The earlier investigators [4] linearized Eqs. 5 and 6 to facilitate analytical solution of their system equations. The exact forms are retained in the present model to allow for cases of deep penetration ($X_P \to 0$ [R]).

Both the earlier and the present model neglect the three-dimensional effects of lateral constraint and load transfer by shear. In effect, the pad is treated as if it were composed of a group of concentric thin-walled circular cylinders, with each cylinder responding independently to its local values of compressive strain and strain rate.

With these preliminaries, the system equations for a rigid sphere colliding with a viscoelastically padded deformable support structure can be written as follows:

$$X_p = X + F/K_s\,(X - X_p) \tag{6}$$

$$r_{max} = \sqrt{2RX_p - (X_p)^2} \quad ; \quad 0 \leq X_p \leq R \tag{7}$$

$$\varepsilon(r) = -W(r)/L = (R/L)\left[1 - \sqrt{1-(r/R)^2}\right] - X_p/L \quad ; \quad 0 \leq r \leq r_{max} \tag{8}$$

$$\dot{\varepsilon} = -\dot{W}/L = -\dot{X}_p/L \tag{9}$$

$$\dot{\sigma}(r) = f\left[\varepsilon(r),\ \dot{\varepsilon},\ \sigma(r)\right] \quad ; \quad 0 \leq r \leq r_{max} \tag{10}$$

$$F = 2\pi \int_0^{r_{max}} \sigma(r)\,r\,dr \quad \text{(subject to } \sigma(r) \leq 0) \tag{11}$$

$$\ddot{X} = F/M \tag{12}$$

with the initial conditions $X = F = 0$ and $\dot{X} = V$ at $t = 0$. There is also a terminal condition $F(T) = 0$ for $t = T > 0$, which defines the end of the impact event as the time when the sphere loses contact with the pad.

Five significant properties of the system equations should be noted. First, the term $K_S(X-X_P)$ in Eq. 6 represents a possibly nonlinear support structure, i.e., K_S is a function of the support deformation $X_S = X - X_P$. In the sequel, this functional relation will be implicitly assumed.

Second, the positive sign of the F/K_S term in Eq. 6 corresponds to the conventions shown in Figure 2-2. The force F and contact stress field σ are negative in compression, while the motion coordinates X and X_P are positive.

Third, the pad penetration X_p is restricted to positive values not exceeding the radius of the sphere. Negative values correspond to loss of contact. Positive values larger than the sphere's radius would require a reformulation of the strain-field description in Eq. 8. This is possible in principle, but is not of practical interest.

Fourth, the constitutive equation, Eq. 10, may be strongly nonlinear. This is the case, for example, when the empirical constitutive equations for Ensolite foam rubber are used. In such cases, the sign conventions for stress and strain must be preserved in the other system equations while working with magnitude in the constitutive equation.

Fifth, a no-tension constraint on $\sigma(r)$ is implicit in the stress integral, Eq. 11. This constraint is needed because the constitutive equation can produce spurious tensile stresses during the rebound phase, when the sphere begins to lose contact at the outer region of the pad's contact zone. The no-tension constraint introduces another strong nonlinearity in the system equations.

2.2 NUMERICAL ANALYSIS PROCEDURE

Together with the initial and terminal conditions, Eqs. 6 through 12 comprise a complete mathematical formulation of the free-impact problem of a rigid sphere contacting an initially flat pad. The system equations are in an implicit form, however, and hence must be solved by means of incremental numerical analysis procedures. Two types of approximation must be introduced for this purpose.

First, the time derivatives of the system variables must be represented by finite-difference approximations[5]. The sphere's evaluation is represented by a second central difference operator:

$$A_k = \ddot{X}_k \tilde{=} (X_{k+1} - 2X_k - X_{k-1}) / (\Delta t)^2 \tag{13}$$

where subscript k refers to the time $t = k\Delta t$ and $X_k \tilde{=} X(k\Delta t)$. This operator is actually used to update the motion coordinate after the reaction force has been calculated:

$$X_{k+1} \tilde{=} 2X_k - X_{k-1} + (F_k/M)(\Delta t)^2 \tag{14}$$

The first forward difference operator is used to represent first derivatives. For example, the sphere's velocity is updated after Eq. 14 has been used:

$$V_k = \dot{X}_k \tilde{=} (X_{k+1} - X_k)/\Delta t \tag{15}$$

Strain rates are computed in a similar manner, and the first forward difference operator is also combined with the constitutive equation to update the stress field:

$$\sigma_{k+1} \tilde{=} \sigma_k + f(\varepsilon_k, \dot{\varepsilon}_k, \sigma_k)\Delta t \tag{16}$$

Second, the trapezoid rule is used to approximate the contact stress integral:

$$2\pi \int_0^{r_{max}} \sigma(r) r dr \tilde{=} \sum_{n=1}^{max} \left[\pi (r_n^2 - r_{n-1}^2)\right]\left[\sigma_n + \sigma_{n-1})/2\right] \tag{17}$$

where $r_\sigma \tilde{=} 0$. Each term in the sum on the right hand side of Eq. 17 is the product of the area of the cylindrical annulus between (r_{n-1}, r_n) and the average stress acting on the annulus.

The numerical analysis procedure must also account for the coupling of variables in the system equations. Specifically, the implicit relation between pad penetration X_p and reaction force F in Eqs. 6 through 11 cannot be made explicit. If the solution is at step k, for example, the penetration $X_{p,k}$ can only be guessed. The force F_k can then be calculated for the trial penetration, but in general, the guess will have to be modified to satisfy Eq. 6. Thus, iteration is required within each step, and this, in turn, requires additional strategies to prevent poor guesses from violating the physical constraints embodied in the system equations.

The impact analysis algorithm has been encoded as Fortran subroutine SPIT (Sphere/Pad Impact Tracker) in accordance with the flow chart shown in Figure 2-4. A user's guide with detailed flow charts appears in Appendix A. The program listing and an example analysis are contained in Appendices B and C, respectively. The remainder of the discussion in this section explains the strategies that are used in the program.

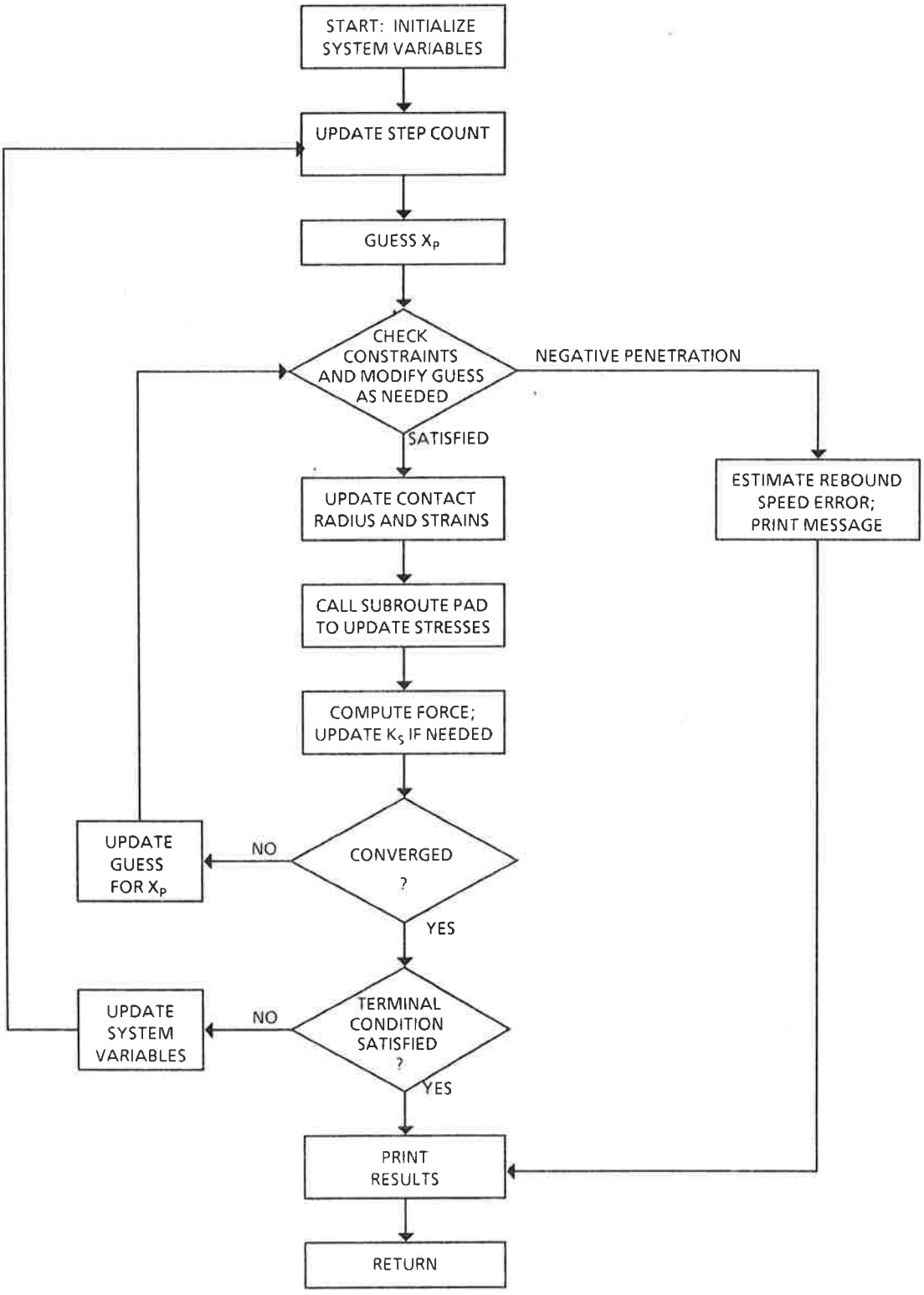

FIGURE 2-4. OVERVIEW OF SUBROUTINE SPIT ALGORITHM

The finite-difference calculations require information from two prior time steps. Vectors of the system variables are started at $t = -\Delta t$, therefore, and are fully initialized at the first two time steps $t = -\Delta t, 0$. The sphere motion must also be estimated for the first step after contact, $X(\Delta t) \cong V\,\Delta t$, where V is the initial velocity. Thus, in the vectors of the system variables, $k = 2$ actually corresponds to the beginning of contact at $t = 0$.

As will be seen in the sequel, three concurrent estimates for the pad penetration are required by the iteration algorithm. The first two are taken as the prior-step penetrations $X_{p,k-2} = Y_1$ and $X_{p,k-2} = Y_2$. The third estimate is the initial guess:

$$Y_3 = Y_2 \pm \Delta Y \tag{18}$$

where

$$\Delta Y = |Y_1 - Y_2| \tag{19}$$

The forces F_{k-1} and F_{k-2} are available, but the force corresponding to the candidate penetration Y_3 is as yet unknown.

The constraints on penetration must now be checked. It is possible that Y_3 may exceed the sphere's radius or the pad thickness simply because the estimate is not accurate. These conditions are treated as "hard-boundary" constraints by reducing the estimate to an appropriate value. A third possibility, $Y_3 < 0$, can occur when the sphere approaches loss of contact in the rebound phase. In this case, as will be seen in the sequel, the computation must be terminated to avoid a numerical instability.

When an estimate Y_3 satisfying the constaints has been obtained, the contact radius, strains, stresses, and force can be calculated. The stress calculations are performed by a second subroutine (PAD), which contains the following options for the constitutive equation:

1. Linear elastic material.
2. Linear viscoelastic model.
3. Rigid foam model (constant crush stress up to a specified strain limit, followed by two-stage piece-wise linear stress increase).
4. Empirical 9-parameter viscoelastic model.
5. Empirical 21-parameter viscoelastic model.

The support structure can be specified as either linear or piece-wise linear. In the second case, the spring rate K_S is treated as a secant stiffness which is updated after the force has been calculated.

Equilibrium and precision convergence tests must now be made to determine whether the estimated penetration Y_3 is sufficiently accurate. The purpose of the equilibrium check is to enforce Eq. 6, which is rewritten for the present case as:

$$f(Y) = F(Y) - K_s Y + K_s X_k \tag{20}$$

where F(Y) is the computed force corresponding to a penetration estimate Y. Evidently, $f(Y)=0$ if, and only if, Y is the exact solution $X_{p,k}$; otherwise f(Y) is the force error. The equilibrium-check criterion is:

$$|f(Y)/F(Y)| \leq \beta \tag{21}$$

where the specified tolerance β is a small number, usually between 0.005 and 0.02.

Even though the equilibrium-check criterion allows some imprecision in $X_{p,k}$, the algorithm may still "dither" trying to find the solution in cases for which the pad has a large tangent stiffness $K_{tan}=dF/dY >> K_s$. The source of the problem is the finite precision of floating-point arithmetic, i.e., adjacent estimate must be separated by at least $dY=PY$, where P is the precision of the computer.

Figure 2-5 illustrates a situation where the pad's tangent stiffness is large enough so that the finite arithmetic precision makes it impossible to satisfy Eq. 21. This occurs when:

$$K_{tan} \geq \frac{2\beta}{p(1-\beta)} K_{sec} = \frac{2\beta}{p} K_{sec} \tag{22}$$

where $K_{sec}=F(Y)/Y$ is the pad's secant stiffness. Typically, $\beta/P \sim 10^4$ and the dithering effect appears when the pad is severely compressed.

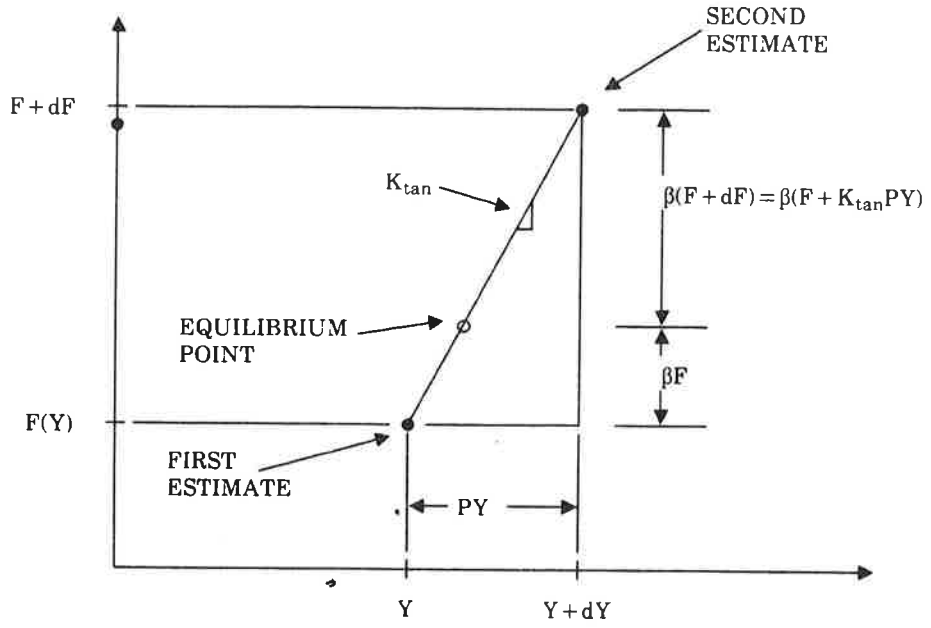

FIGURE 2-5. DITHERING EFFECT FOR A STIFF SYSTEM

The dithering effect is avoided by a precision convergence test. If the two most recent penetration estimates Y_2 and Y_3, satisfy the criterion:

$$|(Y_2-Y_3)/(Y_2+Y_3)| \leq \gamma \tag{23}$$

then Y_3 is accepted as the best estimate for $X_{p,k}$ under the circumstances. Typically, the tolerance γ is set at 10^{-5} for single-precision computing.

Estimates which satisfy neither the equilibrium check nor the convergence test must be improved by iteration before the next time step is taken. Otherwise, the force errors will cause the computed solution to drift away from the exact solution. Because of the nonlinearities in the equilibrium-check function, f(Y), it is essential to use an inherently stable iteration strategy.

An iteration strategy is the set of rules by which a new estimate for the penetration is obtained from the existing estimates. For example, Aitken extrapolation [5] is a very simple strategy that requires only two existing estimates, say Y_1 and Y_2. The new estimate Y_3 is then obtained by linear extrapolation to f(Y)=0:

$$Y_3 = [Y_2 f(Y_1) - Y_1 f(Y_2)]/[f(Y_1)-f(Y_2)] \tag{24}$$

and the iteration is continued by replacing (Y_1,Y_2) with (Y_2,Y_3). Figure 2-6A illustrates a typical iteration step.

In Figure 2-6B, the graphical construction is continued to illustrate the spiral instability which can occur when Aitken extrapolation is applied to inflected curves. The case shown in the figure has been constructed so that the sequence of estimates 1-2-3-4 will repeat indefinitely. A slightly smaller initial estimate for Y_1, however, will cause the iteration path to spiral, as shown by the dashed line, and the succeeding estimates for Y_3 will diverge. The equilibrium-check function is inflected by stress-strain nonlinearity in the pad's constitutive equation (e.g., the empirical models) and is, therefore, subject to spiral instability.

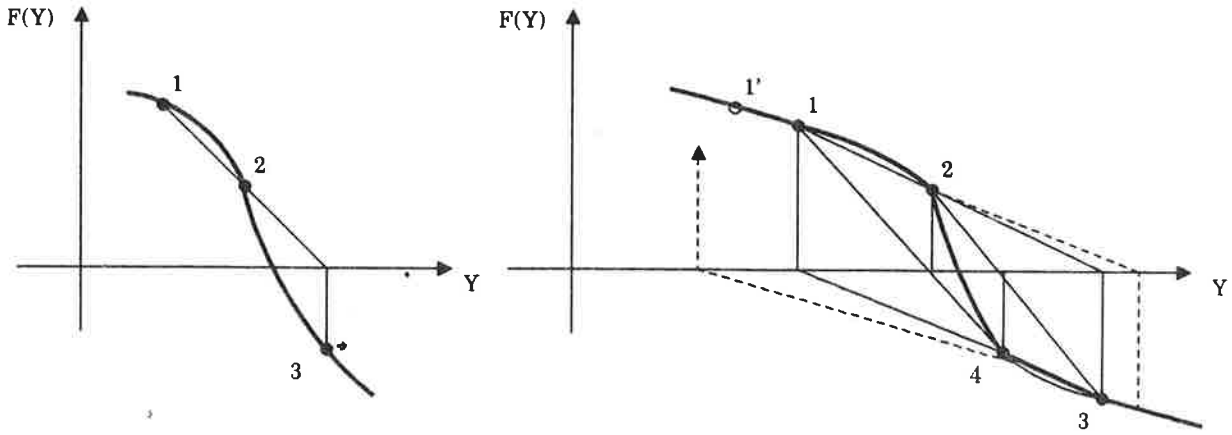

(A) Typical Aitken iteration step (B) Neutrally stable and divergent sequences

FIGURE 2-6. SPIRAL INSTABILITY ASSOCIATED WITH INFLECTED CURVE

Conversely, the bisection method provides a basis for an inherently stable strategy. Suppose, for example, that estimates (Y_1Y_2) have been obtained such that $f(Y_1)$, and $f(Y_2)$ have opposite signs. Then the root of $f(Y)=0$ must lie between these points, and the iteration sequence is:

$$Y_3 = (Y_1+Y_2)/2 \; ; \quad (Y_1,Y_2) \leftarrow (Y_2,Y_3) \tag{25}$$

Succeeding pairs (Y_1,Y_2) will not continue to bracket the root if $f(Y)$ is inflected, however, but bracketing can be assured by working with triplets in the following sequence:

If $f(Y_2)f(Y_3)<0$, then:

$$Y_4 = (Y_2+Y_3)/2 \quad ; \quad (Y_1,Y_2,Y_3) \leftarrow (Y_2,Y_3,Y_4) \tag{26}$$

Otherwise $f(Y_1)f(Y_3)< 0$, then:

$$Y_4 = (Y_1+Y_3)/2 \quad ; \quad (Y_1,Y_2,Y_3) \leftarrow (Y_1,Y_3,Y_4)$$

The triplet bisection method is used in the impact analysis software. However, there still remains the problem of obtaining an initial triplet in which the sign of $f(Y_3)$ is opposite to the sign of either $f(Y_1)$ or $f(Y_2)$. A straight marching sheme is used for this purpose. The initial estimate for Y_3 is either incremented or decremented by $\Delta Y = |Y_1 - Y_2|$ until the first occurrence of $f(Y_2)f(Y_3) < 0$. Thereafter the iteration is switched to triplet bisection.

When a converged estimate $X_{p,k} \cong Y_3$ and the corresponding reaction force F_k have been obtained, an approximate terminal condition is tested to determine whether the impact event has been completed or another time step is needed. The terminal condition is a negative sphere velocity (rebounding) and a force magnitude $|F_k|$ less than the sphere's weight. The residual acceleration of up to 1"g" associated with this criterion is not significant.

Finding the terminal point poses two special problems. First, this point is likely to occur within rather than at the end of a time step. Figure 2-7 illustrates the effect on the equilibrium-check function. The result is that f(Y) has the same sign for all penetration estimates exceeding some negative value, and the iteration algorithm will march to that value. If a negative penetration is found, the solution must be restarted from $(k-1)\Delta t$ with the time-step size cut in half. A few such time-step bisections should be sufficient to reach the 1"g" terminal criterion if conventional material behavior models are used.

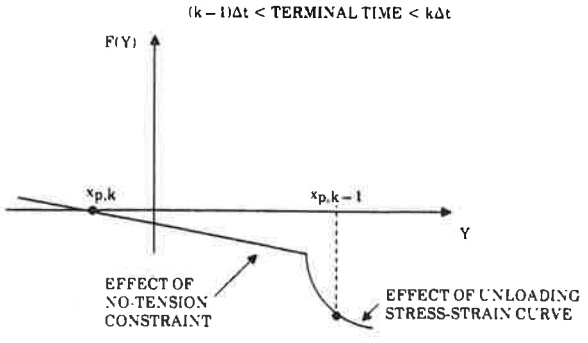

FIGURE 2-7. WITHIN-STEP TERMINATION EFFECT ON EQUILIBRIUM CHECK

The second problem arises if the pad's stress-strain curve is strongly sensitive to strain rate, e.g., when using the multi-parameter empirical constitutive equations. The current computed strain rate magnitude is proportional to $(Y-X_{p,k-1})$ and thus increases as the estimate Y marches toward the origin. In turn, this increases the magnitude of the unloading stress-strain curve and leads to the result shown in Figure 2-8. In such cases, the computing procedure is subject to a rate-sensitive instability artifact, and the calculation must be terminated if several bisections within the same time step have not produced convergence.

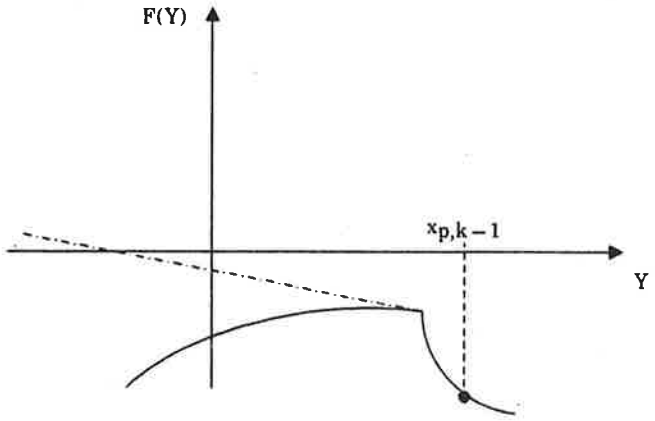

FIGURE 2-8. RATE-SENSITIVITY EFFECT ON EQUILIBRIUM CHECK

The impact analysis software allows up to seven bisection trials within a time step (Δt cut to 1/128 of its original value). A rate-sensitive termination is executed on the eighth trial. The last converged computation V_{k-1} is taken as the approximate rebound velocity, and a velocity error is estimated from:

$$\Delta V/V_{k-1} \cong A_{k-1}(X_{k-1}-L\varepsilon_o)/2V_{k-1}^2 \qquad (27)$$

where A, V, X are respectively the acceleration, velocity, and position of the sphere, L is the pad thickness, and ε_o is the pad residual strain at the center of contact, as projected from the last converged strain-rate value based on the strains at $(k-1)\Delta t$ and $(k-2)\Delta t$. Equation 27 is derived by assuming that the acceleration decreases linearly with respect to time during the final incomplete time step.

2.3 EXAMPLE ANALYSES

The constitutive equations for the multi-parameter empirical models are of the form:

$$\dot{\sigma} = S(\varepsilon,\dot{\varepsilon}) - \sigma h(t) \qquad (\dot{\varepsilon}\geq 0)$$
$$\dot{\sigma} = S(\varepsilon,\dot{\varepsilon},\varepsilon^*) - \sigma h(t) \qquad (\dot{\varepsilon}<0) \tag{28}$$

where ε^* is the maximum strain reached during the loading phase ($\dot{\varepsilon}\geq 0$), and where $S(\varepsilon,\dot{\varepsilon})$ and $S(\varepsilon,\dot{\varepsilon},\varepsilon^*)$ are complicated functions (see Sections 3.2 and 3.3 of Volume II). Therefore, some preliminary analyses were run with prescribed strain-time histories to verify the programming of these constitutive equations.

The first analysis simulated an idealized stress-strain test at constant strain rate. For a given strain rate $\dot{\varepsilon}$ and maximum strain ε^*, the strain-time history:

$$\varepsilon(t) = -\dot{\varepsilon}t \qquad (0\leq t\leq \varepsilon^*/\dot{\varepsilon})$$
$$\varepsilon(t) = -2\varepsilon^* + \dot{\varepsilon}t \qquad (\varepsilon^*/\dot{\varepsilon} \leq t \leq 2\varepsilon^*/\dot{\varepsilon}) \tag{29}$$

was applied in twenty steps for each phase. This analysis revealed a stress-discontinuity artifact arising from the instantaneous reversal of strain rate at the peak strain. The constitutive equations enforce stress continuity from loading to unloading only in the exact sense of a strain rate that passes smoothly through zero. The effect of the finite strain rate at the peak was found to be that the first calculation of stress during unloading exceeded the last calculation of stress during loading.

The idealized stress-strain test is not a realistic representation of the strain-time history during an impact. However, even the expected smoothly varying strain in an impact must be treated numerically in terms of finite steps, and the stress-discontinuity artifact may still appear. Therefore, a second analysis was run to simulate the impact situation by means of the parabolic strain-time history:

$$\varepsilon(t) = \varepsilon^*[\,(t/t_o)^2 - 2(t/t_o)\,] \qquad (0\leq t\leq 2t_o) \tag{30}$$

where $t_o=\varepsilon^*/\dot{\varepsilon}$, and where the time was divided into steps of size $\Delta t=t_o/20$. For this strain-time history, the actual strain rates initially and near the peak strain are given by:

$$d\varepsilon/dt = -2\dot{\varepsilon} \qquad \text{at } t=0$$

$$d\varepsilon/dt \cong \pm\, 2\dot{\varepsilon}^{2}\, \Delta t/\varepsilon^{*} \qquad \text{at } t=t_{o} \pm \Delta t \tag{31}$$

Figures 2-9 and 2-10 show the results of the parabolic strain tests for a maximum strain of 0.95 and for two orders of magnitude in strain rate. The data for $\dot{\varepsilon}=100$ per second correspond to strain rates of the order expected for impacts and to a time step size of the order that should be used in an impact analysis. Neither model shows evidence of the stress-discontinuity artifact for this case. The artifact does appear for the case of $\dot{\varepsilon}=1$ per second in the 9-parameter model, but the effect of the artifact is small. Both models show an increase of hysteresis as the strain rate increases, but the effect is more pronounced in the 9-parameter model than in the 21-parameter model. Also, the 9-parameter model has a higher stress response to loading and a higher peak stress than the 21-parameter model.

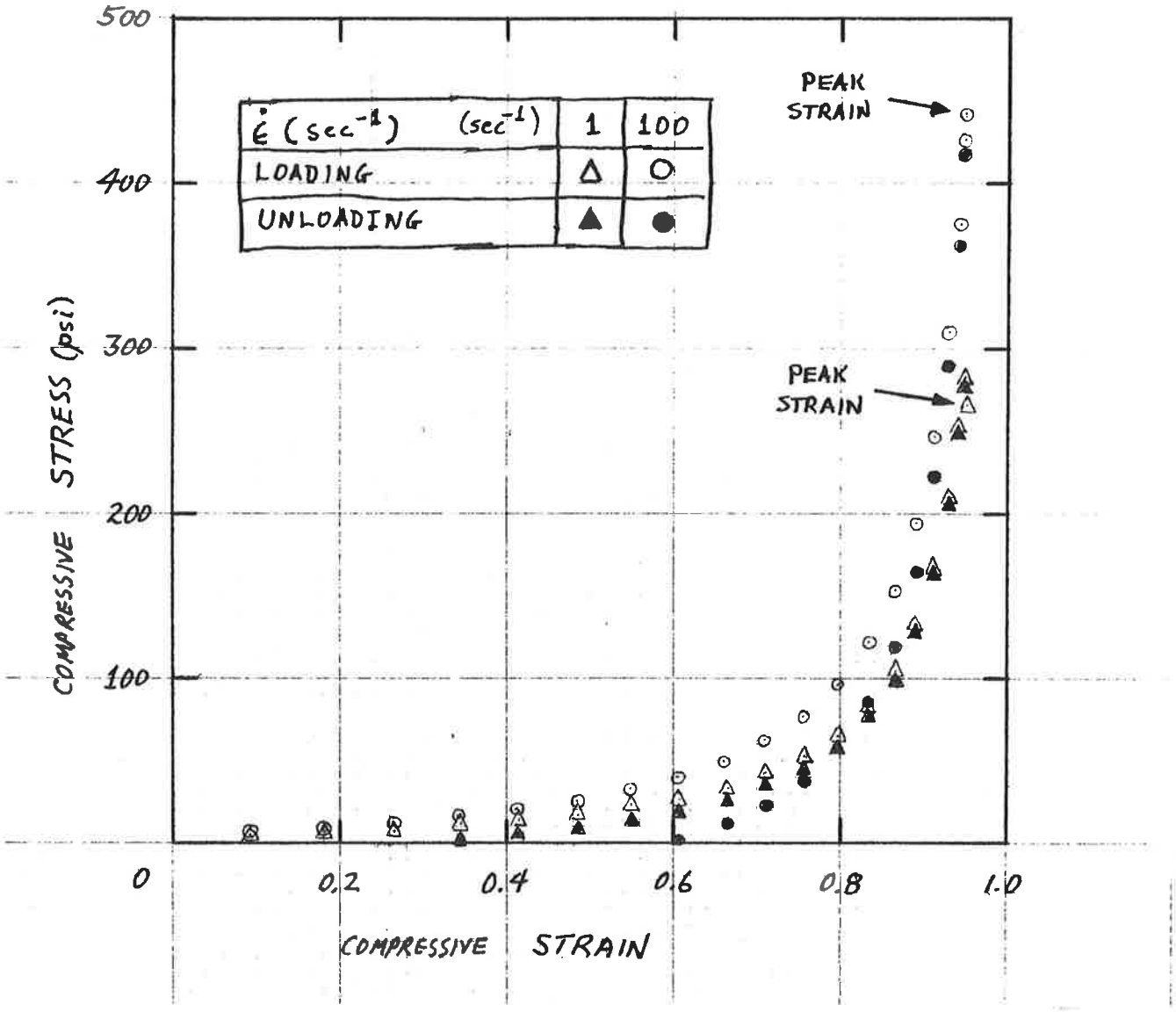

FIGURE 2-9. PARABOLIC STRAIN TEST OF 9-PARAMETER MODEL

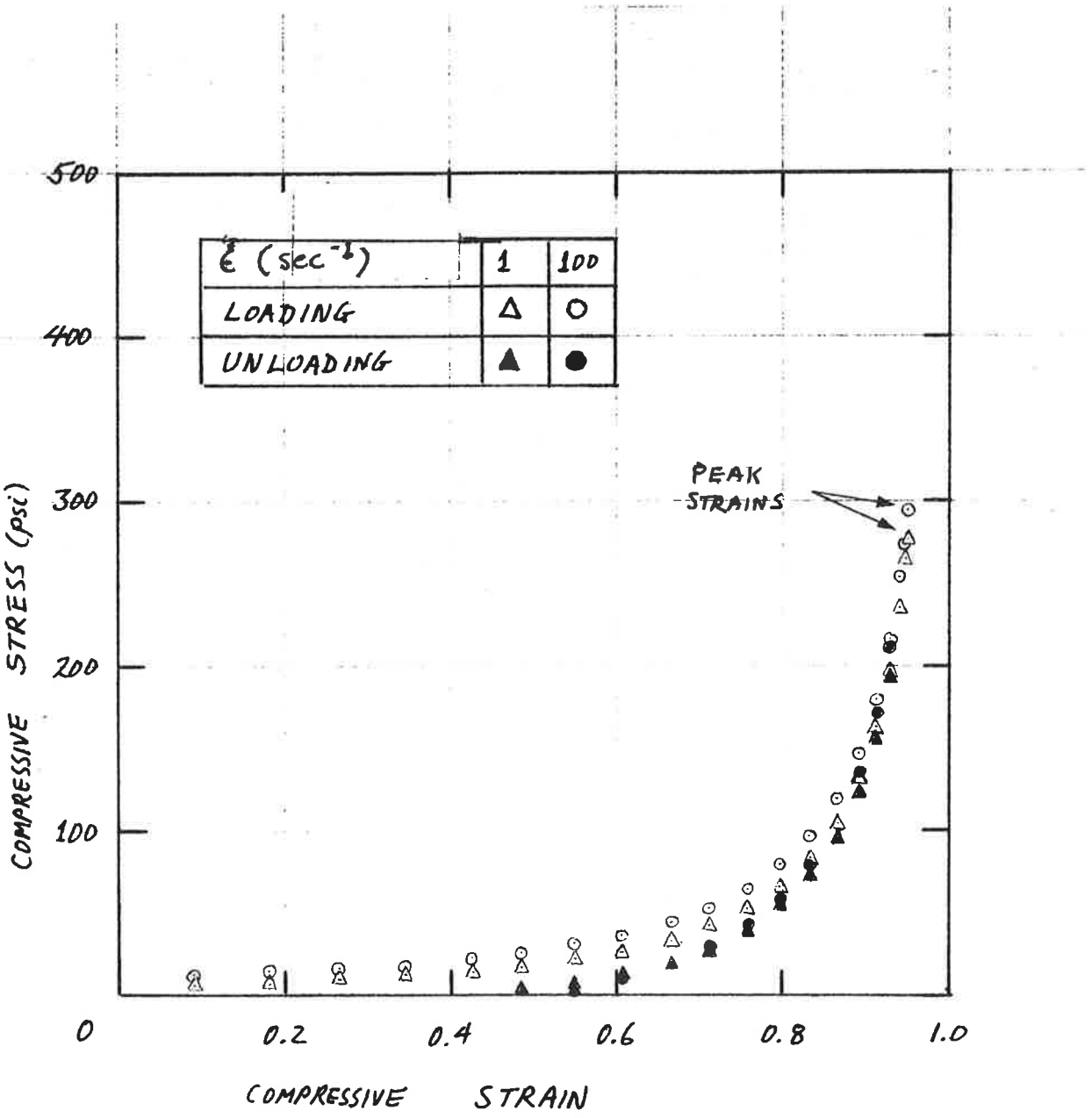

FIGURE 2-10. PARABOLIC STRAIN TEST OF 21-PARAMETER MODEL

Following the parabolic strain test, an example impact analysis was run to test the complete software and to compare the results produced by the 9-parameter and 21-parameter models for Ensolite foam rubber. The input values for the test case were: 3-inch sphere radius; 10-lb. sphere weight; initial speed of 20 mph; 1-inch thick pad; and linearly elastic support structure with a 600 lb/in spring rate. Nominal runs with both models were obtained with a time step size of 0.1 millisecond (ms) and a tolerance factor of 0.02 for the equilibrium-check error. Numerical results of these runs are given in Appendix C and are plotted in Figures 2-11 through 2-14.

Figure 2-11 shows the force-time histories. The 21-parameter model has a peak force about 4 percent higher than that obtained with the 9-parameter model; the time to peak force is 12.9 ms in both cases. A small amount of oscillation is evident in the first few post-peak milliseconds of both models.

Figure 2-12 shows the time histories of the sphere position and pad penetration. Again, the peak values for the 21-parameter model are a few percent higher than those for the 9-parameter model. The "bottoming" effect in the pad is evident in both cases. Also, the group of data points at the right show that the sphere position and pad penetration have become equal, as they should, at the time when contact between the sphere and pad is lost.

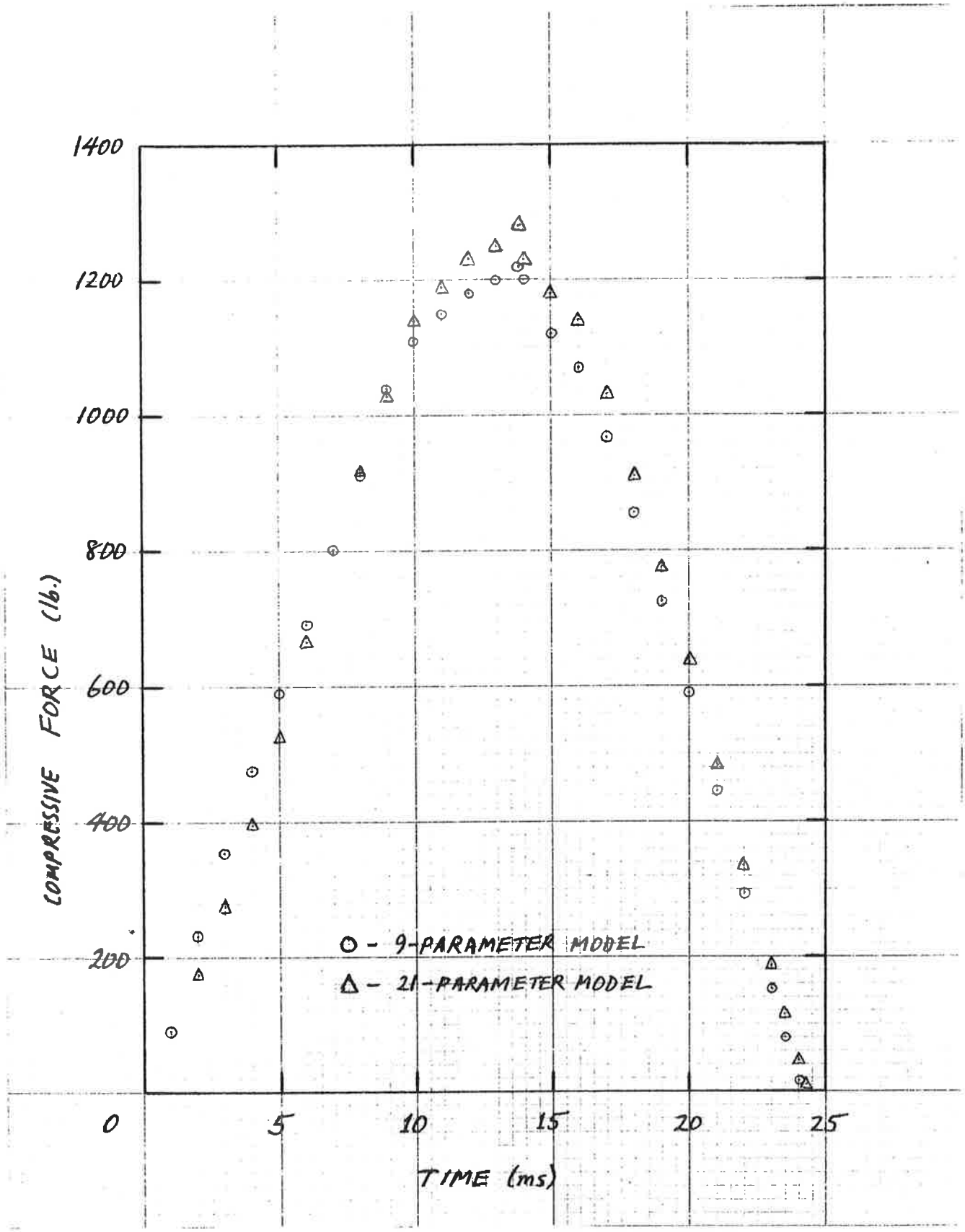

FIGURE 2-11. COMPUTED FORCE-TIME HISTORIES

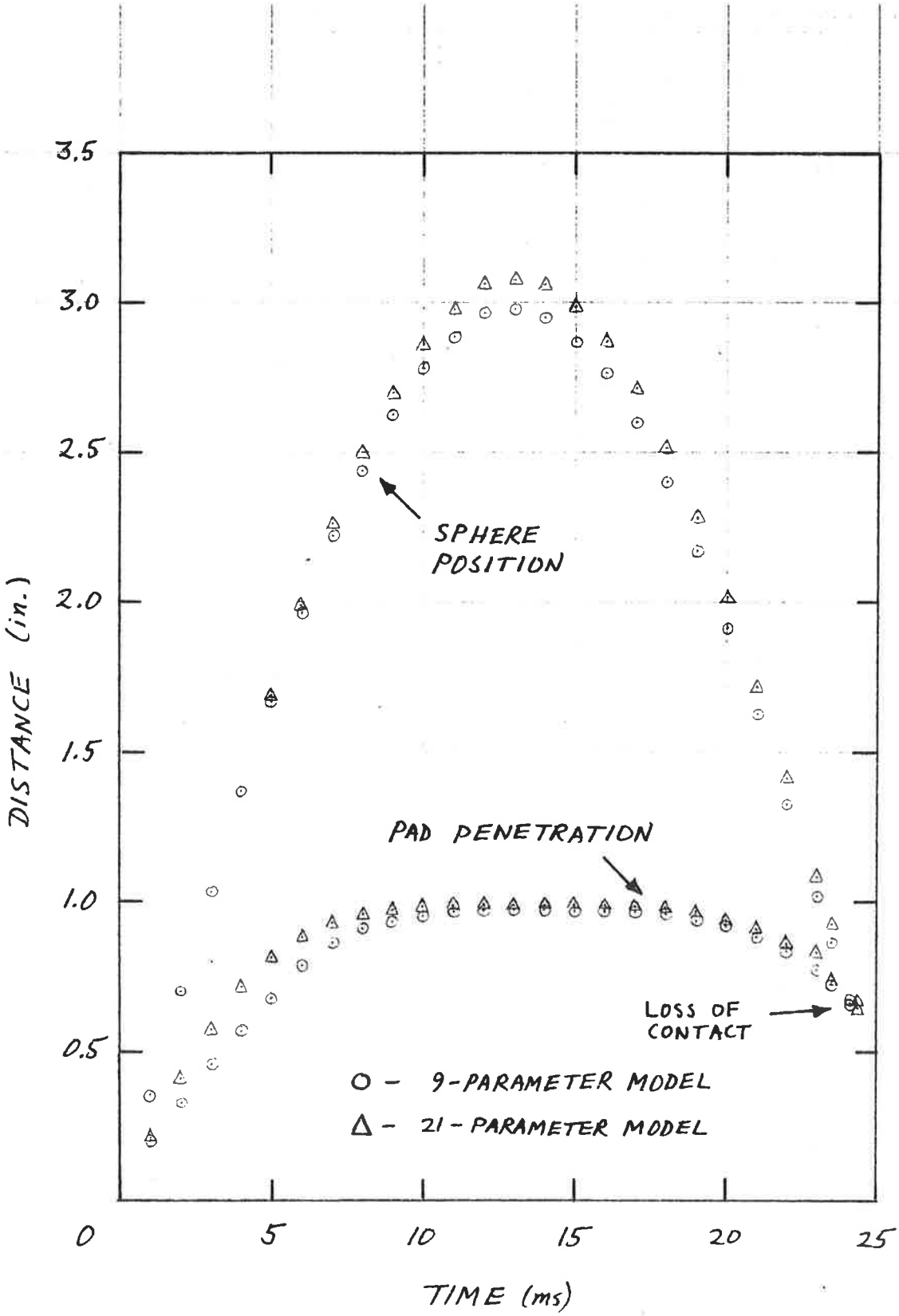

FIGURE 2-12. COMPUTED MOTION-TIME HISTORIES

Figure 2-13 plots the reaction force as a function of pad penetration to highlight the differences and similarities in the dynamic characteristics of the two models. The 21-parameter model has a less-stiff loading response, resulting in a larger peak force, than the 9-parameter model. However, the unloading responses are nearly identical.

Figure 2-13 cannot be interpreted as a true hysteresis plot because some of the impact strain energy is stored in the support structure. The true hysteresis effect can be seen, however, by plotting the reaction force versus the sphere position, as shown in Figure 2-14. Corresponding to the rather modest energy-absorption effects shown in this plot, the computed rebound speed magnitudes were found to be close to the initial speed. The values obtained were 17.9 mph for the 9-parameter model and 18.8 mph for the 21-parameter model. Also, note that a small stress-discontinuity artifact is evident in Figure 2-14 for the 9-parameter model.

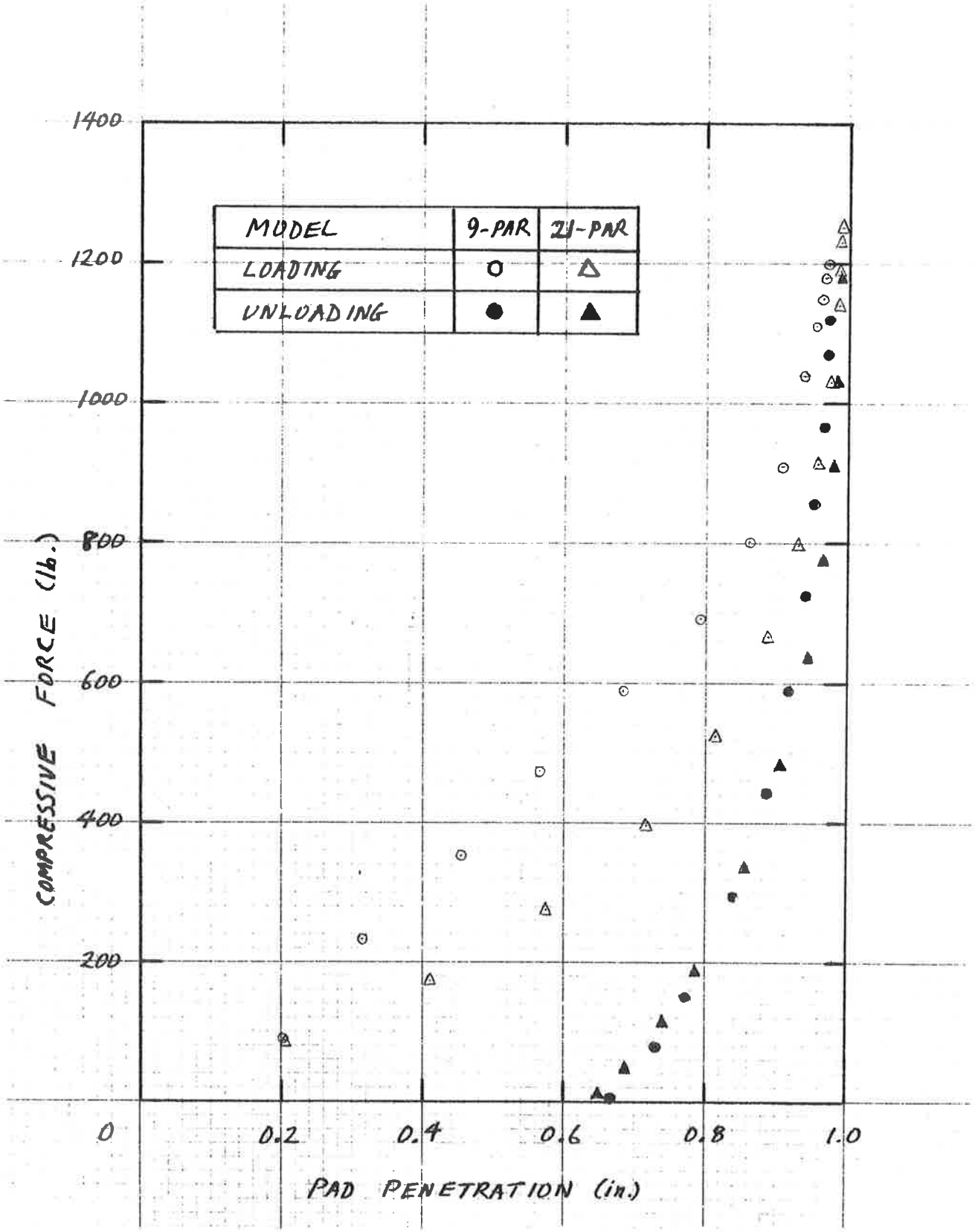

FIGURE 2-13. COMPUTED FORCE VERSUS PENETRATION

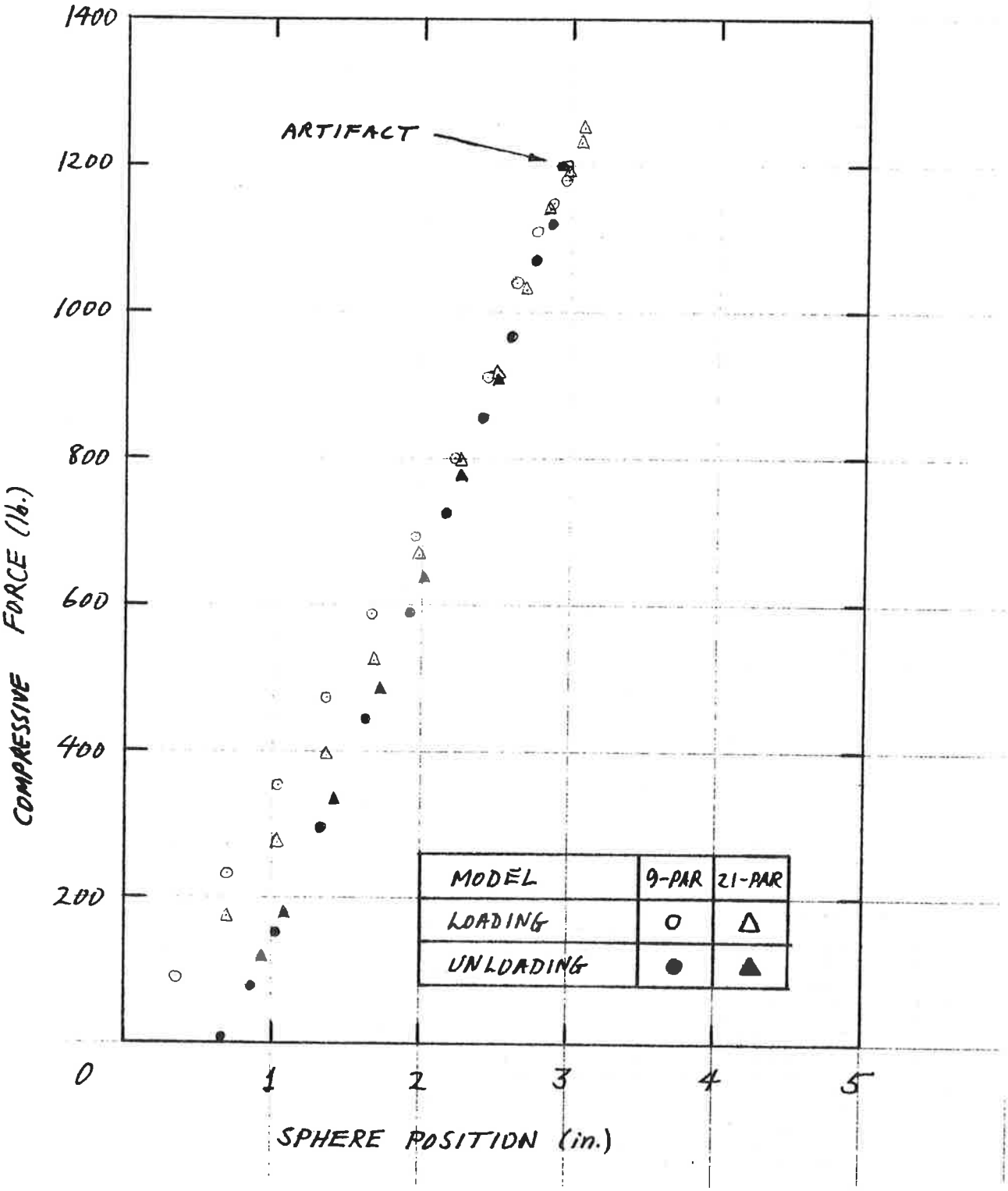

FIGURE 2-14. COMPUTED SYSTEM FORCE-DEFLECTION CURVES

3. VALIDATION EXPERIMENTS

A small apparatus for launching metal projectiles onto padding samples was built and instrumented for measurement of key physical parameters. These experiments tested the performance of Ensolite foam rubber under conditions of spherical contact geometry, typical impact speeds for collisions between an occupant and an automobile interior structure, and supporting structure approximately one order of magnitude stiffer than typical automobile dash boards.

3.1 TEST APPARATUS AND PROCEDURE

Figure 3-1 presents a schematic summary of the validation test apparatus. The main component is a vertical launcher consisting of an open truss framework (not shown) supporting the launching equipment and guide tubing. A bullet-shaped projectile held at the top of the apparatus by a friction-grip collar is launched by means of a hydraulic or mechanical hammer blow. The funnel and inner guide tube deliver the projectile in the proper attitude to the center of the target pad sample, after a vertical drop of 7.5 feet.

The designed vertical drop is equivalent to a nominal impact speed of 15 mph. The actual speed is reduced by guide-tube friction, but can be increased by launching with a heavy hammer blow. Two photocell circuits located near the pad sample are tripped in succession as the projectile approaches the pad, providing a measurement of the impact speed in terms of pulse time delay. The photocell circuits are reset by contact, and a second pulse time delay measures the rebound speed.

In the normal configuration, the pad sample is directly supported by a thick bearing plate, a piezocrystal load cell, and the laboratory floor. A time-of-contact sensor consisting of two thin wires taped to the pad surface is used to trigger the sweep on a digital recording oscilloscope on which the load-time trace from the piezocrystal cell is then displayed. Post-test measurements with the oscilloscope cursor are used to determine the peak load, time to peak load, and impact duration time. The time-of-contact sensor is also used to reset the photocell circuits for rebound speed measurement.

The bearing-plate/load-cell/floor combination is an extremely stiff system for peak loads exceeding 500 pounds. Hence, an alternate structure with more resilience is provided, but load-time measurements are not made when the alternate structure is in place. The alternate structure consists of a flexible aluminum plate supported by two rollers. For the dimensions shown, the alternate support has a calculated stiffness of

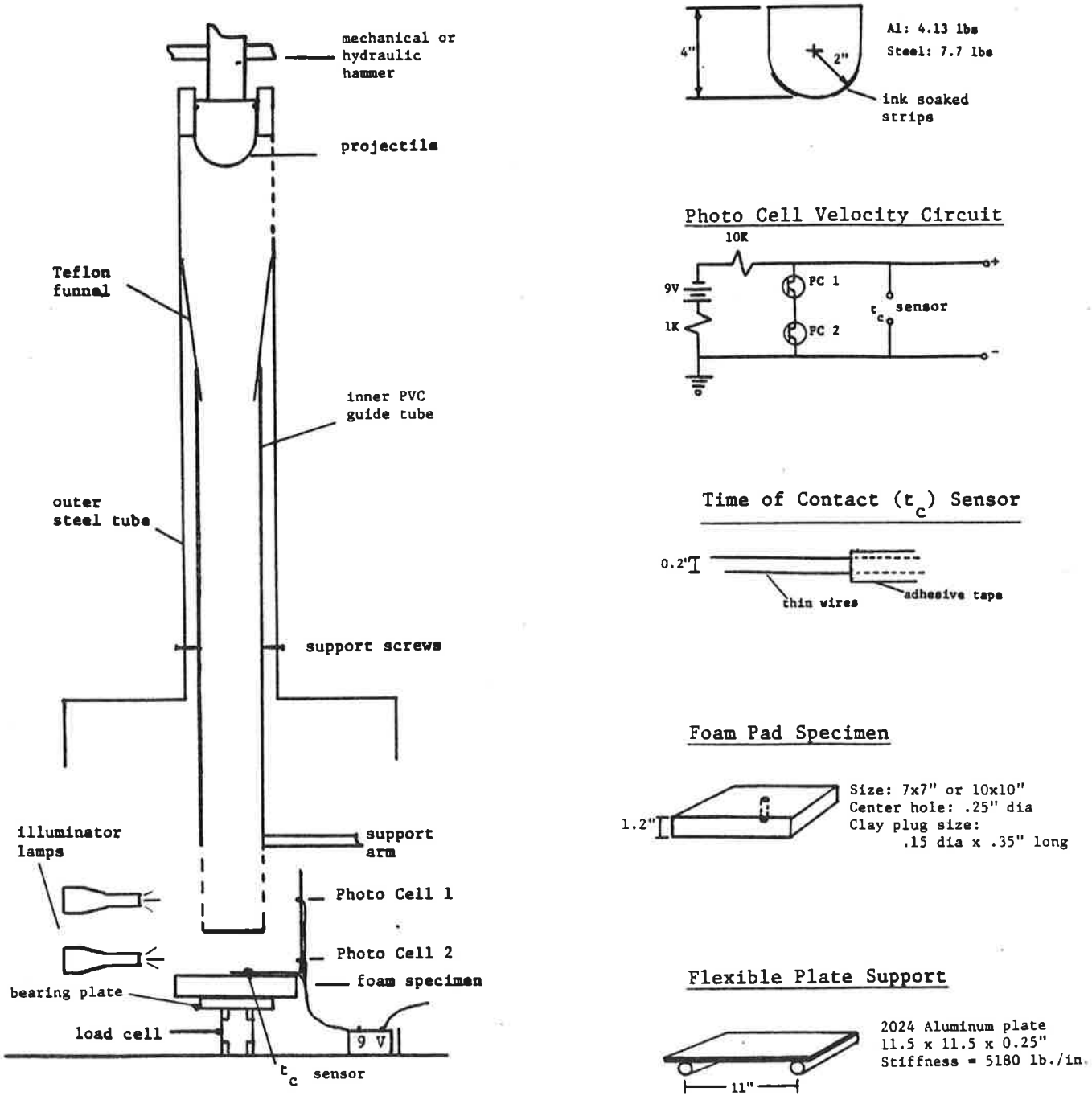

FIGURE 3-1. TEST APPARATUS SCHEMATIC

5,180 lb/in when subjected to a centrally applied concentrated load [6].

Two methods are used to measure peak strain in the pad at the center of contact. In the first method, a 1/4-inch diameter hole is drilled in the center of the pad and a 0.15-inch-diameter x 0.35-inch-long clay plug is inserted in the hole. For tests in which the strain at the center of contact in the 1.2-inch-thick pad exceeds 0.71, the clay plug will be contacted and flattened, providing a post-test record of the peak strain. In the second method, thin cloth strips are glued to the projectile and are soaked with ink just before the test. The ink marks left on the pad measure the maximum contact diameter, and the geometrical relation in Eq. 7 (see Section 2.1) can then be used to estimate the peak strain.

Figure 3-2 shows several photographs of the test apparatus. The apparatus was assembled and the validation tests were conducted at the MIT Department of Materials Science and Engineering.

3.2 SUMMARY OF TESTS AND RESULTS

The objective of the validation test program was to obtain data on the performance of Ensolite foam rubber for typical impact speeds ranging from 10 to 30 mph. The experimenters were able to perform tests at speeds ranging from 10 to 20 mph.

Thirty-three tests were performed altogether: 30 with the load cell in place, and 3 with the flexible plate support. Of the 30 load cell tests, 24 were performed with an aluminum projectile weighing 4.13 lbs, and 6 were performed with a 7.7 lb steel projectile. The aluminum projectile was used in the three tests with the flexible plate support.

Peak strain measurements were made by the clay-plug method in 12 tests and by both clay-plug and contact-diameter methods in 8 tests. Peak loads were measured in 28 of the 30 load cell tests, but were missed when the oscilloscope failed to trigger in the other 2 tests. Fewer than 28 corresponding duration measurements were recorded because it was found difficult to precisely locate the zero-load points on some of the load-time traces.

Table 3-1 summarizes the raw data from the validation tests. The table also includes the initial kinetic energy for each test, as calculated from the initial impact speed.

(A) Overview of launcher and digital oscilloscope.

(B) Mounting projectile in grip collar.

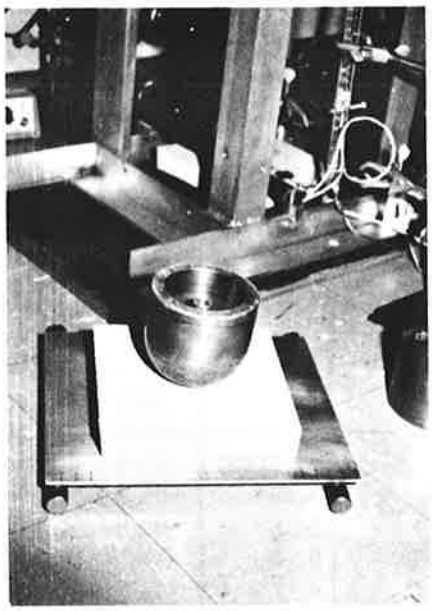

(C) Projectile and pad sample resting on flexible plate (foreground); bottom of launcher with photocell circuits and pad resting on load cell (background).

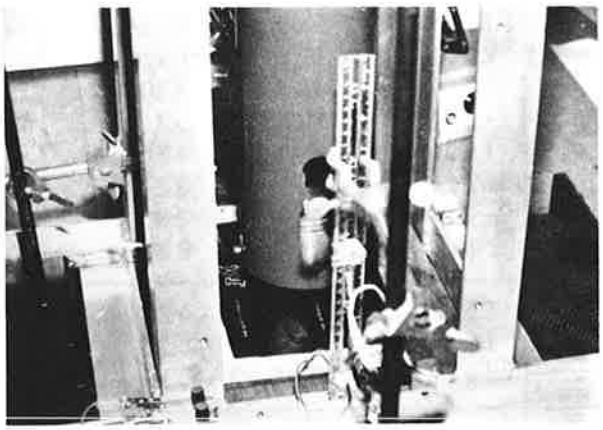

(D) Close-up view of launcher bottom with guide tube and photocell circuits in place for test. Note that the pad sample is covered by a sheet of carbon paper. This method, used in early attempts to measure contact diameter, was later replaced by the ink-soaked strips discussed in the test.

FIGURE 3-2. PHOTOGRAPHS OF TEST APPARATUS

TABLE 3-1. SUMMARY OF VALIDATION TEST RESULTS*

TEST NUMBER	PROJECTILE SPEEDS (mph)		INITIAL KINETIC ENERGY (in.lb.)	DURATIONS (ms)		PEAK FORCE (lb.)	PEAK PAD STRAIN AS MEASURED BY	
	INITIAL	REBOUND		TO PEAK	TOTAL		CLAY PLUG	CONTACT DIAMETER
1	10.6	3.7	187	7.0		486	0.74	0.86
2	11.9	4.6	235				0.99	
3	12.9	6.7	277	7.1		608		
4	12.9	5.6	277	6.5		655	0.84	0.82
5	13.2	6.2	290				0.90	
6	13.5	6.5	303	6.5	11.3	929		
7	14.5	5.7	350	5.8	10.0	872	0.76	
8	14.5	6.7	350	6.0		1253		
9	15.2	6.7	384	5.7	10.3	1060	0.81	
10	14.6	5.8	354.5	7.0	12.5	686	0.85	
11	14.6	5.9	354.5	7.0		636		
12	18.8	8.3	588	5.9		1873		
13	14.1	6.2	331	6.6		819		
14	17.5	8.7	509	5.3	8.5	3022		
15	16.8	8.4	469	6.7		2387		
16	15.4	7.5	394			1838	0.91	
17	19.2	7.5	613	5.0	8.0	3231	0.92	0.98
18	20.0	9.0	665	4.75		5200	0.93	0.94
19	17.7	7.8	521	5.6		2115	0.93	0.94
20	17.8	8.9	527	5.2		3881		
21	16.6	8.8	458	5.0		2990		
22	17.8	8.8	527	5.2	7.7	3375		
23	13.0	4.7	281	6.3	14.0	600	0.80	0.94
24	11.7	4.0	228	7.8	15.0	485		
25	15.9	9.5	420				0.82	
26	19.6	10.7	639				0.84	
27	14.6	9.1	354.5				0.77	
28	14.0	6.7	608	7.4		4390	0.99	0.98
29	14.5	6.9	652	6.6		4309	0.99	
30	14.6	6.8	661	6.6		5265	0.95	0.94
31	15.5	7.1	745	7.0	12.0	5563		
32	14.4	6.6	643	6.7	10.0	4674	0.97	
33	14.6	7.1	661	6.5	10.7	5563	0.97	

*Tests number 1-24: aluminum projectile (4.13 lb.); pad on load cell
Tests number 25-27: aluminum projectile; pad on flexible plate
Tests number 28-33: steel projectile (7.7 lb.); pad on load cell

In addition to the validation tests, several static measurements were made to determine the force-deflection curve of the load cell support system. This curve must be known in order to use the impact analysis software to predict the results of tests performed with the load cell in place. The individual measurements were scattered, and are consequently represented by the averaged force-deflection curve shown in Figure 3-3. Also shown in this figure for comparison is the linear force-deflection relationship calculated for the flexible plate support.

3.3 DATA ANALYSIS

The raw test data were analyzed to assess consistency and identify significant trends. The results of the analysis are as follows.

Figure 3-4 plots the time from initial contact to peak force as a function of the initial impact speed. If the projectile of mass M were interacting with a linearly elastic system of stiffness K, the time to peak force would be given by:

$$T = (\pi/2) \sqrt{M/K} \qquad (32)$$

independent of the initial impact speed. The data in Figure 3-4 show a significant trend, however, of decrease in time with increasing speed. Furthermore, the data are well clustered about a best-fit line VT=constant=1.65 inches, where V is the initial impact speed, and where the best-fit was determined by least-square regression for the constant, assuming that $T \sim 1/V$.

Figure 3-4 is interpreted to mean that the speed of the projectile is nearly constant until it has penetrated deeply into the pad. However, the 1.65-inch travel distance exceeds the pad thickness by 0.45 inch, i.e., much more than one would expect the relatively stiff load cell support system to deflect. A second line shown on the plot, corresponding to VT=1.25 inches, represents the expected results.

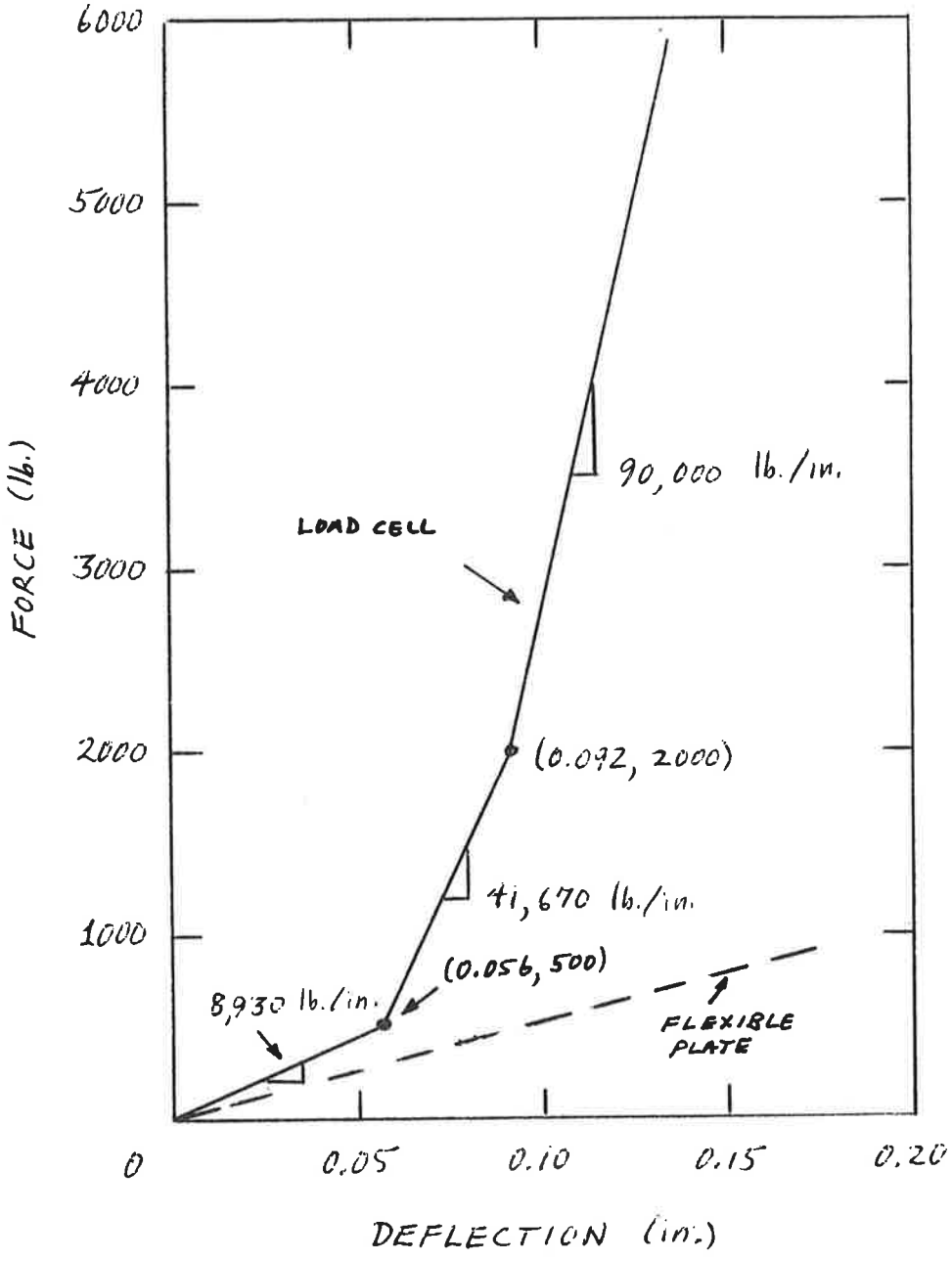

FIGURE 3-3. SUPPORT FORCE-DEFLECTION CURVES

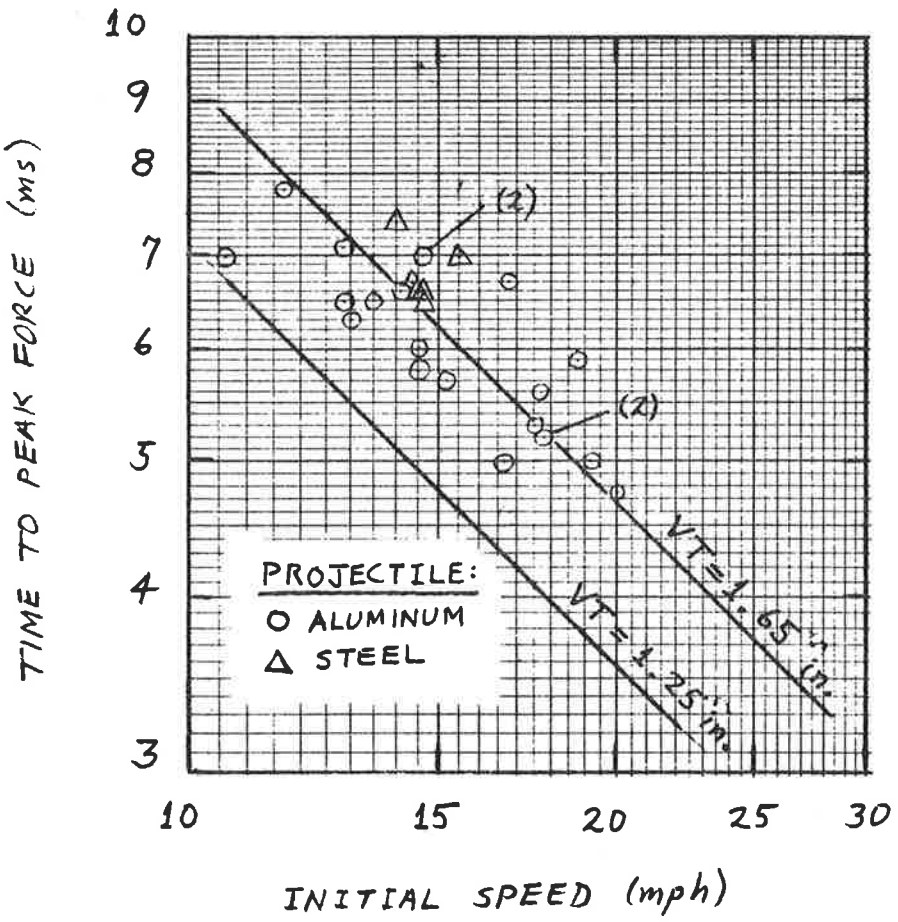

FIGURE 3-4. TIME TO PEAK FORCE VERSUS INITIAL SPEED

The apparent discrepancy can be resolved by recognizing that the measurement of time to peak force actually encompasses two events: the initial penetration at nearly constant velocity, and the subsequent deceleration of the sphere to zero velocity after the pad has been deeply penetrated. The time required by the second event can be roughly estimated by applying Eq. 30 and using data from the load cell force-deflection curve (Figure 3-3) for K. For stiffnesses ranging from 9,000 to 90,000 lb./in. and masses corresponding to the aluminum and steel projectile weights, this calculation gives times ranging from 0.5 to 1.6 ms. Somewhat longer time estimates would result if K were reduced to account for the fact that the pad stiffness is still finite after deep penetration. Returning to Figure 3-4, one can observe that the difference between the best-fit and expected VT lines varies from 1 to 2 ms over the speed range of the data, i.e., the test results are consistent with the expected VT line when the deceleration time is accounted for.

Hence, it is reasonable to interpret the foregoing results in terms of nearly constant velocity during initial penetration, until the pad has been deeply penetrated. This interpretation is also consistent with the results of the example impact analysis discussed in Section 2.3 (see Figure 2-12).

Since the foregoing result also implies that the pad is subjected to a nearly constant strain rate for a large part of the penetration, it is natural to expect that the validation test results should be consistent with laboratory test data which describe the material stress-strain curve for loading at constant strain rate. Conversely, the combination of spherical contact geometry and the nonlinear shape of the material stress-strain curve implies that the stress response in the pad is not homologous, a factor which tends to work against such consistency. Nevertheless, it is still worthwhile to analyze the validation test results for the presence of a trend that would signify consistency with the laboratory test data.

The analysis was performed by using the 9-parameter model for Ensolite foam rubber as a framework. Specifically, the model equation for stress response to loading at constant strain rate (see Volume II) was used to generate a calculated nominal stress based on the validation test measurements:

$$\sigma_{NOM} = \frac{\varepsilon_{PEAK}^{m}}{(1-\varepsilon_{PEAK})^{n}} \left[E_{\infty} + E_{r} (V/L)^{\bar{r}}\right] \tag{33}$$

where ε_{peak} is the peak pad strain, V is the initial impact speed, L is the pad thickness, and E_∞, E_r, m, n, r are assigned the values corresponding to the 9-parameter model of Ensolite. Total consistency implies that σ_{nom} is linearly proportional to the measured peak force, i.e., the test data should fall on a line with unit slope on a log plot.

Figure 3-5 plots the results from the 15 validation tests for which both peak strain and peak force data are available. In those cases for which peak strains were measured by both the clay plug and contact diameter methods, the peak strain was taken to be the average of the two measurements. The data points from 13 of the 15 tests appear to cluster reasonably well. Also shown in the figure is the best-fit line of unit slope based on least-square regression of the 13 clustered points. The result is, perhaps, better than should be expected in view of the imprecision associated with both methods for measuring peak strain. The result implies that the impact analysis software should be expected to yield good predictions for peak force.

Figure 3-6 illustrates peak force as a function of initial speeds for the tests on the load cell support system. Most of these tests resulted in deep penetration of the pad, but a transition region is evident for the aluminum projectile data between 10 and 15 mph. The sharp rise in the peak force between 15 and 20 mph is indirect evidence that these higher-speed tests have engaged the stiffening characteristic of the load cell support system.

Figure 3-7 plots rebound speed as a function of initial speed for all 33 tests. The tests performed on the load cell support system cluster reasonably well around the best-fit line $V_R = 0.44V$, where V and V_R are the initial and rebound speeds, respectively. This result suggests that the system's entire energy absorption capacity has been used at all speeds tested. The three data points from tests on the flexible plate support are distinct from the load cell group. Two of these points (at initial speeds of 14.6 and 15.9 mph, respectively) lie close to the line $V_R = 0.6V$, while the third point at 19.6 mph falls below this line.

The results shown in Figure 3-7 must be considered anomalous if it is assumed that the pad is the only significant source of energy absorption in either system. One would expect that if friction effects in the supports were small, the stiffer load cell should be slightly less absorptive than the flexible plate, and the plate data points should lie within the lower half of the load cell data scatter.

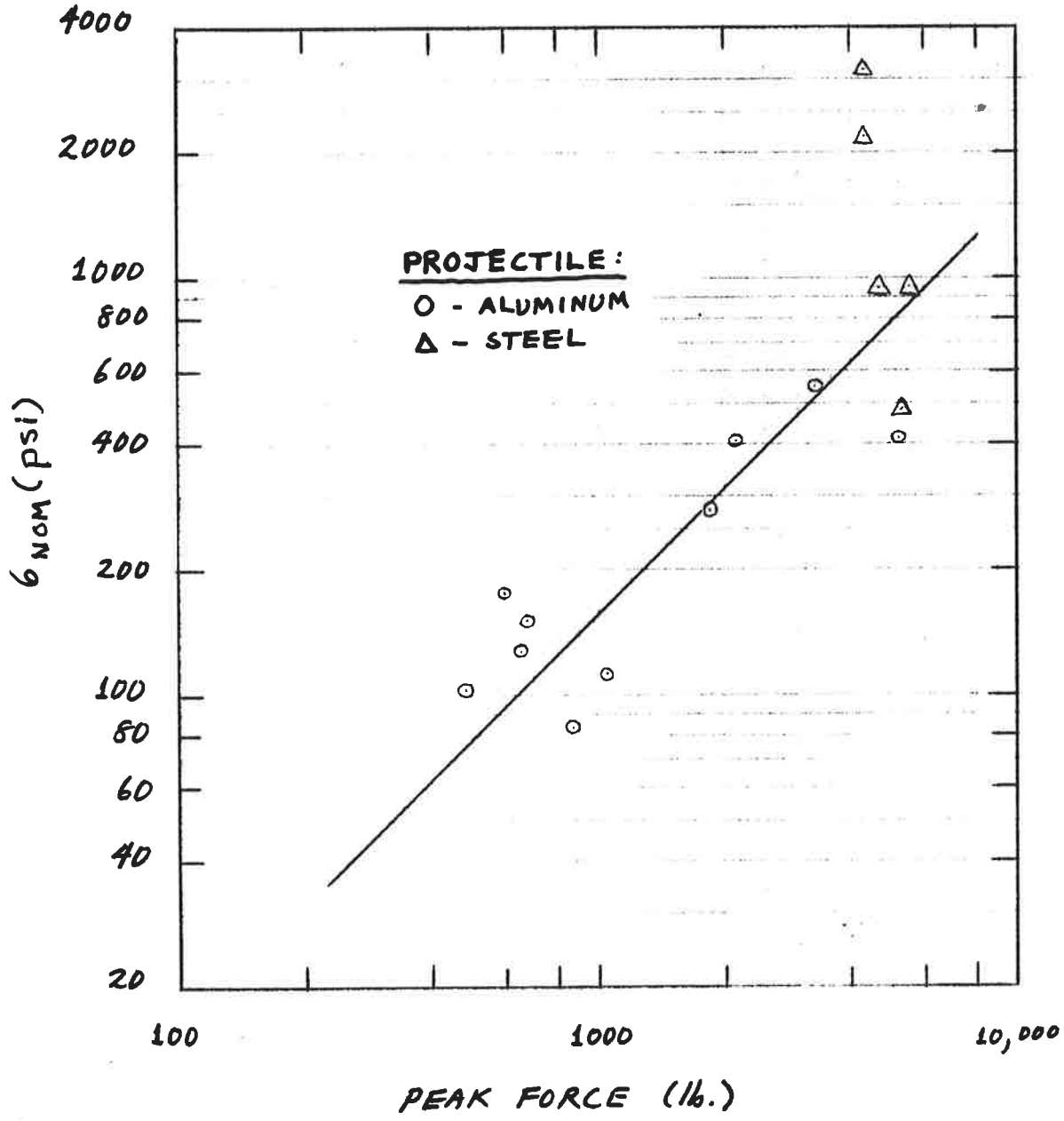

FIGURE 3-5. NOMINAL STRESS VERSUS PEAK FORCE

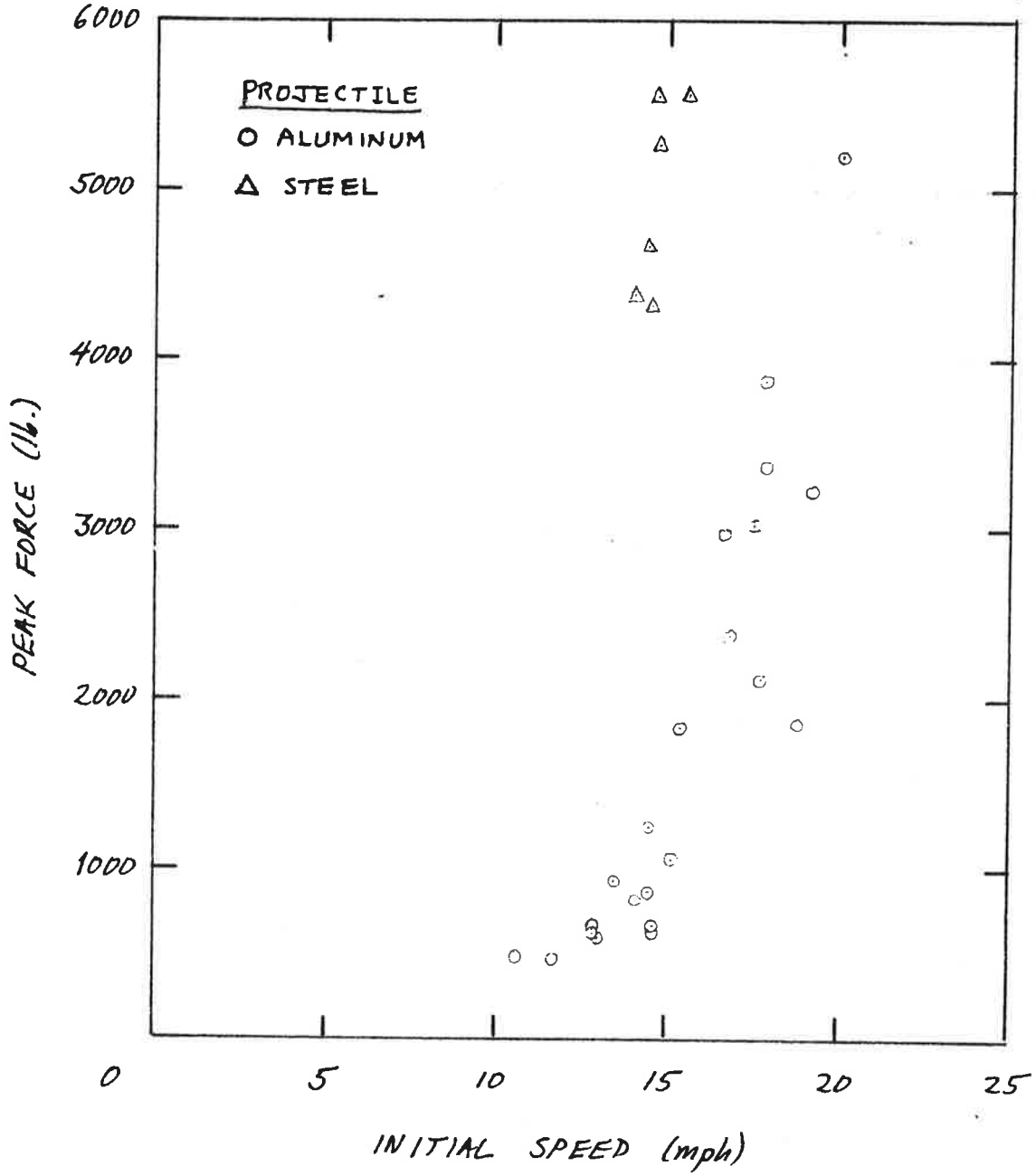

FIGURE 3-6. PEAK FORCE VERSUS INITIAL SPEED

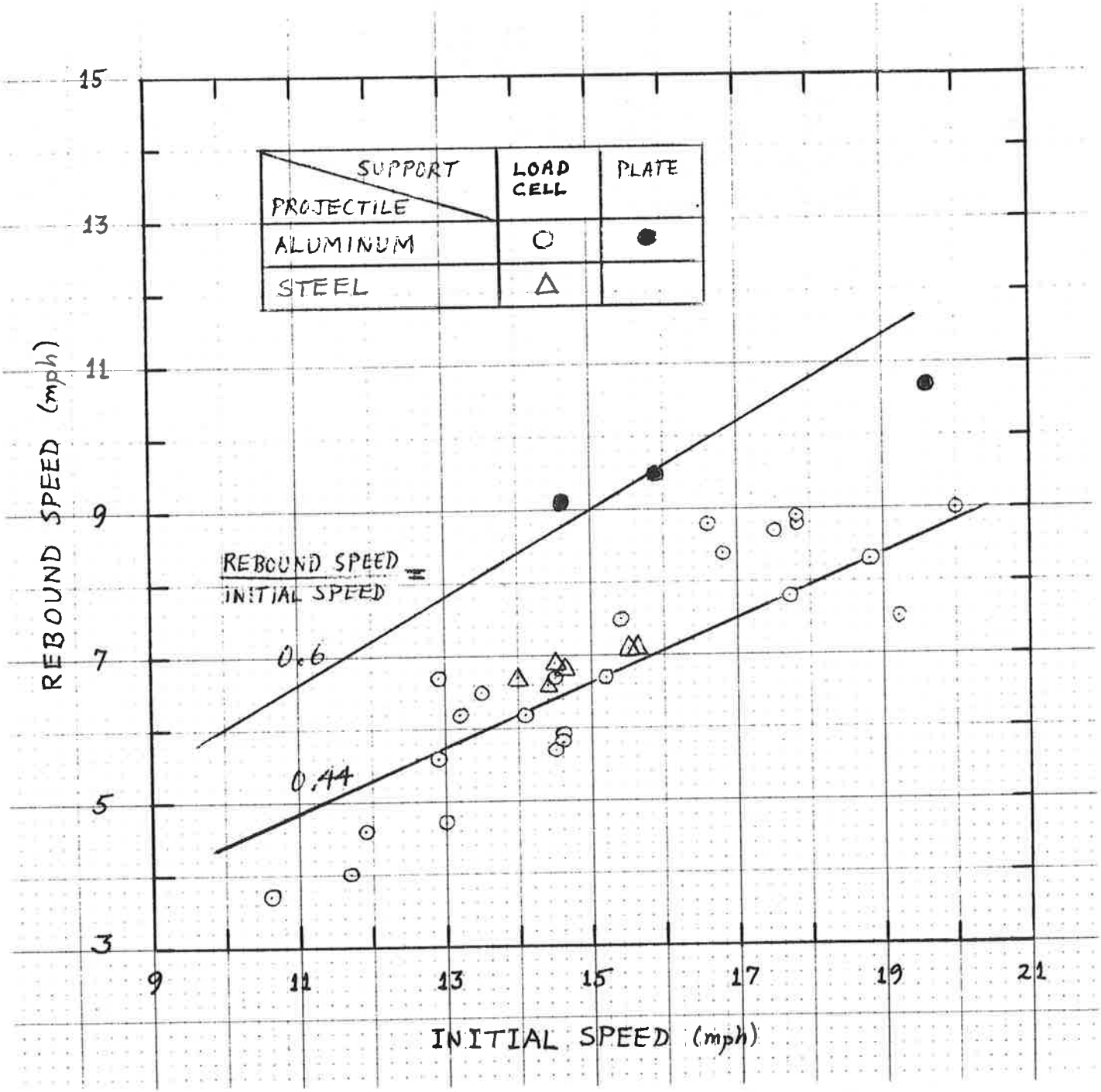

FIGURE 3-7. REBOUND SPEED VERSUS INITIAL SPEED

The appearance of the reverse trend and significant separation between the two groups suggests that there are significant sources of energy absorption associated with the rattling of loose components in the combination of the bearing plate resting on the load cell which in turn rests on the laboratory floor. Also, the failure of the plate test data to follow a trend line suggests the appearance of additional absorption capacity in these tests at high speed. The additional capacity in this case might be provided by either the pad or the support system. The second possibility is suggested by a calculation of peak force assuming a linearly elastic system:

$$F = V\sqrt{KM} \tag{34}$$

where K = 5,180 lb./in. is to be used to represent the flexible plate. For an initial speed of 19.6 mph, Eq. 32 gives a peak force of 2,573 lb. The corresponding plate deflection is about one half inch, i.e., enough to allow the underside of the plate to contact the floor and create an additional source of energy absorption.

The impact analysis software accounts for energy absorption only in the pad. The foregoing results suggest that the predictions of rebound speed should exceed the measurements. Beyond this trend, however, remains the question of how well the model accounts for the energy absorption characteristics of the pad. The energy account cannot be precisely balanced because the energy absorption capacities of the support systems are not known.* Useful bounds can be obtained, however, by comparing the energy storage capacities of the support systems with the total available impact energy. In order to work with the validation test data, it is most convenient to make the comparison by plotting peak force as a function of initial kinetic energy, $MV^2/2$, which has been calculated from the test data (see Table 3-1). The support system storage capacities can be estimated by calculating the elastic work, $W = \int F dX_s$, from the force-deflection curves (Figure 3-3) and expressing the result in terms of the force. For the linearly elastic plate, the result is simply $W = F^2/2K$. For the piece-wise linear curve of the load cell system, the expression:

*Direct measurement by means of impact tests without pads was considered. The idea was abandoned, however, when it became evident that the impact shock stresses from a "bare" test would damage the plate and destroy the load cell.

$$W = W_o + (F^2 - F_o^2)/2K_{tan} \tag{35}$$

can be used, where F_o is the force corresponding to a segment boundary, $W_o = W(F_o)$, $F > F_o$, and K_{tan} is the tangent stiffness for $F > F_o$.

Figure 3-8 compares the force-energy relations. Note that the load cell storage capacity varies from 7 to about 30 percent of the energy available in the tests. These figures represent the upper limit on absorbed energy for which the impact analysis model should not be held accountable. The following logic can then be used to bound the expectation for model performance.

First, estimate the residual kinetic energy $U_R = (V_R/V)^2U$ for a given impact speed V and initial kinetic energy $U = MV^2/2$. Use the best-fit trend line $V_R/V=0.44$ for the load cell support (Figure 3-7). The total energy absorbed is $U-U_R$.

Second, obtain the peak force F corresponding to the energy U from the trend of the test data in Figure 3-8. Read the curve in the figure to obtain the support system's energy storage capacity W_S for the same peak force.

Third, assume that the support absorbs its entire supply of stored energy. The energy absorbed by the pad is then $W_P = U-U_R-W_S$; this is a lower bound.

Fourth, calculate the residual kinetic energy expected from the analysis model: $U_R^*=U-W_P=U_R+W_S$. The corresponding expectation for rebound speed is $V_R^*= \sqrt{(U_R+W_S)/U}\ V$. This is an upper bound. Table 3-2 summarizes two example calculations.

TABLE 3-2. EXAMPLE EXPECTATIONS OF MODEL PREDICTIONS

PROJECTILE	STEEL (7.7 lb.)	ALUMINUM (4.13 lb.)
Initial speed V (mph)	14.6	12
Initial kinetic energy U (in.lb)	661	240
Peak Force F (lb.)	5500	550
Rebound kinetic energy U_R (in.lb.)	128	46
Support capacity W_S (in.lb.)	205	15
$V_R^*/V = (U_R + W_S)/U$	0.71	0.5
Expected rebound speed V_R (mph)	10.4	6

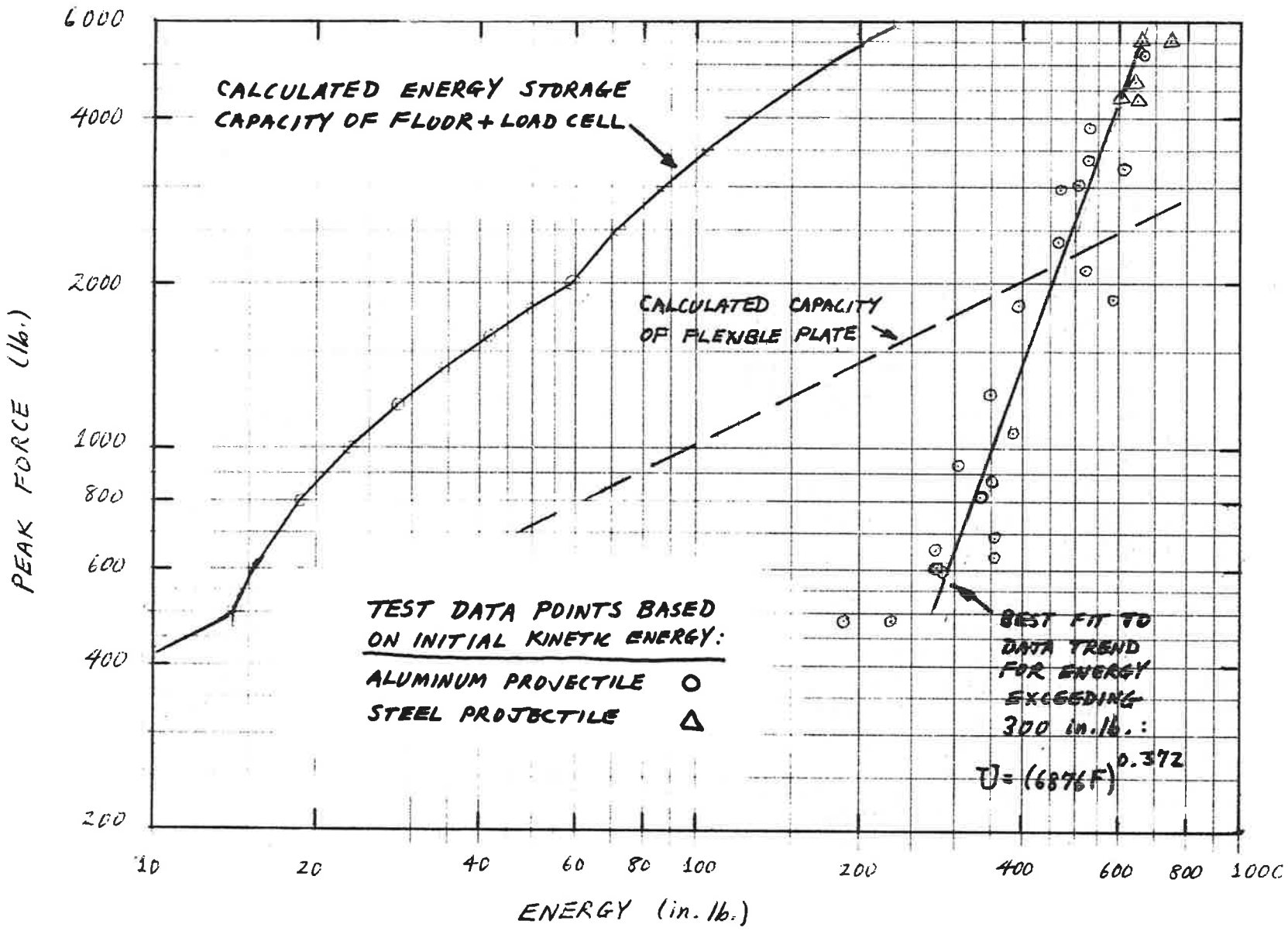

FIGURE 3-8. COMPARISON OF FORCE-ENERGY RELATIONS

The foregoing procedure is less useful for bounding predictions of the flexible-plate-supported tests because the plate is resilient. However, the force-energy relations can also be used to estimate the expected curve of peak force versus initial speed for tests on the plate support. The best-fit trend line in Figure 3-8 represents the sum of energies stored in the pad and load cell support system, as a function of force:

$$U(F) \cong (6876\ F)^{0.372} \tag{36}$$

where the total energy U(F) implicitly includes the support capacity $W_S(F)$. If it is assumed that changing the support does not per se change the storage capacity of the pad, then the relation between force and total energy for tests on the plate support is given by:

$$U^*(F) = U(F) - W_s(F) + F^2/2K \tag{37}$$

where K=5,180 lb./in. is the plate stiffness. The corresponding initial speed is then given by $\sqrt{2U^*/M}$.

The foregoing calculations were made for the aluminum projectile in order to estimate the force-speed curve for tests 25-27. Figure 3-9 illustrates the estimate and compares it with the tests performed on the load cell support. The data points shown in the figure are from tests 1-24 and are the same as those shown in Figure 3-7. Curve "A" is calculated from the best-fit trend line (Figure 3-9 and Eq. 34) for the mass of the aluminum projectile. Curve "B" is the estimate for the plate-supported tests. Both curves have tails based on the data points from tests 1 and 24, which deviate from the trend line. Above the tail, curve "B" is dominated by the $F^2/2K$ term in Eq. 35 and is nearly linear.

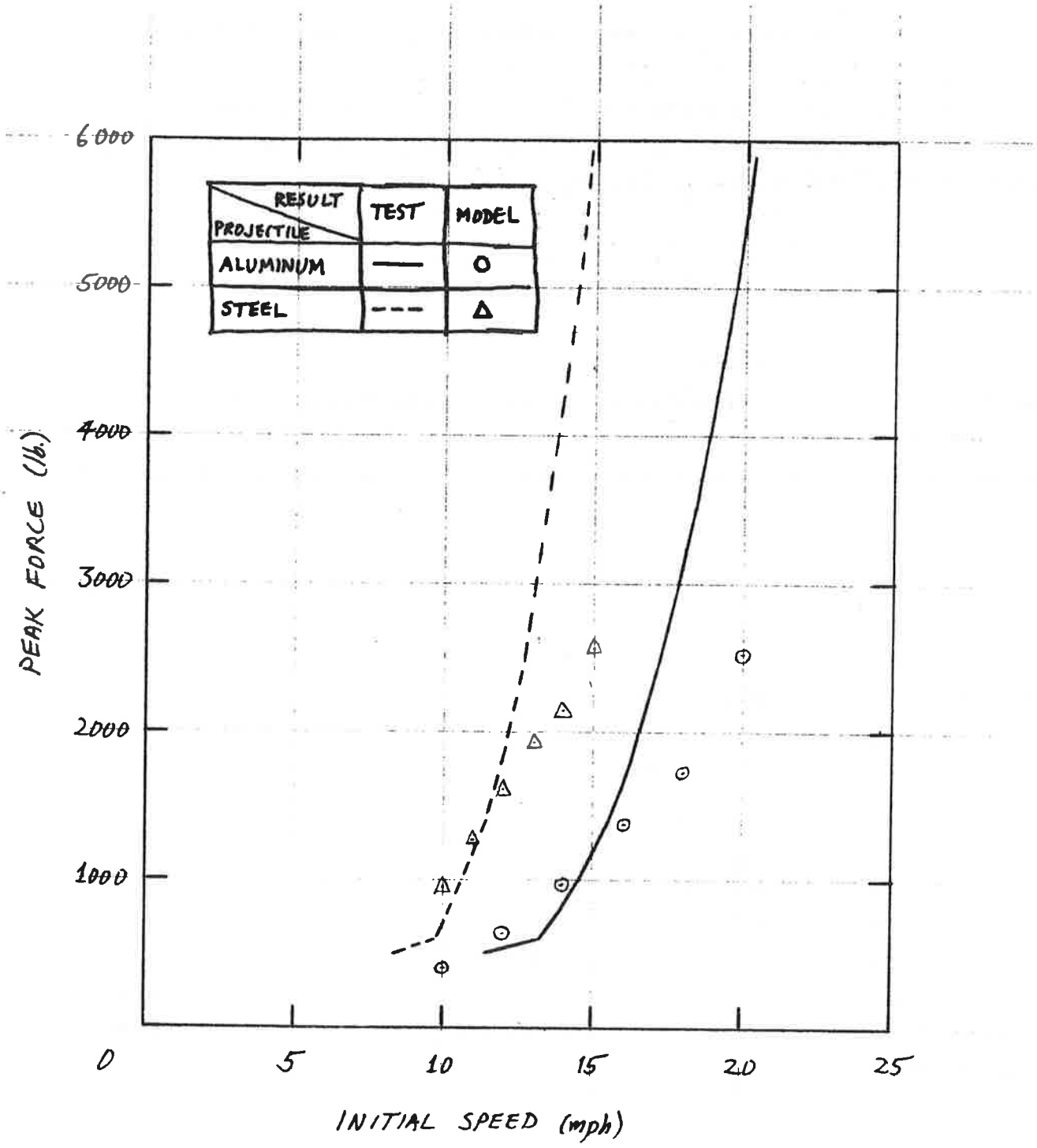

FIGURE 3-9. BEHAVIOR OF PEAK FORCE IN TESTS WITH ALUMINUM PROJECTILE

4. COMPARISON OF MODEL PREDICTIONS WITH VALIDATION TEST RESULTS

Impact simulations were run at initial speeds from 10 to 20 mph in 2-mph increments for the aluminum projectile and at initial speeds from 10 to 15 mph in 1-mph increments for the steel projectile, using the static force-deflection curve of the load cell support (Figure 3-3). Aluminum projectile simulations were also run with the linear elastic support stiffness K=5,180 lb./in. corresponding to the flexible plate. All simulations were run with the 9-parameter model of Ensolite foam rubber.

The simulations covered the speed ranges and projectile masses investigated in the validation tests. For clarity, the model predictions were compared, for the most part, with the best-fit trend lines developed from the data analysis (Section 3.3).

Data for the time T to peak force were available from the tests on the load cell, and were found to cluster along the trend line VT=1.65 inches, where V is the initial impact speed (Figure 3-4). This trend was reconciled to the expected trend line VT=1.25 inches by considering the effect of the support stiffness.

Figure 4-1 reproduces the two trend lines and compares them with the time to peak force predicted by the simulations. Most of the predicted data points appear to follow a similar VT=constant trend line about 2 ms above the expected trend line. If this time difference is attributed to an elastic reversal phase in which the support is engaged, the effective stiffness K can be estimated from Eq. 30, which was previously used to estimate time from stiffness (see Section 3.3). The result of the calculation is K = 6,600 lb/in. for the aluminum projectile simulations and K = 12,300 lb./in. for the steel projectile simulations.

These values are different from the range of 9,000 to 90,000 lb./in. measured statically and found to correlate with the test time differences in Figure 3-4. One would expect similar differences in the peak force data, which should vary according to $F \sim \sqrt{K}$. Also, one would expect the higher test stiffness to correspond to higher initial speed, i.e. the ratio of predicted to measured peak force should vary from 0.9 to 0.3 (aluminum projectile) or 1.2 to 0.4 (steel projectile) as the impact speed varies from low to high.

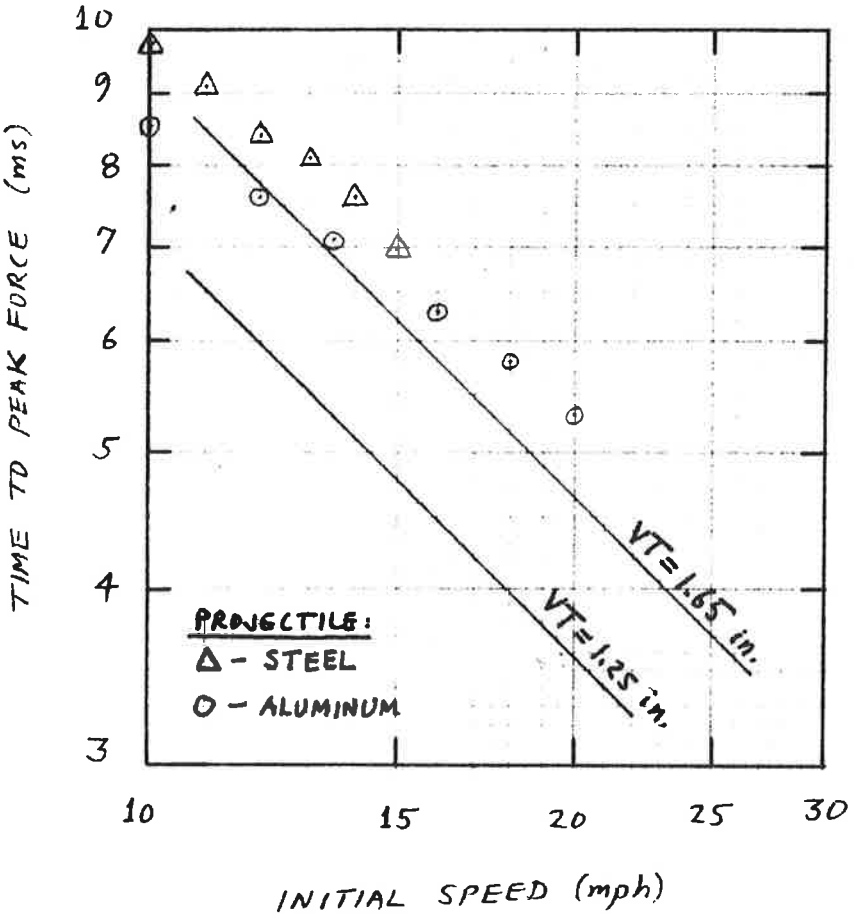

FIGURE 4-1. MODEL PREDICTION OF TIME TO PEAK FORCE FOR TESTS ON LOAD CELL SUPPORT

The peak force data from the tests on the load cell were reconciled by plotting as a function of initial kinetic energy U and determining the best-fit trend line to be $U=(6876F)^{0.372}$ for energies above 300 in./lb. These results were compared with the force-energy relations for the energy-storage capacities of both the load cell and plate supports in Figure 3-8. The best-fit trend was translated into a curve of peak force versus initial speed for the tests of the aluminum projectile on the load cell (curve "A"), and a corresponding curve for the aluminum projectile on the plate was estimated by adjusting for support storage capacity (curve "B") in Figure 3-9.

Figure 4-2 reproduces curve "A" and the corresponding curve for the steel projectile. Also plotted are the data points from the simulations of the tests on the load cell support. The trend of the model predictions reflects the differences in the model and actual support stiffness discussed earlier. In particular, the ratio of predicted to measured force varies from about 1 to 0.4 (aluminum projectile) and 1.4 to 0.4 (steel projectile), in reasonable agreement with the expected variations.

Figure 4-3 reproduces curve "B" and compares it with the simulations of the aluminum projectile on the flexible plate support. In this case, there is reasonable agreement between the prediction and the estimate for test behavior over the entire range of 10 to 20 mph initial speed.

The measurements of rebound speed versus initial speed were seen to cluster along the trend line $V_R/V=0.44$ for the tests on the load cell, while the three data points for tests on the flexible plate were closer to $V_R/V=0.6$ (Figure 3-7). The one high-speed flexible plate test point fell significantly below $V_R/V=0.6$, however. These results suggested that the load cell support system dissipated energy over the entire range of initial speeds tested, while the more resilient plate appeared to dissipate energy only at impact speeds approaching 20 mph.

Figures 4-4 and 4-5 compare the model predictions with the trend lines. As expected, the predicted rebound speeds are much higher than the measured speeds because the impact analysis model accounts for energy absorption only in the pad. A method of adjusting the experimental results to reflect the same accounting was discussed earlier (see Section 3.3 and Table 4-2.) These adjustments are shown as "expected results" in Figures 4-4 and 4-5.

The expected results are based on the assumption that all of the energy stored in the support is absorbed, while none of this absorption is reflected in the model prediction. Hence the model predictions should lie below the expected curves.

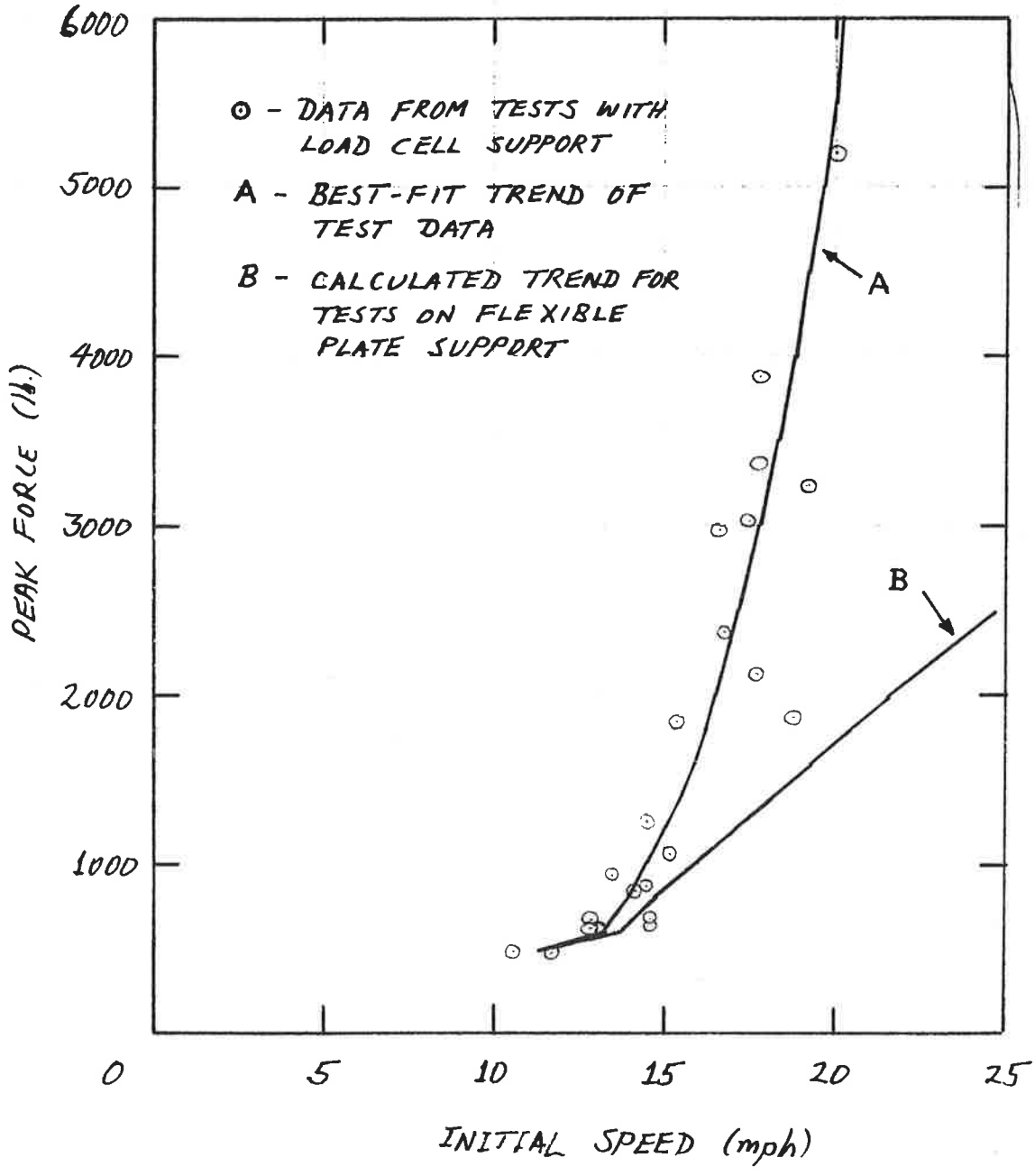

FIGURE 4-2. MODEL PREDICTION OF PEAK FORCE FOR TESTS ON LOAD CELL SUPPORT

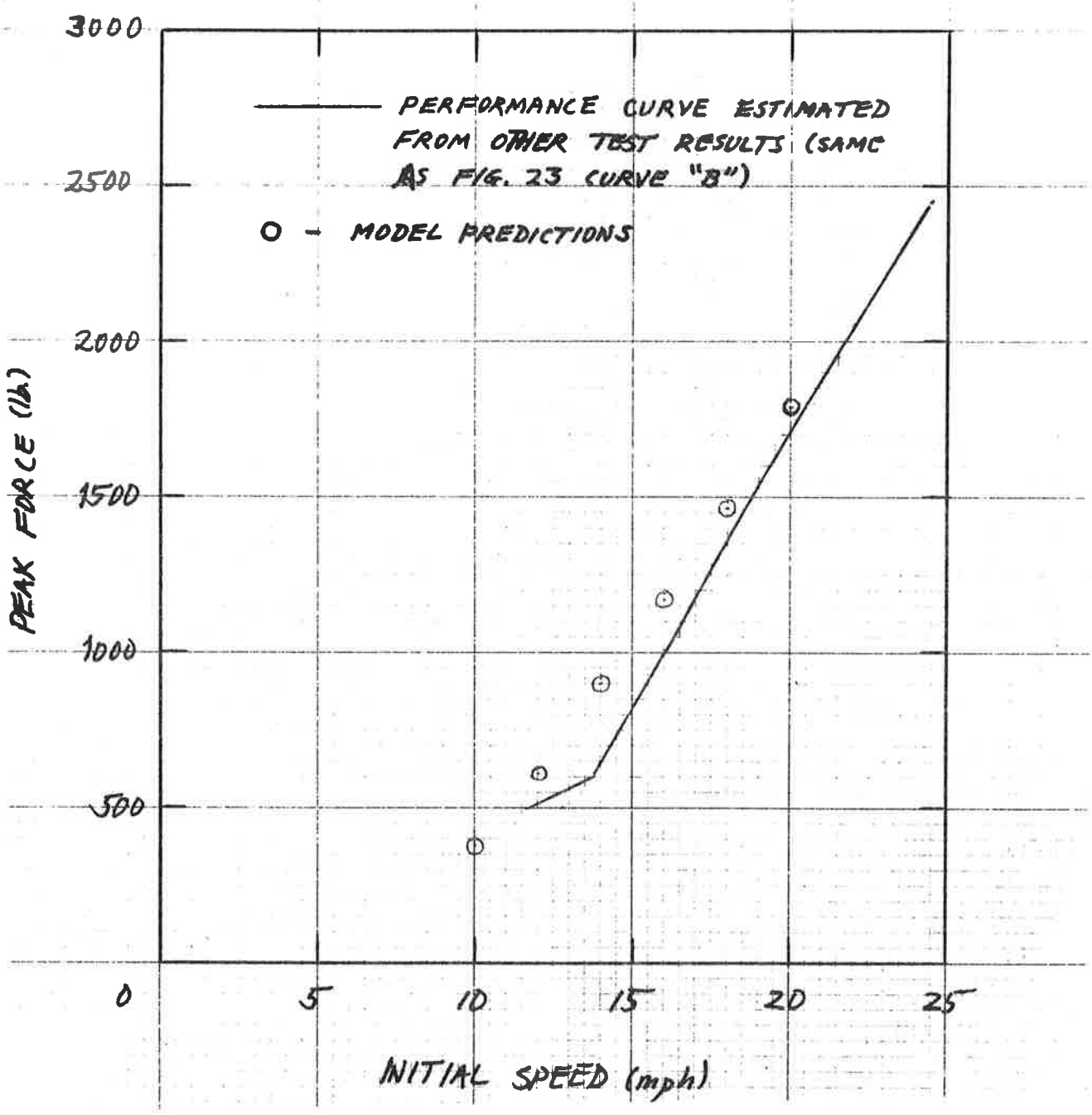

FIGURE 4-3. MODEL PREDICTION OF PEAK FORCE FOR TESTS ON FLEXIBLE PLATE

From Figure 4-4, it is apparent that the model predictions do not conform to the expectations for the tests on the load cell support. This discrepancy suggests either that the combination of the pad material model and the simplified contact strain field under-represent the pad's energy absorption capacity, or that energy absorption in the bearing-plate/load-cell/floor combination is not related to the system's elastic storage capacity.

The comparison for the tests on the flexible plate, shown in Figure 4-5, is more encouraging. In this case the model predictions are consistent with the expected result. Also, the trends of the model predictions and the test data points appear to converge in the low-speed (10 to 15 mph) range. This result for the tests on the flexible plate suggests that most of the discrepancy in the simulation of tests on the load cell should be attributed to lack of understanding of support dynamic energy absorption characteristics.

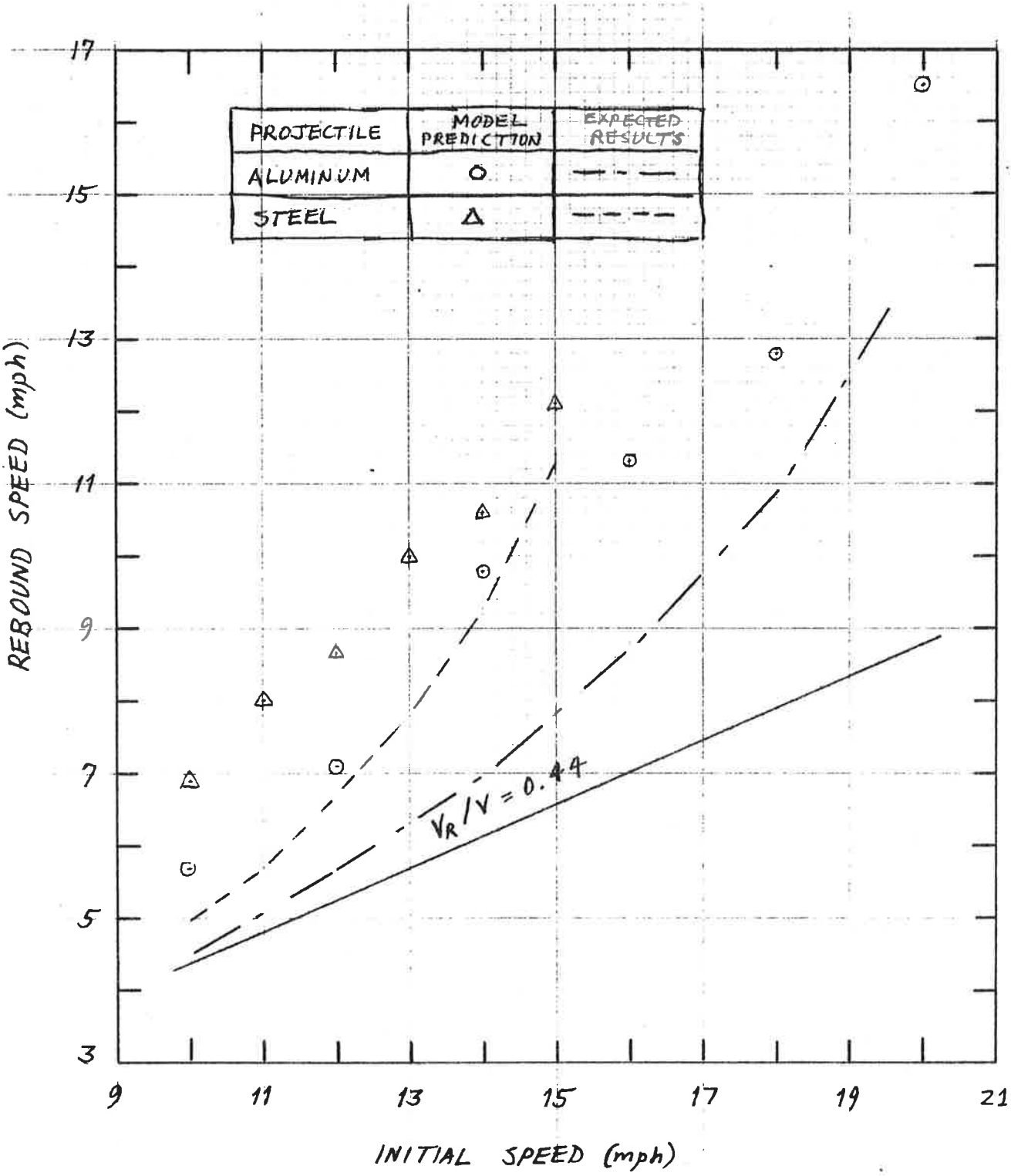

FIGURE 4-4. MODEL PREDICTION OF REBOUND SPEED FOR TESTS ON LOAD CELL SUPPORT

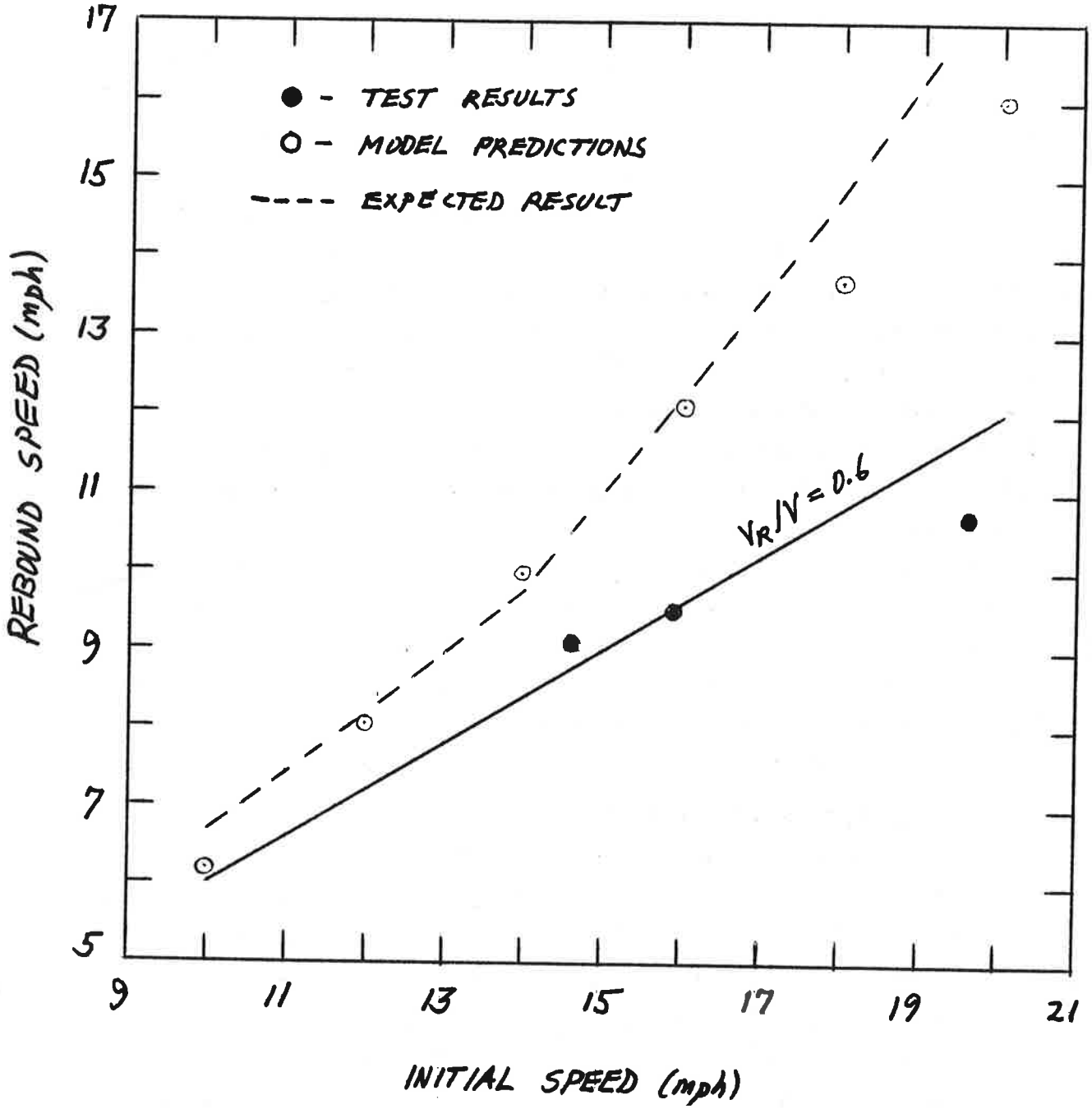

FIGURE 4-5. MODEL PREDICTION OF REBOUND SPEED FOR TESTS ON FLEXIBLE PLATE

5. CONCLUSIONS

The research reported herein comprises the development and validation of a computer program for analyzing impacts between unrestrained occupants and automobile interior structures with crash padding. The computer model uses a rigid spherical mass to approximate the part of the occupant's body involved in the collision. The automobile structure is represented by an elastically supported initially flat pad. The spherical geometry of the rigid mass is assumed to be imposed on the contact region of the pad.

The dynamic mechanical properties of the padding material are characterized by a viscoelastic constitutive equation. Two empirical nonlinear viscoelastic constitutive equations (one with 9 parameters and one with 21 parameters) were previously developed from laboratory tests of Uniroyal Ensolite AAC foam rubber (see Volumes I and II). Ensolite foam rubber pads were used in the validation tests, and the empirical material models were used in the parallel predictive analyses.

The validation tests involved launching metal projectiles with hemispherical noses at target pads. In most of these tests, the pad was supported by the combination of a thick steel bearing plate resting on a load cell which, in turn, rested on the laboratory floor. The presence of the load cell in the support system allowed the measurement of impact duration time and peak force, in addition to the measurements of initial and rebound speed which were made by other means. In a few tests, the pad was supported by a flexible plate, and only speed measurements were made. Separate measurements and calculations were made to determine the static stiffness of each support system.

The following conclusions can be drawn from the results of the research:

- Comparative simulations of a typical 20 mph impact situation showed that there was little difference in the predictions obtained with the 9-parameter versus the 21-parameter model for Ensolite foam rubber. This is likely to be the case for any other material. Consequently, the simpler 9-parameter model was used to predict the results of the validation tests.

- Regarding the tests performed with the load cell support system, the model predictions of time to peak force and peak force value were found to be consistent with a support stiffness somewhat less than the statically measured force-deflection curve.

- The predicted speeds for rebound of the projectile from the pad/bearing-plate/load-cell combination did not agree with the measured speeds. The discrepancy could not be reconciled by accounting for support system energy absorption proportional to elastic energy storage capacity.

- Regarding the tests performed with the flexible plate support, the model predictions for peak force agreed well with expected results developed by adjusting the load cell test data to account for the difference in the static stiffness of the two support systems. Also, the trend of the predicted rebound speeds was in reasonable agreement with the test trend at low speed (10 to 15 mph), and the predicted trend was within expected bounds for energy absorption.

- The foregoing conclusions suggest that the basic sphere/pad/geometry model is valid for Ensolite foam rubber. However, it appears that the dynamic characteristics of the load cell support system are not well understood.

- The flexible plate tests, for which the best agreement between experiment and prediction was obtained, are also the better approximation of an automobile dashboard structure. (The plate stiffness was, however, still about ten times the stiffness of typical dashboards.) The pad was deeply penetrated in these tests. Therefore, it appears that reasonable predictions of padding performance are possible without accounting for the three-dimensional effects of lateral constraint and load transfer by shear.

APPENDIX A
IMPACT ANALYSIS USER'S GUIDE

This appendix contains a complete user's guide to the application of subroutines SPIT and PAD. Figure A-1 illustrates the software architecture required for execution.

FIGURE A-1. SOFTWARE ARCHITECTURE

It is left to the user to write a FORTRAN main program compatible with the user's computing facility. The main program need only perform two functions: acceptance of problem input data and a proper CALL to subroutine SPIT. The example analysis in Appendix C includes a main program that was written for an interactive terminal working with a DECSystem 10 computer.

Subroutines SPIT and PAD have been coded in ANSI FORTRAN-IV to the maximum extent possible. This includes DO-loop initialization of all variables which must have zero initial values. The print formatting is an exception to the standard coding in two respects. First, the formats assume that the printer capacity is 132 characters per line, including the first character for carriage control. However, standard Hollerith formats have been used for all textual messages and headings. Second, the listed output peripheral device code corresponds to print facilities available on the Transportation Systems Center's DECSystem 10 as of December 1984. The user should review the listing of subroutine SPIT in Appendix B to verify or adjust the device code in FORMAT statements 6000 and 600 through 613.

A.1 DIMENSIONING OF VECTORS

Fourteen vectors appearing in the argument list of subroutine SPIT must be dimensioned consistently in the user's main program. These variables are divided into three groups as follows.

Vectors A,F,T,V,X, and XP are the system variables of acceleration, force, time, velocity, sphere position, and pad penetration, respectively. The software is supplied with a dimension of 1000 for each vector. If the dimension is changed, the statement:

```
IF(KP1 .GT. 1000) GO TO 902
```

must be changed to agree with the new dimension.

Vectors EK, EKP1, EMAX, SK, SKP1, and R are the contact field variables of strain (start of step), strain (end of step), maximum strain, stress (start of step), stress (end of step), and integration station radius, respectively. The software is supplied with a dimension of 1000 for each vector. If the dimension is changed, two statements:

```
IF(MAXR .GT. 1000) GO TO 904
```

must be changed to agree with the new dimention.

Vectors PPAR(21) and SPAR(12) store material properties. Vector PPAR contains the parameters for the pad's constitutive equation model. Vector SPAR contains the parameters which describe the support structure stiffness.

A.2 UNITS

The software is programmed to work internally in the unit system of lb. (force), in. (length), sec. (time), and lb. sec.^{2}/in. (mass). Certain inputs and outputs are defined in alternate units for convenience (see Section A.3). Conversion constants C = 17.64 in./sec. per mph and G = 386.4 in./sec.^{2} are stored internally via data statements. Time variables are converted internally between seconds and milliseconds when convenient. Strain variable are dimensionless fractions, and strain rates are expressed in sec.$^{-1}$ internally.

A.3 DEFINITION OF INPUTS

All variables appearing in the argument list of subroutine SPIT must be defined by the user. The meaning and units of each variable are given below in the order in which the arguments appear. The variables are floating-point scalars except where noted.

RAD - Radius of sphere (in.)

VIN - Initial speed of sphere (mph)

WGT - Weight of sphere (lb.)

KEYP - Integer key for type of pad model to be used:

KEYP=1 - Linearly elastic

KEYP=2 - Linearly viscoelastic

KEYP=3 - Rigid foam

KEYP=4 - Nonlinear 9-parameter viscoelastic model

KEYP=5 - Nonlinear 21-parameter viscoelastic model

PPAR(21) - Vector of pad material properties with values stored according to KEYP option, as shown in Table A-1.

THK - Pad thickness (in.)

KEYS - Integer key for type of support stiffness to be used:

KEYS=1 - linear

KEYS=2, 3, or 4 - nonlinear

SPAR(12) - Vector of support stiffness properties with values stored according to KEYS option, as shown in Table A-2.

TABLE A-2. STORAGE CONVENTIONS FOR SPAR(J)

KEYS= \ J=	1	2	3	4	5	6	7	8	9
1									K_S
2	X1	F1	X2	F2					
3	X1	F1	X2	F2	X3	F3			
4	X1	F1	X2	F2	X3	F3	X4	F4	

NOTES:

Blank entries need not be defined.

K_S = spring rate (lb./in.)

(X,F) = points on force-deflection curve: deflection X (in.) and force F (lb.)

For KEYS=2,3,4 - program internally computes and stores tangent spring rates in SPAR(9) through SPAR(12)

DELT - Time step size (milliseconds) - A value of 0.1 ms should be adequate for typical impact analyses. To maintain assurance of stability in the finite-difference algorithm, the user is advised to calculate the following maximum allowable time step size:

TABLE A-1. STORAGE CONVENTIONS FOR PPAR (J)

KEYP = \ J =	1	2	3	4	5	6	7	8	9	10	11	12	13	14	15	16	17	18	19	20	21
1	E																				
2	E_∞	E_0	ι																		
3	S1	E1	S2	E2																	
4	E_∞	m	n	ι	E_r	r	τ^*	P	E_0												
5	E_∞	m	n	A	B	C	σ_r	r	u	v	w	x	y	z	τ^*	P	σ_o	a	b	c	d

NOTES:
Blank entries in table need not be defined

KEYP = 1
E = Young's modules (psi)

KEYP = 2
E_0, E_∞ = moduli (psi)
ι = characteristic decay time (sec.)

KEYP = 4,5
See Volume II of this report
for definition of parameters

KEYP = 3

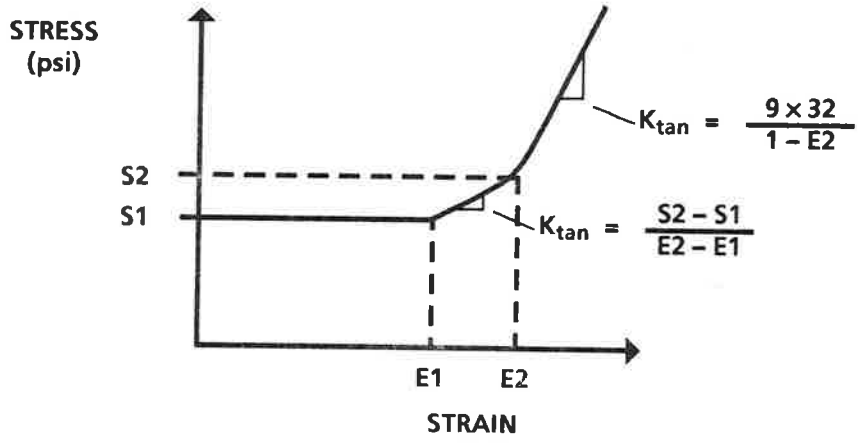

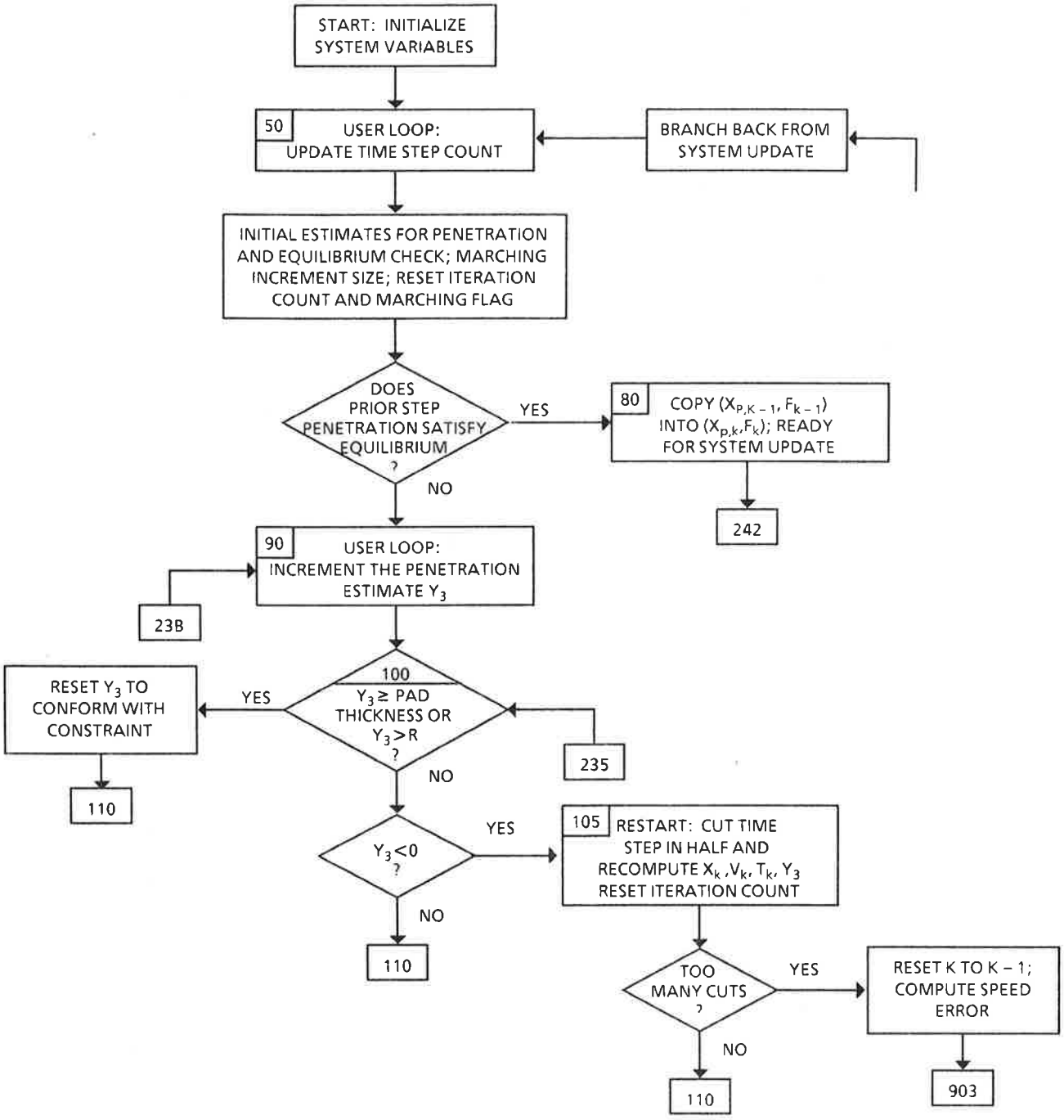

FIGURE A-2. SUBROUTINE SPIT FLOW CHART (Part 1 of 4)

$$\Delta t_{max}\ (\text{sec.}) = 0.25\sqrt{M/K_S}$$

where M (lb.sec.^{2}/in.) is the mass of the sphere and K_S (lb./in.) is the support stiffness. For nonlinear supports the largest tangent stiffness should be used, e.g.:

$$K_S = (F4-F3)/(X4-X3)$$

for KEYS=4.

NDEL - Integer for print control - The results will be printed for every NDELth time step for most of the run. However, every step in the last group of NDEL or fewer steps will always be printed.

A.4 SOFTWARE EXECUTION AND LOGIC

Typical runs with nonlinear viscoelastic models and a 0.1-ms time step size indicate that the simulation-to-real time ratio of the SPIT/PAD software is about 2000 to 1 on a DECSystem 10 computer, i.e., a 20-ms impact consumer about 40 CPU seconds. The ratio on other hardware can be estimated by comparing arithmetic cycle times.

Section 2.2 presented an overview of the algorithm in subroutine SPIT. Figure A-2 presents a detailed flow chart. Key FORTRAN statement numbers are included in the flow chart for easy reference to the listing in Appendix B. A number of minor details in the logic were omitted from the Section 2.2 discussion. These items are principally ABEND branches and/or traps for states which the algorithm may possibly but will not probably reach.

The logic in subroutine PAD can be understood without a flow chart. This subroutine is a stack of five separate branches, one for each of the permitted material models. Within each branch, the appropriate model parameters are transferred from vector PPAR to mnemonic scalars, and a loop is executed over the contact integration stations. At each station, the stress is updated by means of the model's constitutive equation. The strain rate and a strain magnitude at each station are also computed if needed by the model. The empirical nonlinear viscoelastic models work in terms of magnitudes, but preserve and restore the correct sign of the updated stress before

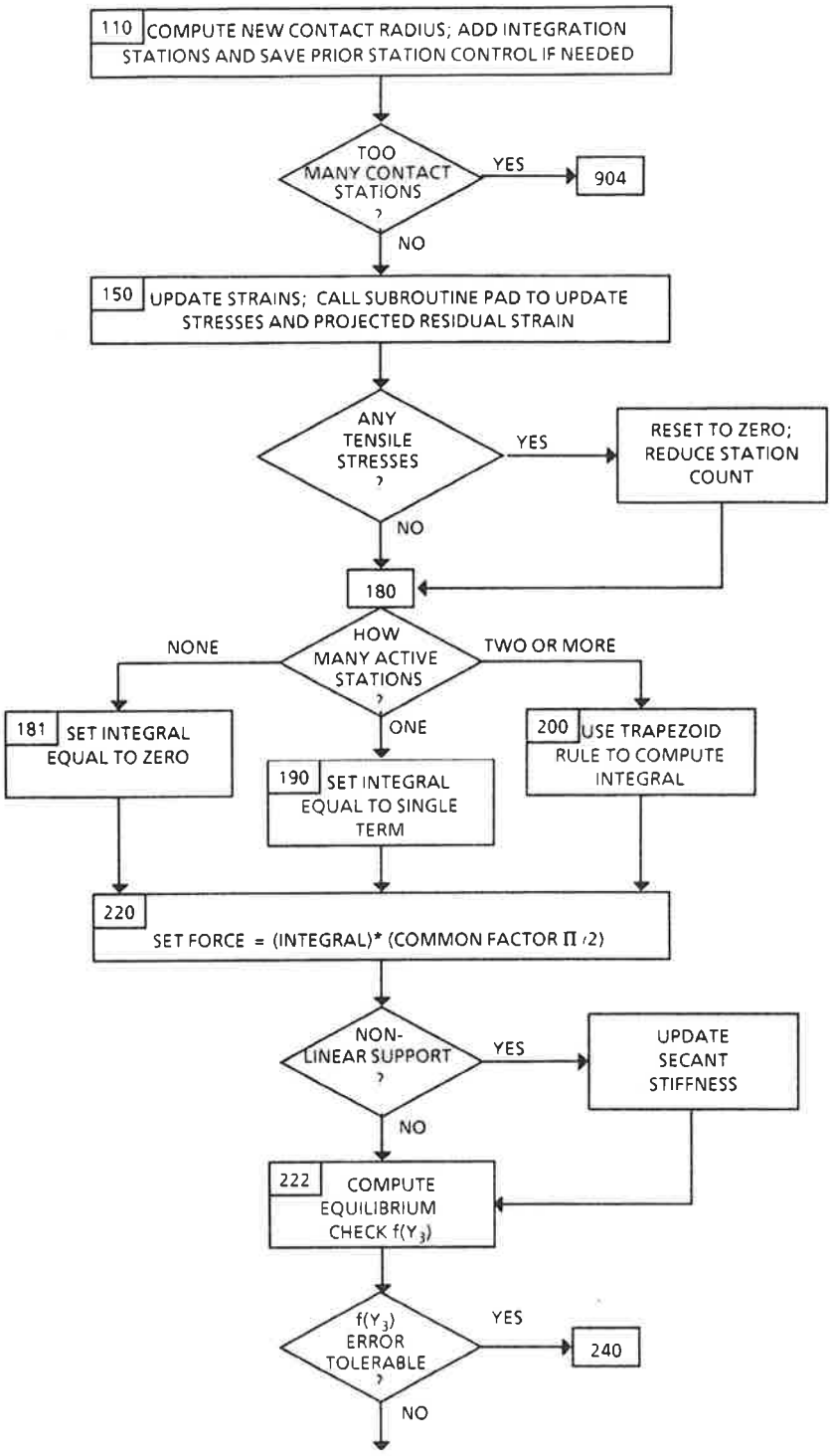

FIGURE A-2. SUBROUTINE SPIT FLOW CHART (Part 2 of 4)

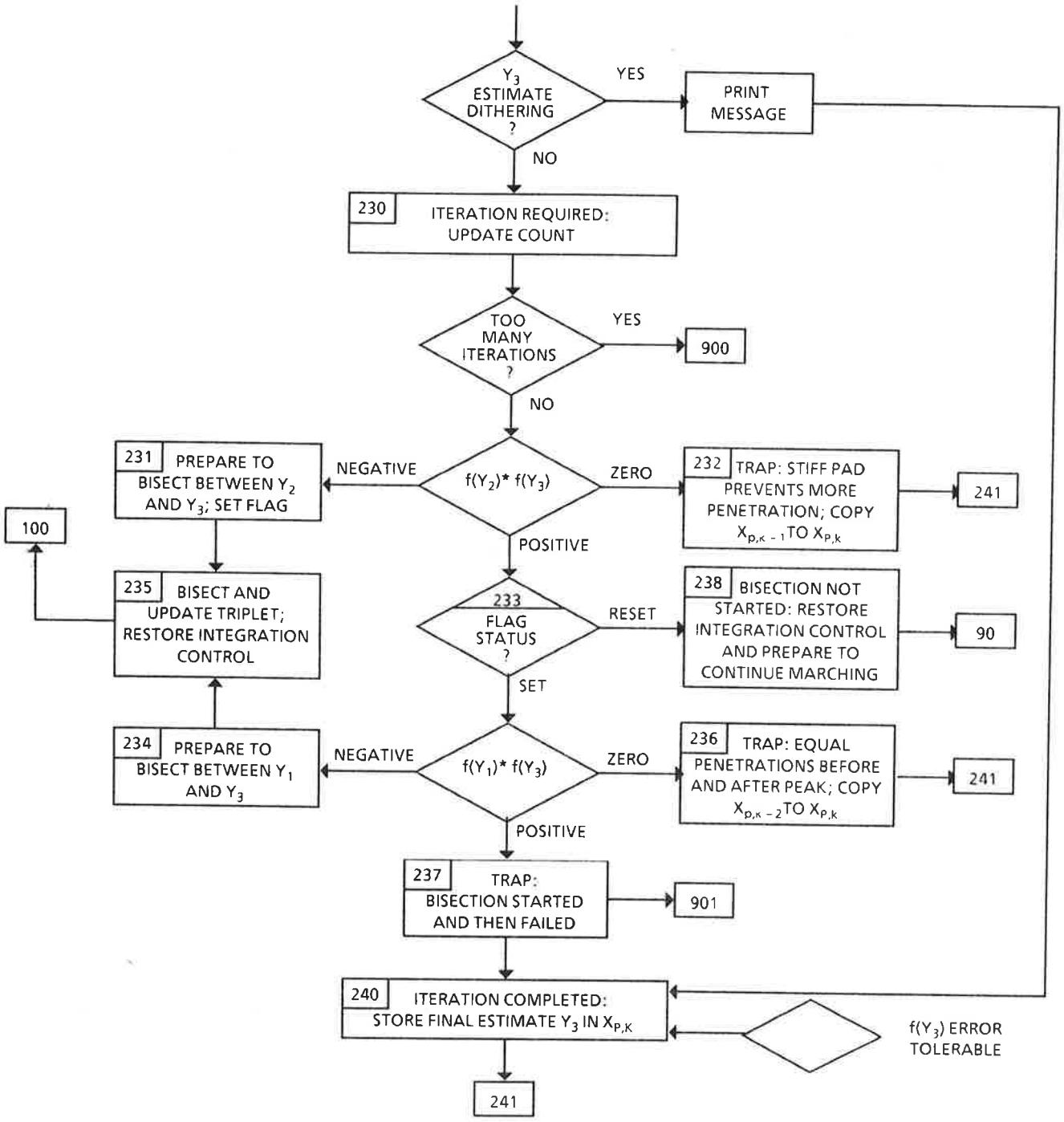

FIGURE A-2. SUBROUTINE SPIT FLOW CHART (Part 3 of 4)

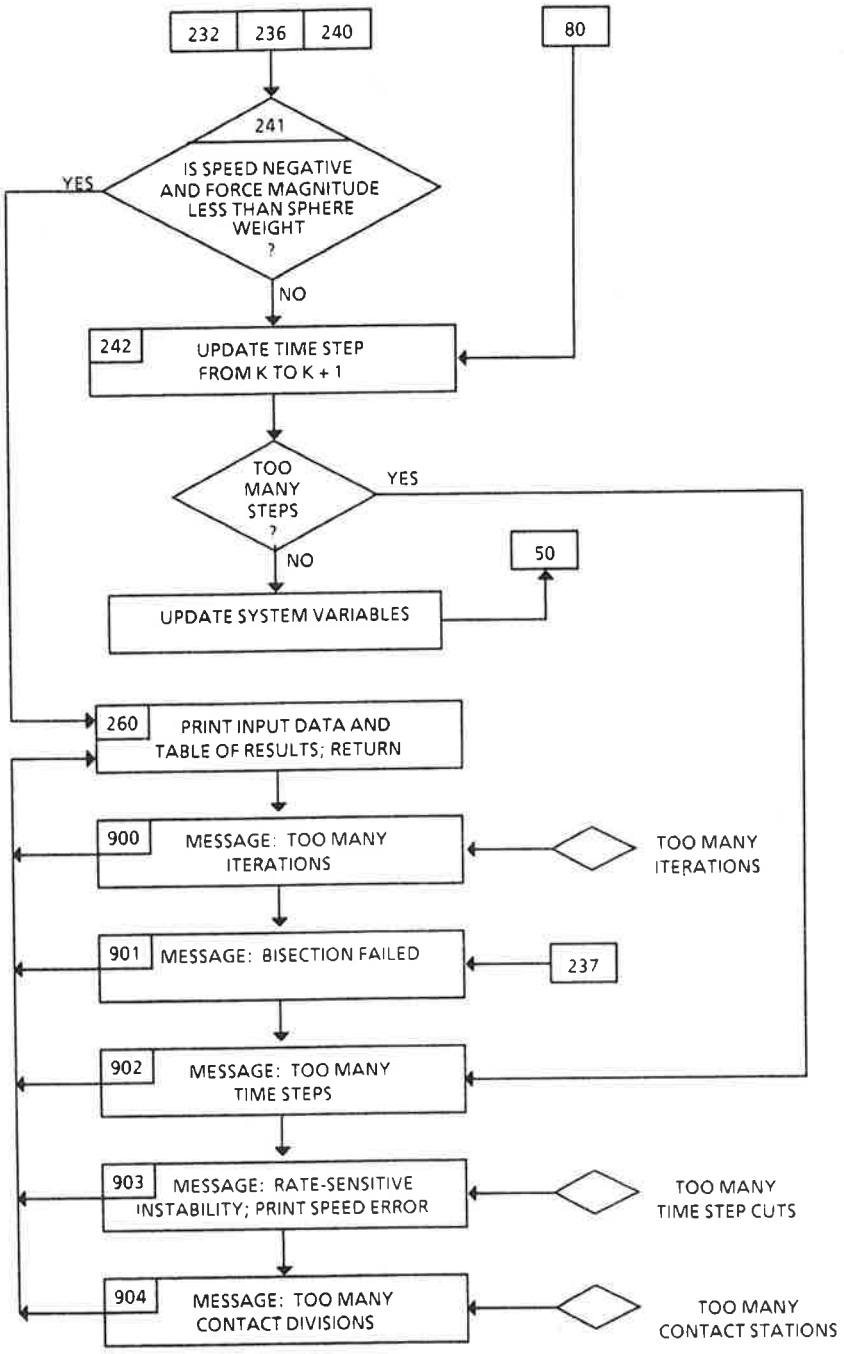

FIGURE A-2. SUBROUTINE FLOW CHART (Part 4 of 4)

returning control to subroutine SPIT. The last step in each branch is a computation of the residual strain (i.e., strain for zero stress on unloading) projected from the current state of stress, strain, and strain rate at the center of contact. The result of this computation is passed back to subroutine SPIT via the argument TIME.

All WRITE and FORMAT statements are located in subroutine SPIT. The print sequence begins with a page-skip and title text executed during the initialization of system variables. During the impact simulation, one line of information is printed each time an iteration has been stopped by attainment of the computing precision limit on pad penetration. The message gives the current step number, current force (lb.), and force error fraction. The force error (lb.) can be calculated as the product of the current force and error fraction. Next in the print sequence is an ABEND message, if any ABEND has occurred. Whether the run is nominal or not, the print sequence continues with a dump of the input data, computed rebound speed, and computed impact duration, and continues with a run summary table of the time (ms) and time histories of force (lb.), acceleration ("g"), speed (in./sec.), sphere position (in.), and pad penetration (in.).

Although the printouts for time and acceleration are converted to milliseconds and "g", respectively, the data in the corresponding vectors T and A are left in seconds and in./sec.^{2}, respectively. The user may access the time history for other purposes by placing the appropriate vectors and the scalar integer K in the argument list of subroutine SPIT. The time history runs from t=0 (vector index 2) to the last computed point before loss of contact at t=(K-2) Δt (vector index K). If an ABEND has occurred in the run, the computed rebound speed, impact duration, and final quantities in the time history correspond to the last valid time step, which is not necessarily close to loss of contact.

A.5 SUGGESTED CORRECTIVE ACTIONS

If a run produces a large number of precision-limit messages, increase the equilibrium-check tolerance limit (TOLMAX) up to 0.02. If this does not solve the problem, try both larger and smaller time step sizes. If the problem persists, reprogram the software with IMPLICIT DOUBLE PRECISION (A-H, O-Z) declarations and decrease the precision tolerance (TOL) to 1.0E-10. The following corrective actions are suggested for ABEND conditions.

900 - TOO MANY ITERATIONS

If ABEND occurs within the impact, the penetration iteration algorithm is converging too slowly. Increase TOLMAX, decrease DELT, or increase the number of

iterations allowed by reprogramming the statement:

IF(ITER.GT.100) GO TO 900

If ABEND occurs near the end of rebound, the problem is likely to be length of marching caused by a rate-sensitive instability. Use next to last time step in run summary as the last valid data point. Estimate speed error $\Delta V/V_{k-1}$ by hand, using Eq. 27 in Section 2.2.

901 - BISECTION FAILED

This ABEND has been included as a logic trap. The triplet bisection algorithm should continue to produce at least one bisectable pair of estimates per iteration step. Failure suggests a highly unusual strain-rate-sensitivity artifact. Re-examine the consitutive equation and material properties being used to represent the pad.

902 - TOO MANY TIME STEPS

The dimension of the system variable vectors is about to be exceeded while the impact is still in progress. Examine the output to estimate the required dimension. Redimension the six system variable vectors and reprogram the statement:

IF (KP1.GT.1000) GO TO 902

to be consistent with the new discussion.

903 - RATE-SENSITIVE INSTABILITY

The algorithm cannot find the terminal point (see discussion in Section 2.2). Accept the results if the printed error, $\Delta V/V_{REBOUND}$, is a small fraction. The corresponding error in the coefficient of restitution is approximately:

2x SPEED ERROR x V_{IN}/V_{REB}

The error effect on injury severity computations can in most cases be neglected, if the solution has progressed to rebound acceleration levels well below the peak acceleration. If the error is not acceptable, rerun the analysis using an initial time step size half the previous size.

904 - TOO MANY CONTACT DIVISIONS

The dimension of the contact field variables is about to be exceeded while the loading phase of the impact is still in progress. Redimension the six contact field variable vectors and reprogram the two statements:

```
IF (MAXR.GT.100) GO TO 904
```

to be consistent with the new dimension.

APPENDIX B
COMPUTER PROGRAM LISTING

This appendix contains FORTRAN source code listings of subroutine SPIT and subroutine PAD. The listed code is Version 2 (December 1984), which supercedes Version 1 (May 1984).

```
      SUBROUTINE SPIT(RAD,VIN,WGT,KEYP,PPAR,THK,KEYS,SPAR,DELT,NDEL)
C     SPHERE/PAD IMPACT TRACKER
C     VERSION 2 (D.Y. JEONG, O. ORRINGER, DEC 1984)
C
C     RAD      = SPHERE RADIUS (INCHES)
C     VIN      = SPHERE INITIAL SPEED (MPH)
C     WGT      = SPHERE WEIGHT (LB)
C     KEYP     = PADDING PROPERTIES KEY
C              1: LINEAR ELASTIC
C              2: LINEAR VISCOELASTIC
C              3: RIGID/CONSTANT CRUSH STRESS
C              4: NINE-PARAMETER VISCOELASTIC
C              5: 21-PARAMETER VISCOELASTIC
C     PPAR(21)= VECTOR OF PADDING PARAMETERS (SEE SUBR PAD)
C     THK      = PAD THICKNESS (INCHES)
C     KEYS     = SUPPORT KEY
C              0: RIGID
C              1: LINEAR ELASTIC
C              2 TO 4: PIECEWISE LINEAR ELASTIC
C     SPAR(12)= SUPPORT PROPERTIES VECTOR:
C     KEYS = SPAR(J), J = 1  2  3  4  5  6  7  8  9  10  11  12
C     0        NOT USED
C     1        (LB/INCH)   *  *  *  *  *  *  *  * KS   *   *   *
C     2        (IN,LB)     X1 F1 X2 F2
C     3        (IN,LB)     X1 F1 X2 F2 X3 F3
C     4        (IN,LB)     X1 F1 X2 F2 X3 F3 X4 F4
C
C     DELT     = INITIAL TIME STEP SIZE (MS)
C     NDEL     = PRINT INTERVAL (MULTIPLE OF DELT)
C
      DIMENSION PPAR(21),SPAR(12)
C
C     TIME HISTORY VARIABLES
      DIMENSION A(1000),F(1000),T(1000),V(1000),X(1000),XP(1000)
C
C     CONTACT FIELD VARIABLES
      DIMENSION EK(1000),EKP1(1000),EMAX(1000),
     1 SK(1000),SKP1(1000),R(1000)
C
C     PHYSICAL CONSTANTS (1 MPH = 17.64 IN/SEC)
      DATA C,G,PI/17.64,386.4,3.141593/
C
C     ITERATION TOLERANCE
      DATA TOL,TOLMAX/1.E-5,0.02/
C
C     IINITIALIZATION (INCLUDING CONSISTENT UNITS)
C
C     STANDARD DELTA-RAD FOR CONTACT SUBDIVISIONS
      DR=RAD/100.
      VZ=C*VIN
      AMASS=WGT/G
      IF(KEYS.EQ.1) GO TO 20
C     CALCULATE SUPPORT TANGENT STIFFNESS
      SPAR(9)=SPAR(2)/SPAR(1)
      DO 10 N=2,KEYS
      J=2*N
10    SPAR(N+8)=(SPAR(J)-SPAR(J-2))/(SPAR(J-1)-SPAR(J-3))
20    DT=DELT/1000.
      DDT=DT
C     CONTACT BOUNDARY PARAMETERS
      MAXR=1
```

```
      RMAX=0
      RLAST=0
C     INITIALIZE
      DO 30 N=1,1000
      EK(N)=0.0
      EMAX(N)=0.0
30    SK(N)=0.0
      FMAX=0.0
      TMAX=0.0
C     INITIAL CONDITIONS
      STIF=SPAR(9)
C     LOOP FOR CONVENIENCE: I.C. ON A(3),F(3),XP(3) WILL BE REPLACED
      DO 40 K=1,3
      T(K)=FLOAT(K-2)*DDT
      A(K)=VZ*T(K)
      V(K)=VZ
      A(K)=0.0
      F(K)=0.0
40    XP(K)=0.0
C     CONTACT STARTS AT T=0.0; THEREAFTER TIME=(K-2)*DT EXCEPT WHEN
C     ALGORITHM CUTS TIME STEP
      K=2
      WRITE(5,6000)
      WRITE(21,6000)
6000  FORMAT(26H1SPHERE/PAD IMPACT TRACKER/)
C
C     BEGIN USER LOOP FOR IMPACT TRACKING
C
50    CONTINUE
C     UPDATE STEP
      KM2=K-1
      KM1=K
      K=K+1
C     COMPUTE INITIAL PENETRATION AND EQUILIBRIUM-CHECK
C     ESTIMATORS
      Y1=XP(KM2)
      F1=F(KM2)+STIF*(A(K)-XP(KM2))
      Y2=XP(KM1)
      F2=F(KM1)+STIF*(A(K)-XP(KM1))
C     ITERATION CONTROL
      ITER=0
      NEXP=0
C     RESET FLAG FOR MARCHING
      IFLAG=0
      DY=ABS(Y2-Y1)
      IF(DY.LT.0.005*ABS(Y2)) DY=0.005*ABS(Y2)
      IF(DY.EQ.0.0) DY=0.005*THK
      IF(F2) 70,80,90
70    DY=-DY
      GO TO 90
80    XP(K)=XP(KM1)
      F(K)=F(KM1)
      GO TO 242
C     BEGIN USER LOOP FOR MARCHING ITERATION
90    Y3=Y2+DY
C     CHECK PENETRATION ESTIMATES; ADJUST FOR HARD BOUNDARY OR
C     EXIT IF REQUIRED; ALSO BEGIN USER LOOP FOR BISECTION
100   IF(Y3.GE.THK) Y3=0.5*(THK+XP(KM1))
      IF(Y3.GT.RAD) Y3=RAD
      IF(Y3.GE.0.0) GO TO 110
C     OVERSTEP EXIT; RESTART THIS STEP AT HALF DELTA-T
```

```
105     DDT=0.5*DDT
        X(K)=X(KM1)+V(KM1)*DDT
        V(K)=V(KM1)+A(KM1)*DDT
        T(K)=T(KM1)+DDT
        NEXP=NEXP+1
        Y3=XP(KM1)+(XP(KM1)-XP(KM2))*(0.5**NEXP)
        ITER=0
        IF(NEXP.LE.7) GO TO 110
C       STRAIN-RATE-SENSITIVE INSTABILITY CANNOT BE
C       DAMPED OUT; ESTIMATE VELOCITY ERROR AND QUIT
        K=KM2
C       ESTIMATE RETREATS TWO STEPS TO ACCESS BETTER DATA
        AA=0.5*A(K)*(X(K)-THK*ERES)/V(K)**2
        GO TO 903
C       ESTIMATE IS OK; FIND NEW CONTACT RADIUS AND ADD
C       INTEGRATION STATIONS IF NEEDED
110     RMAX=2.*RAD*Y3-Y3**2
        RMAX=SQRT(RMAX)
        IF(RMAX.LE.RLAST) GO TO 150
        RL=RLAST
        LAST=MAXR
        N=INT((RMAX-RLAST)/DR)
        IF(N.EQ.0) GO TO 130
        DO 120 J=1,N
        MAXR=MAXR+1
        IF(MAXR.GT.1000) GO TO 904
120     R(MAXR)=R(MAXR-1)+DR
130     AA=(RMAX-R(MAXR))/DR
        IF(AA.LT.0.1) GO TO 140
        MAXR=MAXR+1
        IF(MAXR.GT.1000) GO TO 904
        R(MAXR)=RMAX
140     RLAST=RMAX
C       COMPUTE STRAINS AT END OF TIME STEP
150     DO 160 N=1,MAXR
        AA=1.-(R(N)/RAD)**2
        EKP1(N)=(RAD*(1.-SQRT(AA))-Y3)/THK
160     CONTINUE
C       UPDATE STRESSES WITH CONSTITUTIVE EQUATION
        TIME=T(K)
C
        CALL PAD(DDT,PPAR,KEYP,EK,EKP1,EMAX,SK,SKP1,MAXR,TIME)
C
C       PROJECTED RESIDUAL STRAIN IS RETURNED IN VARIABLE "TIME";
C       PICKED UP AT END OF STEP
C
C       CHECK FOR TENSION (RESET TO ZERO) AND REDUCE CONTACT
C       RADIUS IF FULLY UNLOADED
        DO 170 N=MAXR,1,-1
        IF(SKP1(N).LE.0.0) GO TO 180
        MAXR=MAXR-1
        SKP1(N)=0.0
170     CONTINUE
180     IF(MAXR-1) 181,190,200
C       ALL STRESSES ZERO IF MAXR=0, COMPRESSION ONLY ON LINE
C       OF APPROACH IF MAXR=1
181     AA=0.0
        GO TO 220
190     AA=SKP1(1)*R(2)**2
        GO TO 220
C       IF MAXR.GT.1, TRAPEZOID INTEGRATION TO FIND FORCE
```

```
200     AA=0.0
        DO 210 N=2,MAXR
210     AA=AA+(SKP1(N)+SKP1(N-1))*(R(N)**2-R(N-1)**2)
220     F(K)=PI*AA/2.
        IF(KEYS.EQ.1) GO TO 222
C       UPDATE SECANT STIFFNESS OF NONLINEAR SUPPORT
        XS=X(K)-Y3
        STIF=SPAR(9)
        DO 221 N=2,KEYS
        J=2*N-3
        AA=1.-SPAR(J)/XS
        IF(AA.GT.1.0) STIF=STIF+SPAR(N+8)*AA
221     CONTINUE
222     F3=F(K)+STIF*(X(K)-Y3)
C       EQUILIBRIUM CHECK
        AA=F3
        IF(F(K).NE.0.0) AA=AA/F(K)
        IF(ABS(AA).LE.TOLMAX) GO TO 240
C       CONVERGENCE CHECK
        IF(Y2+Y3.EQ.0.0) GO TO 230
        BB=(Y2-Y3)/(Y2+Y3)
        IF(ABS(BB).GT.TOL) GO TO 230
C       CONVERGED ON PRECISION ONLY; PRINT FORCE ERROR MESSAGE
        WRITE(5,613) K,F(K),AA
613     FORMAT(5H0STEP,I5,7H FORCE=,E10.3,7H ERROR=,E10.3)
        GO TO 240
C       ITERATION REQUIRED
230     ITER=ITER+1
        IF(ITER.GT.100) GO TO 900
C       FIRST ATTEMPT INITIAL BISECTION
        IF(F2*F3) 231,232,233
C       PRIMARY BISECTION IS AVAILABLE
231     Y1=Y2
        F1=F2
        Y2=Y3
        F2=F3
C       SET FLAG TO CONTINUE BISECTIONS
        IFLAG=1
        GO TO 235
C       TRAP: STIFF PAD - NO PENETRATION CHANGE
232     XP(K)=XP(KM1)
        GO TO 241
233     IF(IFLAG.EQ.0) GO TO 238
C       SECONDARY BISECTION IF BISECTING STARTED AND PRIMARY
C       NOT AVAILABLE
        IF(F1*F3) 234,236,237
C       SECONDARY AVAILABLE
234     Y2=Y3
        F2=F3
235     Y3=0.5*(Y1+Y2)
C       RESTORE INTEGRATION CONTROL TO PRIOR VALUES
        MAXR=LAST
        RMAX=RLAST
        RLAST=RL
        GO TO 100
C       TRAP: EQUAL PENETRATIONS JUST BEFORE AND AFTER
C       START OF REBOUND
236     XP(K)=XP(KM2)
        GO TO 241
C       BISECTION FAILED
237     GO TO 901
```

```
C       BISECTION NOT STARTED: CONTINUE MARCHING
238     Y1=Y2
        F1=F2
        Y2=Y3
        F2=F3
        MAXR=LAST
        RMAX=RLAST
        RLAST=RL
        GO TO 90
C       ITERATION COMPLETED
240     XP(K)=Y3
C       CHECK FOR TERMINATION
241     AA=F(K)
        IF(V(K).LT.0.0.AND.ABS(AA).LT.WGT) GO TO 260
C       UPDATE TIME STEP AND MOTION
242     KP1=K+1
        IF(KP1.GT.1000) GO TO 902
        A(K)=F(K)/AMASS
C       CENTRAL DIFFERENCE UPDATES FOR MOTIONS;
C       FORWARD DIFFERENCE FOR SPEED
        X(KP1)=2.*X(K)-X(KM1)+A(K)*DDT**2
        V(KP1)=(X(KP1)-X(K))/DDT
        T(KP1)=T(K)+DDT
C       SWITCH NEW STRESS AND STRAIN TO OLD, GO TO NEXT STEP
        DO 250 N=1,MAXR
        EK(N)=EKP1(N)
        AA=ABS(EK(N))
        IF(EMAX(N).LT.AA) EMAX(N)=AA
250     SK(N)=SKP1(N)
C       PICK UP PROJECTED RESIDUAL STRAIN
        ERES=TIME
C       UPDATE PEAK FORCE AND TIME OF OCCURRENCE
        IF(FMAX.LT.F(K)) GO TO 251
        FMAX=F(K)
        TMAX=1000.*T(K)
251     GO TO 50
C       NORMAL TERMINATION: COMPUTE REBOUND SPEED (MPH) AND
C       PRINT RESULTS
260     VREB=V(K)/C
        WRITE(5,601) RAD,WGT,VIN,VREB,KEYP,THK
        WRITE(21,601) RAD,WGT,VIN,VREB,KEYP,THK
601     FORMAT(14H0SPHERE PARMS:,/8H0RADIUS=,12X,E10.3,
        1 7H INCHES,/8H WEIGHT=,12X,E10.3,4H LBS,
        2 /15H0INITIAL SPEED=,5X,E10.3,4H MPH,
        3 /15H REBOUND SPEED=,5X,E10.3,4H MPH,
        4 /15H0PAD MATL TYPE=,10X,I5,/11H THICKNESS=,9X,
        5 E10.3,7H INCHES,/12H PROPERTIES=)
        WRITE(5,602) (PPAR(N),N=1,21)
        WRITE(21,602) (PPAR(N),N=1,21)
602     FORMAT(1X,8E15.3)
        WRITE(5,603) KEYS,(SPAR(N),N=1,7,2)
        WRITE(21,603) KEYS,(SPAR(N),N=1,7,2)
603     FORMAT(14H0SUPPORT TYPE=,11X,I5,/4H X= ,4E15.3)
        WRITE(5,604) (SPAR(N),N=2,8,2)
        WRITE(21,604) (SPAR(N),N=2,8,2)
604     FORMAT(4H F= ,4E15.3)
        WRITE(5,605) (SPAR(N),N=9,12)
        WRITE(21,605) (SPAR(N),N=9,12)
605     FORMAT(4H K= ,4E15.3)
        AA=1000*T(K)
        WRITE(5,606) DELT,AA,TMAX,FMAX
```

```
      WRITE(21,606) DELT,AA,TMAX,FMAX
606   FORMAT(17H0INITIAL DELTA-T=,3X,E10.3,3H MS,
     1 /17H IMPACT DURATION=,3X,E10.3,3H MS,
     2 /20H TIME TO PEAK FORCE=,E10.3,3H MS,
     3 /12H PEAK FORCE=,8X,E10.3,3H LB,
     4 /12H1RUN SUMMARY,/1H0,6X,9HTIME (MS),5X,
     5 10HFORCE (LB),6X,9HACCEL (G),4X,11HSPEED (IPS),
     6 4X,11HMOTION (IN),4X,11HPENETR (IN)/)
C
      LAST=K-NDEL
      IF(LAST.LT.2) GO TO 280
      DO 270 N=2,LAST,NDEL
      TIME=1000.*T(N)
      AA=A(N)/G
      WRITE(5,607) TIME,F(N),AA,V(N),X(N),XP(N)
      WRITE(21,607) TIME,F(N),AA,V(N),X(N),XP(N)
270   CONTINUE
280   LAST=LAST+1
      DO 290 N=LAST,K
      TIME=1000.*T(N)
      AA=A(N)/G
      WRITE(5,607) TIME,F(N),AA,V(N),X(N),XP(N)
      WRITE(21,607) TIME,F(N),AA,V(N),X(N),XP(N)
290   CONTINUE
607   FORMAT(1X,6E15.3)
281   RETURN
C     ABENDS
900   WRITE(5,608)
      WRITE(21,608)
608   FORMAT(28H0ABEND - TOO MANY ITERATIONS)
      GO TO 260
901   WRITE(5,609)
      WRITE(21,609)
609   FORMAT(25H0ABEND - BISECTION FAILED)
      GO TO 260
902   WRITE(5,610)
      WRITE(21,610)
610   FORMAT(28H0ABEND - TOO MANY TIME STEPS)
      GO TO 260
903   WRITE(5,611) AA
611   FORMAT(50H0ABEND - RATE-SENSITIVE INSTABILITY - SPEED ERROR=,
     1 E10.3)
      GO TO 260
904   WRITE(5,612)
612   FORMAT(35H0ABEND - TOO MANY CONTACT DIVISIONS)
      END
```

```
      SUBROUTINE PAD(DELT,PROPS,KEY,EK,EKP1,EMAX,SK,SKP1,LASTR,TIME)
C
C     VERSION 2 (D.Y.JEONG, O.ORRINGER, DEC 1984)
C
C     CONTAINS FIVE CONSTITUTIVE EQUATIONS (C.E.) CORRESPONDING TO
C     VALUE OF "KEY" PARAMETER. USES C.E. TO FIND UPDATED STRESSES
C     SKP1 FROM UPDATED STRAINS EKP1 AND PREVIOUS STATE (SK,EK)
C     EACH C.E. IS PROGRAMMED AS A FIRST FORWARD DIFFERENCE
C
C     ABSOLUTE TIME FROM START OF IMPACT IN ARGUMENT "TIME" IS USED BY
C     21-PARAMETER MODEL; SUBROUTINE RETUNS PROJECTED RESIDUAL
C     STRAIN IN ARGUMENT 'TIME' (ALL MODELS)
C
C     CONVENTIONS FOR MATERIAL PROPERTIES STORAGE-PROPS(J)
C     KEY     J =   1   2   3   4   5   6   7   8   9
C     1             EI
C     2             EI  EZ   T
C     3             S1  E1  S2  E2
C     4             EI  EM  EN   T  ER   R  TS   P  EZ
C     5 (J=1,9)     EI  EM  EN  AA  BB  CC  SR   R   U
C       (J=10,18)    V   W   X   Y   Z  TS   P  SZ   A
C       (J=19,21)    B   C   D
C
C     DEFINITIONS AND UNITS
C
C     KEY= 1 (LINEAR ELASTIC SOLID)
C     EI       = YOUNG'S MODULUS (PSI)
C
C     KEY      = 2 (LINEAR VISCOELASTIC SOLID)
C     EI       = ASYMPTOTIC MODULUS (PSI)
C     EZ       = ZER-TIME MODULUS (PSI)
C     T        = RELAXATION TIME CONSTANT (SEC)
C
C     KEY=3 (IDEALIZED RIGID FOAM)
C     S1       = CRUSH STRENGTH (PSI)
C     E1       = BOTTOMING STRAIN (IN/IN)
C     S2,E2    = SECOND STRESS-STRAIN DATA POINT (PSI,IN/IN)
C     MODEL FOR LOADING ASSIGNS: STRESS S1 UP TO STRAIN E1;
C     STRESS INCREASES PROPORTIONAL TO TANGENT MODULUS BETWEEN
C     DATA POINTS 1 AND 2 UP TO STRAIN E2; STRESS INCREASES
C     PROPORTIONAL TO 9*S2/(1-E2) AT STRAINS EXCEEDING E2
C
C     KEY=4 (9-PARAMETER VISCOELASTIC MODEL)
C     EI       = ASYMPTOTIC MODULUS (PSI)
C     EM,EN    = ASYMPTOTIC STRAIN EXPONENTS M,N
C     T        = RELAXATION ME CONSTANT (SEC)
C     ER       = STRAIN-RATE MODULUS (PSI)
C     R        = STRAIN-RATE EXPONENT
C     TS       = RESIDUAL STRAIN SCALE FACTOT (SEC)
C     P        = RESIDUAL STRAIN EXPONENT
C     EZ       = ZERO-TIME MODULUS (PSI), NOT USED IN C.E.
C
C     KEY=5 (21-PARAMETER VISCOELASTIC MODEL)
C     EI       = ASYMPTOTIC MODULUS (PSI)
C     EM,EN    = ASYMPTOTIO STRAIN EXPONENTS M,N
C     AA,BB,CC= RELAXTION TIME SCALING PARAMETERS
C     SR       = STRAIN-RATE-SENSITIVE STRESS FACTOR (PSI)
C     R        = STRAIN-RATE EXPONENT
C     U,V      = STRAIN-SCALING FACTORS IN STRAIN-RATE EXPONENT
C     W,X,Y,Z  = STRAIN-SCALING FACTORTS IN STRAIN-RATE-SENSITIVE
C                STRESS
```

```
C       TS      = RESIDUAL STRAIN SCALE FACTORS (SEC)
C       P       = RESIDUAL STRAIN EXPONNENT
C       SZ      = ZERO-TIME STRESS FACTOR (PSI), NOT USED IN C.E.
C       A,B,C,D = STRAIN-SCALING FACTORS IN ZERO-TIME STRESS;
C                 NOT USED IN C.E.
C
      DIMENSION PROPS(21)
      DIMENSION EK(1000),EKP1(1000),EMAX(1000),SK(1000),SKP1(1000)
C
C
      LAST=LASTR-1
C
C     SELECT MATERIAL TYPE
C
      GO TO (100,200,300,400,500) KEY
C
C     ELASTIC
C
100   EI= PROPS(1)
      DO 101 I=1, LASTR
101   SKP1(I)= EI*EKP1(I)
C     RESIDUAL STRAIN
      TIME=0.0
      RETURN
C
C     LINEAR VISCOELASTIC
C
200   EI= PROPS(1)
      T=PROPS(3)
      EZ= PROPS(2)
      A= 1. - DELT/T
      B= EZ - EI*DELT/T
      DO 201 I=1, LASTR
201   SKP1(I)= A*SK(I) + EZ*EKP1(I) - B*EK(I)
C     RESIDUAL STRAIN
      EDOT=(EKP1(1)-EK(1))/DELT
      A=SKP1(1)-EZ*T*EDOT-EI*EKP1(1)
      TIME=EKP1(1)+SKP1(1)*T*EDOT/A
      RETURN
C
C     RIGID FOAM
C
300   S1=PROPS(1)
      S2=PROPS(3)
      E1=PROPS(2)
      E2=PROPS(4)
      A= (S2 - S1)/ (E2 - E1)
      B= 9.*S2 / (1. - E2)
      DO 307 I=1, LASTR
      EDOT= EKP1(I) - EK(I)
      IF (EDOT) 301,301,306
C
CC    LOADING
C
301   EKM=ABS(EKP1(I))
      IF(EKM-E1) 302,302,303
302   SKP1(I)= -S1
      GO TO 307
303   IF (EKM-E2) 304,304,305
304   SKP1(I)= A* (E1-EKM) - S1
      GO TO 307
```

```
      I
305   SKP1(I)= B*(E2-EKM) - S2
      GO TO 307
C
CC    UNLOADING
306   SKP1(I)= 0.
307   CONTINUE
C     RESIDUAL STRAIN
      TIME=EMAX(1)
      RETURN
C
CC    9-PARAMETER
C
400   IF(LAST.EQ.0) RETURN
      EI=PROPS(1)
      EM=PROPS(2)
      EN=PROPS(3)
      T =PROPS(4)
      ER=PROPS(5)
      R =PROPS(6)
      TS=PROPS(7)
      P =PROPS(8)
C
      EDOT=(EK(1)-EKP1(1))/DELT
      EDOTM=ABS(EDOT)
999   DO 405 I=1,LAST
      EKM=ABS(EK(I))
      IF(EKM.EQ.0) EKM=(EKM+ABS(EKP1(I)))/2.
      SKM=ABS(SK(I))
      ISGN=-1
      IF(SKM.NE.0) ISGN=INT(1.1*SKM/SK(I))
      A=(EKM**EM)/((1.-EKM)**EN)
      B=EI+ER*EDOTM**R
      C=((EM/EKM)+(EN/(1.-EKM)))*EDOT+1./T
      IF (EDOT) 402,401,401
C
CC    LOADING
401   Q=A*B*C
      GOTO 404
C
CC    UNLOADING
402   D=(TS*EDOTM)**P
      E=(EKM-EMAX(I)*D)/(EKM*(1.-D))
      D=EDOT*EMAX(I)*D/(EKM*EKM*(1.-D))
      Q=A*B*(D+E*C)
404   SKP1(I)= ISGN*(SKM+(Q-SKM/T)*DELT)
      IF(ISGN.EQ.1) SKP1(I)=ABS(SKP1(I))
405   CONTINUE
      SKP1(LASTR)=0.0
C     RESIDUAL STRAIN
      EKM=ABS(EMAX(1))
      TIME=EKM*(TS*EDOTM)**P
      RETURN
C
CC    21-PARAMETER
C
500   IF(LAST.EQ.0) RETURN
      EI=PROPS(1)
      EM=PROPS(2)
      EN=PROPS(3)
      AA=PROPS(4)
      BB=PROPS(5)
```

```
      CC=PROPS(6)
      SR=PROPS(7)
      R =PROPS(8)
      U =PROPS(9)
      V =PROPS(10)
      W =PROPS(11)
      X =PROPS(12)
      Y =PROPS(13)
      Z =PROPS(14)
      TS=PROPS(15)
      P =PROPS(16)

      EDOT=(EK(1)-EKP1(1))/DELT
      EDOTM=ABS(EDOT)
C
      DO 505 I=1,LAST
      EKM=ABS(EK(I))
      IF(EKM.EQ.0.0) EKM=(EKM+ABS(EKP1(I)))/2.
      SKM=ABS(SK(I))
      ISGN=-1
      IF(SKM.NE.0) ISGN=INT(1.1*SKM/SK(I))
      A=EI*(EKM**EM)/((1.-EKM)**EN)
      SIN=A
      A=((EM/EKM)+(EN/(1.-EKM)))*EDOT
      B=AA*(TIME**(AA-1.))/(BB*(CC**EKM))
      Q=(A+B)*SIN
      C=0.0
      IF(EDOTM.EQ.0) GO TO 501
      EKU=EKM**U
      EKW=EKM**W
      EKY=EKM**Y
      IF(EKU/V.GE.50.) EXU=0.0
      IF(EKU/V.LT.50.) EXU=EXP(-EKU/V)
      EXW=EXP(EKW/X)
      IF(EKY/Z.GE.50.) EXY=0.0
      IF(EKY/Z.LT.50.) EXY=EXP(-EKY/Z)
      SR1=SR*(EDOTM**(R*EKU))
      SR2=EDOT*((W*EKW*EXW/X)+(Y*EKY*EXY/Z))/EKM
      SR3=EDOT*R*U*EKU*EXU*ALOG(EDOTM)/(V*EKM)
      C=SR1*(SR2+(B-SR3)*(EXW-EXY))
C
CC    LOADING
C
501   Q=Q+C
      IF(EDOT.GE.0.0) GO TO 504
C
CC    UNLOADING
C
      D=(TS*EDOTM)**P
      E=(EKM-EMAX(1)*D)/(EKM*(1.-D))
      D=EDOT*EMAX(I)*D/(EKM*EKM*(1.-D))
      Q=D*(SIN+SR1*(EXW-EXY))+E*Q
C
504   SKP1(I)=ISGN*(SKM+(Q-B*SKM)*DELT)
      IF(ISGN.EQ.1) SKP1(I)=ABS(SKP1(I))
505   CONTINUE
      SKP1(LASTR)=0.0
C     RESIDUAL STRAIN
      EKM=ABS(EMAX(1))
      D=(TS*EDOTM)**P
      TIME=EKM*D
```

```
RETURN
END
```

APPENDIX C
EXAMPLE ANALYSIS

This appendix contains an example of impact analysis with subroutines SPIT and PAD. Pages C-2 and C-3 contain a FORTRAN source code listing of the MAIN program which was used to drive the software on a DECSystem 10 computer. This MAIN was written for interactive input from a remote terminal. DATA statements for vectors PAR9 and PAR21 define the parameter values for the 9-parameter and 21-parameter models of Ensolite AAC foam rubber.

Following the MAIN program are printouts of the example impact analysis discussed in Section 2.3. Results are given for both the 9-parameter and 21-parameter models.

```
C
C       ENSOL   SPIT/PAD TESTER W/ ENSOLITE PARAMETERS
C
C
        DIMENSION SPAR(12),PPAR(21),PAR9(9),PAR21(21)
C
C       DATA FOR 9-PARAMETER MODEL OF ENSOLITE AAC FOAM RUBBER
        DATA PAR9/7.96,0.675,1.09,8.81E-03,5.45,0.166,
        1       9.76E-06,0.0987,22.127/
C
C       DATA FOR 21-PARAMETER MODEL OF ENSOLITE AAC FOAM RUBBER
        DATA PAR21/7.96,0.675,1.09,0.13,0.156,3.08,4.153,0.19,3.17,0.58,
        1 2.57,0.296,2.23,1.64E-3,9.76E-6,0.0987,66.0,10.12,0.279,
        2 1.94,0.029/
C
C       INPUT
C
        WRITE(5,500)
500     FORMAT(1X,'SPHERE/PAD IMPACT TRACKER VERSION 2-DEC 1984')
C       CHOOSE MODEL
10      WRITE(5,510)
510     FORMAT(1X,'PLEASE CHOOSE MODEL: 1 = ELASTIC,'
        1 /22X,'2 = LINEAR V.E.',/22X,'3 = RIGID-FOAM',
        2 /22X,'4 = 9-PARAMETER',/22X,'5 = 21-PARAMETER: '$)
        READ(5,596) KEYP
596     FORMAT(I)
C       KEYP    = 1: ELASTIC
C               = 2: LINEAR V.E.
C               = 3: RIGID-FOAM
C               = 4: 9-PARAMETER
C               = 5: 21-PARAMETER
C
C       CHOOSE IMPACT TYPE/INPUT
15      WRITE(5,520)
520     FORMAT(/1X,'PLEASE ENTER: 1 = LINEAR ELASTIC SUPPORT',/15X,
        1       '2 = PIECEWISE LINEAR SUPPORT (2 SLOPES)',/15X,
        2       '3 = PIECEWISE LINEAR SUPPORT (3 SLOPES)',/15X,
        3       '4 = PIECEWISE LINEAR SUPPORT (4 SLOPES): '$)
        READ(5,596) KEYS
        WRITE(5,530)
530     FORMAT(/1X,'ENTER SPHERE RADIUS (IN.): '$)
        READ(5,592) RAD
592     FORMAT(E10.0)
        WRITE(5,999)
999     FORMAT(1X,'ENTER INITIAL SPEED (MPH): '$)
        READ(5,592) VIN
        WRITE(5,531)
531     FORMAT(1X,'ENTER WEIGHT (LBS): '$)
        READ(5,592) WGT
        WRITE(5,535)
535     FORMAT(1X,'ENTER FOAM THICKNESS (IN.): '$)
        READ(5,592) THK
        WRITE(5,998)
998     FORMAT(1X,'INITIAL TIME STEP SIZE (MSEC): '$)
        READ(5,592) DELT
        WRITE(5,996)
996     FORMAT(1X,'ENTER PRINT INTERVAL, NDEL: '$)
        READ(5,596) NDEL
C
C       PROGRAM SUPPORT STIFFNESS
C
```

```
      I
      IF(KEYS.GE.2) GO TO 650
600   WRITE(5,601)
601   FORMAT(1X,'ENTER SUPPORT STIFFNESS (LB/IN): '$)
      READ(5,592) SPAR(9)
      GO TO 900
650   WRITE(5,651)
651   FORMAT(1X,'ENTER BREAK POINTS FOR PIECEWISE LINEAR SUPPORT: ')
      DO 662 I=1,KEYS
      WRITE(5,652)I
652   FORMAT(1X,'DEFLECTION-LOAD PAIR ',I2,1H:$)
      J=2*I
      READ(5,653) SPAR(J-1),SPAR(J)
653   FORMAT(2F)
662   CONTINUE
C
900   GO TO (950,950,950,920,940) KEYP
920   DO 930 I=1,9
      PPAR(I)=PAR9(I)
930   CONTINUE
      GO TO 950
940   DO 945 I=1,21
      PPAR(I)=PAR21(I)
945   CONTINUE
C
C     PERFORM SPIT/PAD TRACKING AND OUTPUT
950   CALL SPIT(RAD,VIN,WGT,KEYP,PPAR,THK,KEYS,SPAR,DELT,NDEL)
C
25    CALL EXIT
      END
```

```
SPHERE/PAD IMPACT TRACKER


SPHERE PARMS:

RADIUS=              0.300E+01 INCHES
WEIGHT=              0.100E+02 LBS

INITIAL SPEED=       0.200E+02 MPH
REBOUND SPEED=      -0.179E+02 MPH

PAD MATL TYPE=               4
THICKNESS=           0.100E+01 INCHES
PROPERTIES=
      0.796E+01      0.675E+00      0.109E+01      0.881E-02      0.545E+01      0.166E+00      0.976E-05      0.987E-01
      0.221E+02      0.000E+00      0.000E+00      0.000E+00      0.000E+00      0.000E+00      0.000E+00      0.000E+00
      0.000E+00      0.000E+00      0.000E+00      0.000E+00      0.000E+00

SUPPORT TYPE=                1
X=       0.000E+00      0.000E+00      0.000E+00      0.000E+00
F=       0.000E+00      0.000E+00      0.000E+00      0.000E+00
K=       0.600E+03      0.000E+00      0.000E+00      0.000E+00

INITIAL DELTA-T=     0.100E+00 MS
IMPACT DURATION=     0.241E+02 MS
TIME TO PEAK FORCE=  0.129E+02 MS
PEAK FORCE=         -0.122E+04 LB
```

RUN SUMMARY

TIME (MS)	FORCE (LB)	ACCEL (G)	SPEED (IPS)	MOTION (IN)	PENETR (IN)
0.000E+00	0.000E+00	0.000E+00	0.353E+03	0.000E+00	0.000E+00
0.100E+01	-0.908E+02	-0.908E+01	0.351E+03	0.352E+00	0.203E+00
0.200E+01	-0.234E+03	-0.234E+02	0.345E+03	0.701E+00	0.314E+00
0.300E+01	-0.355E+03	-0.355E+02	0.334E+03	0.104E+01	0.454E+00
0.400E+01	-0.477E+03	-0.477E+02	0.318E+03	0.137E+01	0.566E+00
0.500E+01	-0.589E+03	-0.589E+02	0.298E+03	0.167E+01	0.681E+00
0.600E+01	-0.693E+03	-0.693E+02	0.273E+03	0.196E+01	0.792E+00
0.700E+01	-0.801E+03	-0.801E+02	0.244E+03	0.222E+01	0.860E+00
0.800E+01	-0.911E+03	-0.911E+02	0.211E+03	0.244E+01	0.906E+00
0.900E+01	-0.104E+04	-0.104E+03	0.174E+03	0.263E+01	0.938E+00
0.100E+02	-0.111E+04	-0.111E+03	0.133E+03	0.278E+01	0.953E+00
0.110E+02	-0.115E+04	-0.115E+03	0.891E+02	0.289E+01	0.962E+00
0.120E+02	-0.118E+04	-0.118E+03	0.437E+02	0.296E+01	0.968E+00
0.130E+02	-0.120E+04	-0.120E+03	-0.275E+01	0.298E+01	0.971E+00
0.140E+02	-0.120E+04	-0.120E+03	-0.490E+02	0.295E+01	0.974E+00
0.150E+02	-0.112E+04	-0.112E+03	-0.941E+02	0.287E+01	0.971E+00
0.160E+02	-0.107E+04	-0.107E+03	-0.137E+03	0.276E+01	0.970E+00
0.170E+02	-0.966E+03	-0.966E+02	-0.177E+03	0.260E+01	0.964E+00
0.180E+02	-0.858E+03	-0.858E+02	-0.213E+03	0.240E+01	0.956E+00
0.190E+02	-0.725E+03	-0.725E+02	-0.244E+03	0.217E+01	0.940E+00
0.200E+02	-0.590E+03	-0.590E+02	-0.269E+03	0.191E+01	0.919E+00
0.210E+02	-0.444E+03	-0.444E+02	-0.290E+03	0.163E+01	0.887E+00
0.220E+02	-0.296E+03	-0.296E+02	-0.304E+03	0.133E+01	0.840E+00
0.230E+02	-0.151E+03	-0.151E+02	-0.313E+03	0.102E+01	0.772E+00
0.232E+02	-0.124E+03	-0.124E+02	-0.314E+03	0.960E+00	0.757E+00
0.233E+02	-0.107E+03	-0.107E+02	-0.315E+03	0.929E+00	0.749E+00
0.234E+02	-0.945E+02	-0.945E+01	-0.315E+03	0.897E+00	0.740E+00
0.235E+02	-0.802E+02	-0.802E+01	-0.315E+03	0.866E+00	0.730E+00
0.236E+02	-0.691E+02	-0.691E+01	-0.316E+03	0.834E+00	0.721E+00
0.237E+02	-0.553E+02	-0.553E+01	-0.316E+03	0.802E+00	0.712E+00
0.238E+02	-0.438E+02	-0.438E+01	-0.316E+03	0.771E+00	0.699E+00
0.239E+02	-0.266E+02	-0.266E+01	-0.316E+03	0.739E+00	0.696E+00
0.240E+02	-0.184E+02	-0.184E+01	-0.316E+03	0.708E+00	0.677E+00
0.241E+02	-0.733E+01	0.000E+00	-0.317E+03	0.676E+00	0.664E+00

```
SPHERE/PAD IMPACT TRACKER


SPHERE PARMS:

RADIUS=              0.300E+01 INCHES
WEIGHT=              0.100E+02 LBS

INITIAL SPEED=       0.200E+02 MPH
REBOUND SPEED=      -0.188E+02 MPH

PAD MATL TYPE=               5
THICKNESS=           0.100E+01 INCHES
PROPERTIES=
      0.796E+01       0.675E+00       0.109E+01       0.130E+00       0.156E+00       0.308E+01       0.415E+01       0.190E+0
      0.317E+01       0.580E+00       0.257E+01       0.296E+00       0.223E+01       0.164E-02       0.976E-05       0.987E-0
      0.660E+02       0.101E+02       0.279E+00       0.194E+01       0.290E-01

SUPPORT TYPE=                1
K=        0.000E+00       0.000E+00       0.000E+00       0.000E+00
F=        0.000E+00       0.000E+00       0.000E+00       0.000E+00
K=        0.600E+03       0.000E+00       0.000E+00       0.000E+00

INITIAL DELTA-T=     0.100E+00 MS
IMPACT DURATION=     0.243E+02 MS
TIME TO PEAK FORCE= 0.129E+02 MS
PEAK FORCE=         -0.128E+04 LB
```

RUN SUMMARY

TIME (MS)	FORCE (LB)	ACCEL (G)	SPEED (IPS)	MOTION (IN)	PENETN (IN)
0.000E+00	0.000E+00	0.000E+00	0.353E+03	0.000E+00	0.000E+00
0.100E+01	-0.866E+02	-0.866E+01	0.352E+03	0.352E+00	0.208E+00
0.200E+01	-0.174E+03	-0.174E+02	0.346E+03	0.701E+00	0.410E+00
0.300E+01	-0.278E+03	-0.278E+02	0.338E+03	0.104E+01	0.576E+00
0.400E+01	-0.397E+03	-0.397E+02	0.325E+03	0.137E+01	0.719E+00
0.500E+01	-0.524E+03	-0.524E+02	0.308E+03	0.169E+01	0.814E+00
0.600E+01	-0.664E+03	-0.664E+02	0.285E+03	0.199E+01	0.885E+00
0.700E+01	-0.798E+03	-0.798E+02	0.257E+03	0.226E+01	0.931E+00
0.800E+01	-0.914E+03	-0.914E+02	0.224E+03	0.250E+01	0.958E+00
0.900E+01	-0.103E+04	-0.103E+03	0.186E+03	0.270E+01	0.976E+00
0.100E+02	-0.114E+04	-0.114E+03	0.145E+03	0.286E+01	0.986E+00
0.110E+02	-0.119E+04	-0.119E+03	0.998E+02	0.298E+01	0.989E+00
0.120E+02	-0.123E+04	-0.123E+03	0.526E+02	0.306E+01	0.992E+00
0.130E+02	-0.125E+04	-0.125E+03	0.435E+01	0.308E+01	0.993E+00
0.140E+02	-0.123E+04	-0.123E+03	-0.441E+02	0.306E+01	0.993E+00
0.150E+02	-0.118E+04	-0.118E+03	-0.915E+02	0.299E+01	0.992E+00
0.160E+02	-0.114E+04	-0.114E+03	-0.137E+03	0.287E+01	0.991E+00
0.170E+02	-0.103E+04	-0.103E+03	-0.179E+03	0.271E+01	0.987E+00
0.180E+02	-0.909E+03	-0.909E+02	-0.217E+03	0.251E+01	0.980E+00
0.190E+02	-0.775E+03	-0.775E+02	-0.250E+03	0.228E+01	0.967E+00
0.200E+02	-0.638E+03	-0.638E+02	-0.277E+03	0.201E+01	0.944E+00
0.210E+02	-0.483E+03	-0.483E+02	-0.299E+03	0.172E+01	0.907E+00
0.220E+02	-0.337E+03	-0.337E+02	-0.316E+03	0.141E+01	0.857E+00
0.230E+02	-0.187E+03	-0.187E+02	-0.326E+03	0.109E+01	0.785E+00
0.234E+02	-0.128E+03	-0.128E+02	-0.328E+03	0.962E+00	0.748E+00
0.235E+02	-0.115E+03	-0.115E+02	-0.329E+03	0.929E+00	0.738E+00
0.236E+02	-0.101E+03	-0.101E+02	-0.329E+03	0.896E+00	0.729E+00
0.237E+02	-0.875E+02	-0.875E+01	-0.330E+03	0.863E+00	0.718E+00
0.238E+02	-0.724E+02	-0.724E+01	-0.330E+03	0.830E+00	0.709E+00
0.239E+02	-0.595E+02	-0.595E+01	-0.330E+03	0.797E+00	0.699E+00
0.240E+02	-0.463E+02	-0.463E+01	-0.331E+03	0.764E+00	0.688E+00
0.241E+02	-0.334E+02	-0.334E+01	-0.331E+03	0.731E+00	0.675E+00
0.242E+02	-0.217E+02	-0.217E+01	-0.331E+03	0.698E+00	0.662E+00
0.243E+02	-0.999E+01	0.000E+00	-0.331E+03	0.665E+00	0.648E+00

REFERENCES

1) J. T. Fleck and F. E. Butler, "Validation of the Crash Victim Simulator" (4 volumes), CALSPAN Corporation, Buffalo, NY, Report No. ZS5881, final report to NHTSA, Contract DOT-HS-6-01300, 1982.

2) R. H. Eppinger, "Proposed Injury Criteria and Mathematical Analogs for Selected Body Areas", National Highway Traffic Safety Administration (NRD-12), Washington, DC, memorandum to A. C. Malliaris, July 6, 1982.

3) O. Orringer, K. T. Knadle, and J. F. Mandell, "Crash Padding Mechanical Properties and Impact Response Analysis," in Mathematical Simulation of Occupant and Vehicle Kinematics (S. H. Backaitis and R. L. Strombotne, ed.), Society of Automotive Engineers, Inc., Warrandale, PA, Special Publication P-146, May 1984.

4) F. J. Lockett, R. R. Cousins, and D. Dawson, "Engineering Basis for Selection and Use of Crash Padding Materials," Plastics and Rubber Processing and Applications, Vol. 1 No. 1 (1981), 25-37.

5) G. Dahlquist and A. Bjork, Numerical Methods, Prentice-Hall, Englewood Cliffs, NJ, 1974.

6) R. J. Roark and W. C. Young, Formulas for Stress and Strain, McGraw-Hill, New York, 5th edition, 1975.

64 copies